

Lessons Learned from a Decade-Long Assessment of Asphaltenes by Ultrahigh-Resolution Mass Spectrometry and Implications for Complex Mixture Analysis

Martha L. Chacón-Patiño,* Murray R. Gray, Christopher Rüger, Donald F. Smith, Taylor J. Glatcke, Sydney F. Niles, Anika Neumann, Chad R. Weisbrod, Andrew Yen, Amy M. McKenna, Pierre Giusti, Brice Bouyssiere, Caroline Barrère-Mangote, Harvey Yarranton, Christopher L. Hendrickson, Alan G. Marshall, and Ryan P. Rodgers*

Cite This: *Energy Fuels* 2021, 35, 16335–16376

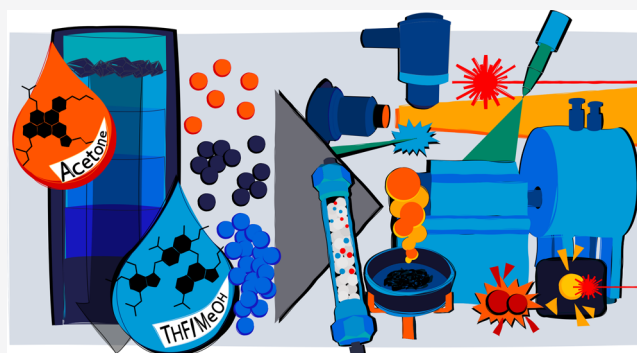
Read Online

ACCESS |

Metrics & More

Article Recommendations

ABSTRACT: Recent advances in instrumentation for high-field Fourier transform ion cyclotron resonance mass spectrometry (FT-ICR MS) have enabled access to ~70 000 unique molecular formulas in broadband mass spectral characterization of unfractionated/whole asphaltenes. The results accumulated over a decade highlight the need for an asphaltene molecular model that acknowledges the coexistence of (1) monofunctional and polyfunctional species; (2) island and archipelago structural motifs; and (3) heteroatom-depleted/highly aromatic compounds, as well as atypical species with low aromaticity but increased heteroatom content. Collectively, results from FT-ICR MS, preparatory-scale separations (extrography/interfacial material), gel permeation chromatography, precipitation behavior in heptane:toluene, thermal decomposition, and aggregate microstructure by atomic force microscopy (among other techniques), suggest that the strong aggregation of asphaltenes results from the synergy between several intermolecular forces: π -stacking, hydrogen bonding, London forces, and acid/base interactions. This review presents general features of asphaltene molecular composition reported over the past five decades. We focus on mass spectrometry characterization and expose the reasons why early results supported the dominance of single-core motifs. Then, the discussion shifts to recent advances in instrumentation for high-field FT-ICR MS, which have enabled the detection of thousands of species in asphaltene samples, whose molecular composition and fragmentation behavior in ultrahigh vacuum agree with the coexistence of single-core and multicore structural motifs. Furthermore, evidence that highlights the limitations of commercially available/custom-built ion sources and selective ionization effects is presented. Consequently, the limitations require separations (e.g., chromatography, extrography) to gain more-comprehensive molecular-level insights into the composition of these complex organic mixtures. The final sections present evidence for the role of aggregation in selective ionization and suggest that advanced characterization by both thermal desorption/decomposition and liquid chromatography with online FT-ICR MS detection can be employed to mitigate the effects of aggregation and provide unique insights in molecular composition/structure.



INTRODUCTION

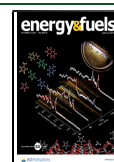
Asphaltenes are arguably the most complex fraction derived from the most polydisperse natural mixture, petroleum; thus, their molecular characterization is a difficult task that has been the subject of several long-lasting controversies.^{1–4} Extensive discussions regarding whether asphaltene molecules or “monomers” have a high (>4000 g/mol) or low (<1200 g/mol) molecular weight were the focus of literature reports between the 1970s and the 2000s.^{5–11} Eventually, that controversy reached a consensus: asphaltene monomers are now accepted as low-molecular-weight (LMW) species with

the most abundant masses between 250 g/mol and 1200 g/mol and an average molecular weight (AMW) of ~700 g/mol.^{12,13} However, the true upper molecular weight boundary (the tailing region of the molecular weight distribution)

Received: June 25, 2021

Revised: September 16, 2021

Published: October 12, 2021



remains unknown, as inefficient/lack of ionization of species >1200 g/mol could also arise from their low volatility/ultrahigh boiling points (>1200 °F). The disparities in molecular weight were caused by aggregation. Today, questions about asphaltene chemistry focus on the molecular structure, single-core or “island” versus multicore or “archipelago”, and the nature of the molecular interactions involved in asphaltene self-aggregation.¹⁴

Repeatedly, experimental results have shown that molecular-level understanding of asphaltenes is hindered by nano-aggregation.^{14,15} Initial works on MW, by vapor pressure osmometry (VPO) and gel permeation chromatography (GPC), suggested that petroleum asphaltenes exhibited high masses in the range of $\sim 4 \times 10^3$ – 1×10^5 g/mol.^{16–21} Petroleum scientists soon realized that MW results, apart from being sample-dependent, varied based on the analytical technique(s) and analysis conditions (e.g., solvents, eluents, temperature). Thus, concerns about the innate, self-aggregation nature of asphaltenes and its impact on MW results ignited discussion about their plausible low MW. It was suggested that asphaltenes (heptane insoluble/toluene soluble) molecular weights should be within the same range of maltenic petroleum compounds (heptane soluble).⁸

Boduszynski was among the first scientists who promoted such an idea in the early 1980s,^{8,11,22} and he based his hypothesis on trends in bulk elemental composition of petroleum distillation cuts/residue solubility fractions, and MW distributions as measured by field desorption/field ionization low-resolution mass spectrometry (FD/FI LRMS).²³ It is known that heteroatom concentration gradually and continuously increases as a function of increasing petroleum boiling point. Indeed, distillation residues and asphaltenes contain the highest heteroatom content. Moreover, FD/FI LRMS results suggested that the average MW increased, and the MW range broadened concurrently with increased boiling point. For a given distillation cut, bulk compositional trends suggested that species with a lower MW must have a higher number of aromatic rings or heteroatoms to remain within the same boiling point range. Thus, stronger intermolecular interactions, such as π -stacking and hydrogen bonding, are offset by lower carbon content. Boduszynski hypothesized that distillation residues, enriched in asphaltenes, had a high boiling point, not because of continuously increasing MW, but instead due to increased heteroatom content and increased hydrogen deficiency (aromaticity) that result in stronger intermolecular interactions. Boduszynski concluded that asphaltenes, among other compound families present in distillation residues (e.g., resins, tetracarboxylic acids), could exhibit several heteroatoms per molecule, resulting in multiple intermolecular interactions that considerably impact properties such as solubility, aggregation, and boiling point. Many of the early Boduszynski's hypotheses were recently confirmed through molecular-level characterization of petroleum by Fourier transform ion cyclotron resonance mass spectrometry (FT-ICR MS).^{4,24}

Molecular Features Responsible for the Solubility Behavior of Asphaltenes. In routine analyses, petroleum is fractionated into heptane (nC_7) insolubles (*asphaltenes*) and nC_7 solubles (*maltenes*). Maltenes are further separated by liquid chromatography with silica/alumina into saturates (hexane-eluted), aromatics (hexane/toluene-eluted), and resins (dichloromethane/methanol-eluted). In other words, resins are the “polar” petroleum fraction soluble in nC_7 .^{25,26}

Therefore, understanding the compositional differences between asphaltenes and resins, two “polar” fractions of petroleum, could shed some light on the reason behind their different solubility behavior.

Speight et al.^{22,27} studied crude oil resins and asphaltenes from several geological origins by bulk elemental analysis, ¹H nuclear magnetic resonance (NMR), and GPC. The authors concluded that the major differences were hydrogen deficiency and oxygen content. Resins revealed H:C ratios between ~ 1.38 and 1.69, whereas asphaltene ratios ranged between ~ 0.98 and 1.56. The oxygen concentration was ~ 3 -fold higher for asphaltenes. The authors hypothesized that asphaltenes were composed of several smaller interconnected aromatic units (archipelago structures), whereas resins were less polydisperse.

Boduszynski et al.²⁸ found that separation of distillation residues into fractions enriched with acids, bases (pyridinic nitrogen), neutral Lewis bases, aromatics, and saturates, without prior asphaltene removal, caused asphaltene aggregation behavior to “vanish”. For this reason, the authors published their work titled “Asphaltenes, Where Are You?”²⁸ The authors discovered that the MW of the individual fractions and their subsequently separated heptane insolubles, accessed by VPO, ranged between 1000 g/mol and 2300 g/mol. Conversely, nC_7 asphaltenes isolated from the whole residues, without prior removal of acids and bases, exhibited apparent MWs of >4000 g/mol. Thus, the authors hypothesized that acid/base interactions play a central role in asphaltene chemistry, as their samples were found to lose their intrinsic aggregation tendency once those functionalities were separated from each other. It is likely that such interactions are also present in petroleum resins; however, aggregation is not extensive, because resins are most likely monofunctional species or have a much lower proportion of functionalities than petroleum fractions with strong aggregation tendencies. Conversely, asphaltenes consist of molecules with several functionalities that promote stronger aggregation, because they can establish multiple intermolecular interactions with two or more neighboring molecules.

Based on the theoretical foundations of petroleum solubility, largely developed by Hildebrand and Scott,^{29,30} Boduszynski and co-workers concluded that asphaltene insolubility in heptane is dictated by the synergistic effect between (1) hydrogen bonding resulting from increased heteroatom content, (2) dipolar interactions between aromatic rings and heteroatom-containing groups, and (3) molecular size. Boduszynski et al.^{28,31–34} also hypothesized the existence of nC_7 -insoluble species with high heteroatom content, low molecular weight (<1900 g/mol), and low aromaticity. Therefore, hydrogen bonding and π -stacking were both suggested to be critical in asphaltene solubility, whereas MW did not seem as crucial. The authors also hypothesized an additional factor for the solubility behavior: the existence of multiple “polar” functionalities per asphaltene molecule. Even in the presence of solvents in which asphaltenes are arguably highly soluble, such “multifunctional” species can exhibit both intermolecular (aggregation) and intramolecular (cross-linking) interactions, decreasing their solubility. Boduszynski's ideas regarding asphaltenes as low MW species were later supported by other techniques that indicated the presence of significant concentrations of low-molecular weight compounds, such as time-resolved fluorescence depolarization and mass spectrometry assisted by soft ionization. These methods, along with the dependence of apparent molecular weight with

concentration by vapor-pressure osmometry, converged on a monomeric MW range between ~ 250 g/mol and 1200 g/mol, with an average of ~ 700 g/mol.^{35–39}

Asphaltene Molecular Structure. Recent advances for single-molecule atomic force microscopy (AFM) have enabled the direct imaging of hundreds of molecules present in asphaltene samples.^{40,41} The results suggest that single-core motifs (island) are dominant (>90%). Only a few multicore structures (archipelago), with only aryl–aryl linkages between the cores, were identified in UG8 and shale oil bitumen asphaltenes. Regardless of the intrinsic bias toward the selective detection of quasi-planar—and, thus, single-core—molecules,⁴² AFM has strengthened the notion of the dominance of single-core structures in coal and petroleum asphaltenes. It is important to highlight that, in AFM, the sample undergoes sublimation under ultrahigh vacuum via rapid resistive heating up to ~ 1000 K; thus, individual molecules are evaporated and deposited onto a cold Cu(111) surface held at 10 K. Molecular imaging by AFM has revealed abundant island-type molecules, with predominant H:C ratios below ~ 0.70 , which is much lower than the values reported by combustion elemental analyses and FT-ICR MS.^{40,41,43} Furthermore, as mentioned above, a few multicore molecules have been detected but the bridges between the aromatic cores were noted as aryl–aryl linkages,⁴⁰ or short alkyl chains (C_1 – C_3) in the case of petroleum pitch.⁴⁴ In a separate study, the authors reported that simple archipelago model compounds, with both short (C_2) and long alkyl bridges (C_{20}), can be successfully deposited and detected by AFM.⁴⁵ Note that the analyzed model compounds are too simple and do not represent the molecular complexity of asphaltenes, and future advances likely require the synthesis and characterization of more “complex” mixtures of molecules involving island/archipelago structures, multiple heteroatom-containing functionalities, and naphthenic moieties, which should present a strong aggregation behavior consistent with petroleum asphaltenes.⁴⁶ Moreover, it is important to highlight that, in the analysis of real petroleum samples, such as unprocessed bitumen, a significant fraction of the imaged asphaltene molecules were not assigned an exact structure, because of the nonplanarity of the detected species.⁴¹ The fact that AFM is limited to planar molecules is well-documented. For instance, Zhang et al.⁴⁷ investigated the molecular structure of petroleum porphyrins by AFM molecular imaging. The authors reported difficulties in the access of the structures as vanadyl porphyrins exhibit a pronounced repulsive feature in the center, because of the pyramidal geometry of the vanadyl group.

Generally, AFM molecular imaging results support the dominance of island structures, which is consistent with the modified Yen model,⁴⁸ based on the work of Groenzin and Mullins on time-resolved fluorescence depolarization (TRFD).^{5,49} The authors concluded that island model compounds and asphaltenes exhibit similar rotational diffusion rates in TRFD. Conversely, archipelago model structures exhibit a different trend; although that claim was not validated by measurements on known/reported archipelago model compounds; it was concluded that asphaltenes consist of *mostly* island structures. Thus, the predominant structural motif in asphaltenes is a “single, moderate-sized polycyclic aromatic hydrocarbon (PAH) ring system with peripheral alkane substituents”.⁴⁸ Specific structural features include a prevalent ring number of ~ 7 , and heteroatoms, often present

within the core, lead to dipole–dipole interactions. Thus, asphaltene molecules aggregate via π -stacking; other forces, such as acid/base interactions and hydrogen bonding, are excluded from the modified Yen model.^{12,48,50}

The Reason Behind Asphaltene Structural Debate.

The controversy around the asphaltene structure is rooted in the molecular composition of the products from thermal cracking or catalytic hydroconversion of asphaltenes. Both theory and experiments on model compounds show that thermal cracking of large and pericondensed single-core molecules, such as the structure shown in Figure 1a, would

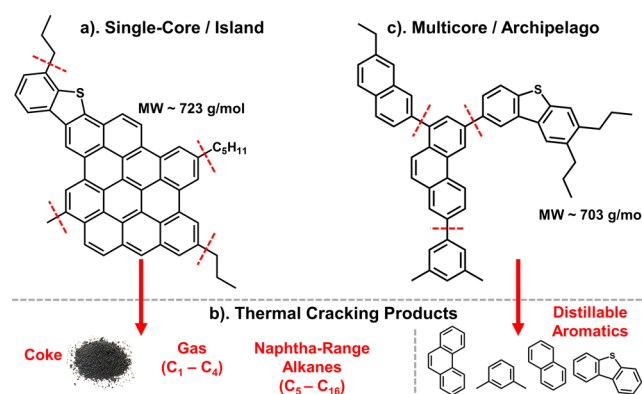


Figure 1. Proposed structures for petroleum asphaltenes: (a) a single-core or island motif; (b) thermal cracking products from asphaltenes, including coke, C_{1-4} gas, naphtha-range alkanes, and alkyl-substituted polycyclic aromatic hydrocarbons (PAHs); and (c) a multicore or archipelago structure. The production of alkyl-substituted small PAHs upon thermal cracking is inconsistent with the notion that single-core molecules are dominant in petroleum asphaltenes.

preferentially produce coke from the core, and gas (C_1 – C_4) and naphtha-range alkanes (C_5 – C_{16}) from the alkyl-side chains, as illustrated by the red lines.^{51–57} However, it is well-known that asphaltenes also produce significant yields of distillable alkyl-substituted 1–4 ring aromatics, such as alkyl benzene, naphthalene, phenanthrene, and dibenzothiophene (Figure 1b), upon thermal processing. These products are unique to multicore motifs, in which there is more than one aromatic core linked by covalent bridges.^{58–61} Those structures, also known as *archipelago* (Figure 1b), can “crack” between the aromatic cores upon thermal processing (red lines) to produce small/alkyl-substituted PAHs.⁵⁸ The nature of the “archipelago bridges” is another subject of discussion and has been suggested to exist as one single bond (aryl–aryl),⁴⁰ linear alkyl chain,^{52,62,63} or multiple bonds, as in naphthenic rings.⁶⁴ It has been suggested that aryl–aryl linkages do not dissociate in thermal cracking or gas-phase fragmentation, and they could thus be considered as similar to single-core structures.⁶⁵ However, molecular fragmentation is dependent on structure. For instance, rubrene, which is a four-core aromatic molecule with four additional phenyl groups connected by aryl linkages, readily cracks in tandem-MS to lose two of the pendent phenyl units.⁶⁶

Several authors attempted to tackle the structural interrogation of asphaltenes via organic reactions and mild thermal cracking, and early results suggested coexistence of island and archipelago structural motifs. For instance, Strausz et al.^{67,68} used ruthenium-ion-catalyzed oxidation (RICO) and thermal cracking to access asphaltene structures for oils such as Boscan,

Athabasca bitumen, and Cold Lake. The authors concluded the existence of multicore motifs with covalent bridges consisting of aryl–aryl linkages and alkyl chains, sometimes with oxygen and sulfur as ether and sulfide functionalities.⁶² They also found evidence for abundant naphthenic carbon in several asphaltene samples. In another work, Strausz et al.⁶⁸ used Ni₂Br reduction to target sulfide bonds in Athabasca bitumen asphaltenes. The authors concluded that asphaltenes produced 5–18 wt % of alkane solubles (maltenes). The saturate fraction from the soluble products revealed an abundant content of biomarkers such as steranes and hopanes, which were believed to consist of pendant groups in asphaltenes.⁶⁸ Thus, archipelago molecules were proposed to coexist with island motifs. However, the proposed structures featured a molecular weight (6239 g/mol) that exceeded the currently accepted range (~250–1200 g/mol), because it was determined by VPO and GPC, which are susceptible to large MW errors, because of aggregation.⁶⁹ Strausz et al.⁷⁰ emphasized that mild thermal cracking (~430 °C) of highly condensed aromatic structures (e.g., coronene; see Figure 2a, left) would not

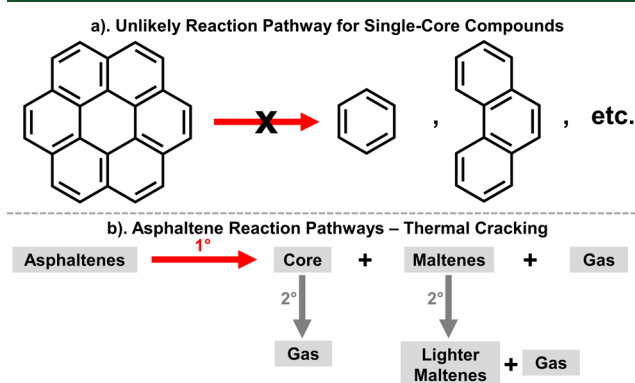


Figure 2. (a) Single-core structures such as coronene (7-ring) are not suited to produce smaller PAHs such as benzene (1-ring) and phenanthrene (3-ring). [Reproduced with permission from ref 70. Copyright 1999, American Chemical Society, Washington, DC.] (b) Primary and secondary reactions in asphaltene thermal cracking. Primary reactions yield dealkylated aromatic cores (coke precursors), alkane-soluble species (naphtha-range alkanes and small alkyl-PAHs), and gas (H₂S, CO₂, C_{1–4} alkanes). Secondary reactions can potentially produce lighter maltenes and additional gas. [Reproduced with permission from ref 73. Copyright 1985, American Chemical Society, Washington, DC.]

produce lower-MW polycyclic aromatic hydrocarbons such as benzene and phenanthrene (Figure 2a, top right panel), which are commonly produced upon thermal cracking of asphaltenes. Instead, coronene would undergo condensation reactions to produce a coke-like material.⁷⁰

By a similar approach, Gray,⁵¹ Karimi,⁵² Nomura,⁷¹ and Schenck et al.⁷² confirmed structural features that converged with Strausz's view. Furthermore, in several works, Klein et al.^{73–76} highlighted the need for distinguishing between primary and secondary reactions in thermal cracking to determine product structural features. The authors proposed that primary reactions in low-temperature cracking of sulfide (R–S–R) and carboxylic acid (R–COOH) asphaltene moieties would yield H₂S and CO₂ gas. The subsequent increase in temperature would induce primary reactions that cause C–C bond cleavage, producing C_{1–4} gases and maltenic compounds comprised of cycloalkanes, C_{5–C}₁₆

paraffins, and 1–4 ring alkyl-substituted PAHs. In some instances, secondary reactions can yield lighter paraffins that arise from naphthenic C–C scission. Primary and secondary reactions are summarized in Figure 2b. The primary formation of toluene and xylenes at 400 °C indicates that single-ring aromatic moieties are likely bound to a larger asphaltene core, which supports the existence of multicore species.

Do Secondary Reactions “Undermine” Structural Conclusions from Thermal Cracking? Several reports reiterate that the composition of the products from asphaltene thermal cracking is unreliable evidence for the existence of multicore motifs.^{12,48,77–79} The reason is simple: secondary reactions occur in the bulk phase and lead to data misinterpretation. A report by Gray et al.⁸⁰ is often used, by Mullins et al.,^{48,77,79} to challenge thermal cracking/pyrolysis data. In Gray's work, island model compounds, such as the structure displayed in Figure 3a, were subjected to mild

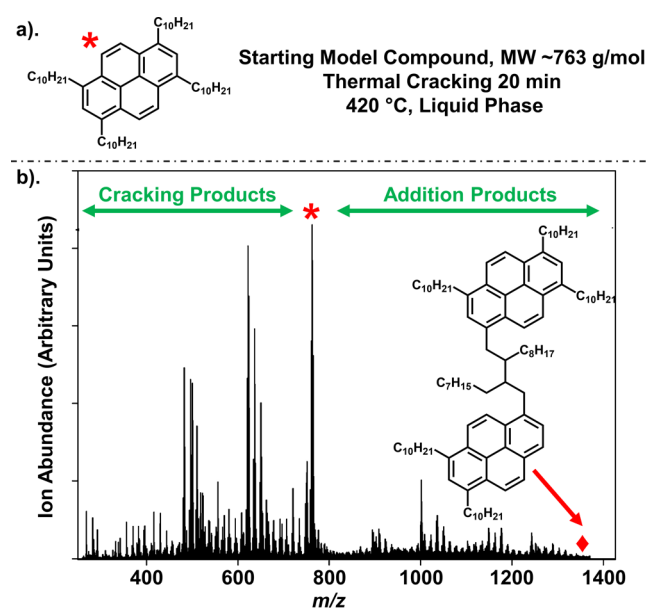


Figure 3. (a) Single-core model compound subjected to mild thermal cracking in liquid phase at 420 °C for 20 min; (b) MALDI TOF mass spectrum for the cracked products. The starting model compound (MW ≈ 763.31 g/mol) is highlighted with a red asterisk. Dealkylation ($m/z < 750$) and addition products ($m/z > 763$) are evident. NMR enabled the structural identification of some of the addition products. One example is highlighted with a red arrow and demonstrates that secondary reactions produce alkyl-bridged multicore motifs.⁸⁰ Gray et al. have hypothesized that geological conditions (temperature/pressure) during petroleum generation, similar to mild thermal cracking, could yield archipelago species. [Reproduced with permission from ref 80. Copyright 1985, American Chemical Society, Washington, DC.]

thermal cracking conditions in the liquid phase (420 °C, 20 min). The authors observed, via matrix-assisted laser desorption ionization (MALDI) MS, cracking products with lower molecular mass ($m/z < 750$) that resulted from the stepwise fragmentation of the alkyl side chains. The cracking products are evident in the mass spectrum in Figure 3b, because they present a lower MW than the starting model compound (highlighted with the red asterisk). However, ~40% of the products, as determined by MS, had a higher MW and were derived from addition reactions; some structures were determined by NMR (one is shown in Figure 3b, right side).

Therefore, addition reactions can yield multicore motifs. The authors concluded that alkyl side chains in island compounds are fragmented via free-radical reactions and yield intermediate compounds that contain olefinic moieties, which, in many cases, are adjacent to the aromatic cores. The high MW products result from secondary reactions in the liquid phase by free-radical addition to these olefinic moieties. The authors suggested an analogy between mild thermal cracking and the geochemical processes that yielded light petroleum compounds, and complex/heavier species, such as asphaltenes. It was concluded that addition reactions favored the generation of new alkyl-bridged archipelagos that can be readily fragmented in tandem MS studies.

Gas-Phase Fragmentation of Asphaltenes: Early Stages of Collision Induced Dissociation of Petroleum.

Concerns about the misinterpretation of thermal cracking data have been suggested, because side/secondary reactions potentially produce archipelago structures.⁷⁹ Instead, it has been proposed that gas-phase fragmentation is ideal for structural studies, because the intermolecular interactions and side reactions that occur in bulk phase (i.e., liquid phase, ≥ 760 Torr) are precluded in the gas phase (i.e., CID with helium, $\sim 10^{-3}$ Torr, or infrared multiphoton dissociation (IRMPD) performed at $< 10^{-10}$ Torr).⁴⁸ Structural studies performed at The National High Magnetic Field Laboratory (NHMFL) in 2007, via electrospray ionization coupled to CID with helium and FT-ICR MS, suggested that petroleum species with basic N-containing functionalities were comprised of single-core/island motifs.^{81,82} Figure 4a presents the isoabundance contour

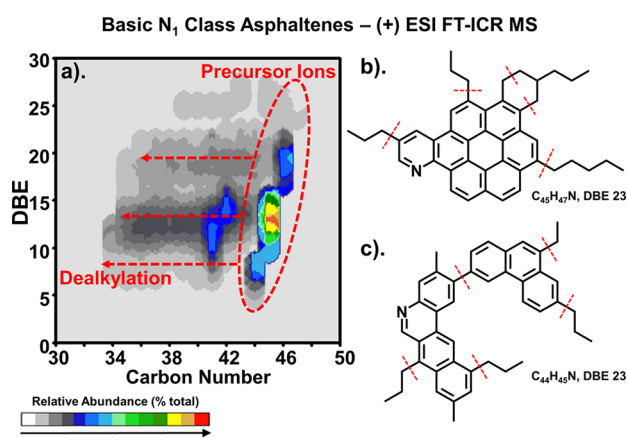


Figure 4. (a) Isoabundance-contoured plot of double bond equivalents (DBE = number of rings plus double bonds to carbon) versus carbon number for basic N₁ asphaltene precursor ions (red circles) and their CID fragments. (b) Single-core and (c) multicore model compounds and their possible fragmentation pathway (red dotted line) via CID. The “archipelago bridges” are represented as a single bond; however, there is debate about their nature and the possible existence of alkyl-chain/naphthenic bridges.^{81,82}

plot of double bond equivalents (DBE = number of rings plus double bonds to carbon) versus carbon number for precursor ions, selected through a quadrupole mass filter (circled in red), and their CID products. Figure 4a displays the common way of representing the molecular composition data derived from FT-ICR MS studies. In these plots, a higher DBE implies a higher aromaticity, and the color scale represents the relative abundance. The results demonstrate that the precursor ions have DBE values between ~ 4 and 27, which undergo

dealkylation because they only lose carbon number. The fragments remain in the DBE range of the precursor ions, as highlighted by the horizontal red arrows. This fragmentation pathway is consistent with single-core model compounds (Figure 4b), that decrease in carbon number due to dissociation of the alkyl-side chains but maintain the precursor DBE (aromaticity) because CID causes no fragmentation across the aromatic cores. Conversely, multicore model compounds (Figure 4c) can lose both carbon number and DBE; however, this fragmentation pathway is not clearly evident in the DBE vs carbon number plot of Figure 4. Given the wide DBE range of the precursor ions, it is not possible to conclude whether or not the high DBE precursors produce low DBE fragments, which is the basis to determine the existence of archipelago/multicore motifs. Thus, the results support an island asphaltene structural motif. However, these experiments were performed prior to understanding the importance of several methods that are critical for accurate asphaltene compositional/structural determination by mass spectrometry, namely extensive washing to remove coprecipitated maltenic material (as discussed below).

Limitations of Conventional Gas-Phase Fragmentation Studies. It is critical to highlight that structural/compositional studies of asphaltenes, performed in the 2000s at the NHMFL, suffered several limitations. First, the experiments were performed on whole/unfractionated asphaltene samples. Recent works have demonstrated that the characterization of whole asphaltenes is limited, because of the wide range of ionization efficiencies inherent to the myriad unique compounds present in asphaltenes (selective ionization).⁸³ Furthermore, positive-ion electrospray ionization [(+) ESI] was the ion source of choice; however, (+) ESI has been demonstrated to preferentially ionize those molecules with one or more basic functionalities but is unable to produce ions efficiently from species that lack basic groups. Importantly, asphaltenes are comprised of a high portion of aromatic hydrocarbons with no basic functionalities,^{84,85} and access to these species is improved by (+) atmospheric pressure photoionization (APPI), which has been employed more recently for asphaltene studies in our laboratory.^{36,66,86} Asphaltene MS analysis assisted by ESI is also limited by solvent conditions: usually a toluene/methanol ratio of 7:3 (v/v) with a modifier (e.g., formic acid) that facilitates protonation. Under these conditions, asphaltenes exhibit strong aggregation/precipitation issues, which decreases their ionization efficiency.

Second, the isolated precursor ions spanned a wide range of DBE values (~ 4 –27), which contradicts the “classical” view of asphaltene chemistry, based on the dominance of highly aromatic structures of ~ 7 -fused rings (DBE ~ 19 –21).⁴⁸ Given the wide DBE range of the precursor ions, it is impossible to determine if the high-DBE ions produce low-DBE fragments upon CID, or if exclusively, low-DBE precursors undergo dealkylation to produce low-DBE fragments.

Third, it is demonstrated that conventional CID with helium (low energy) does not usually provide the energy required for complete dissociation of covalent bonds in alkyl side chains of single-core compounds and alkyl/aryl bridges in multicore motifs. Nyadong et al.⁸⁷ demonstrated that accurate structural characterization of petroleum model compounds requires high-energy CID (HCD). The authors performed dissociation of island and archipelago model compounds by conventional CID and HCD. The experiments were performed under several

collision energies, adjusted to reach a final precursor relative abundance of 100%, 25%, and 0% after fragmentation. Figure 5

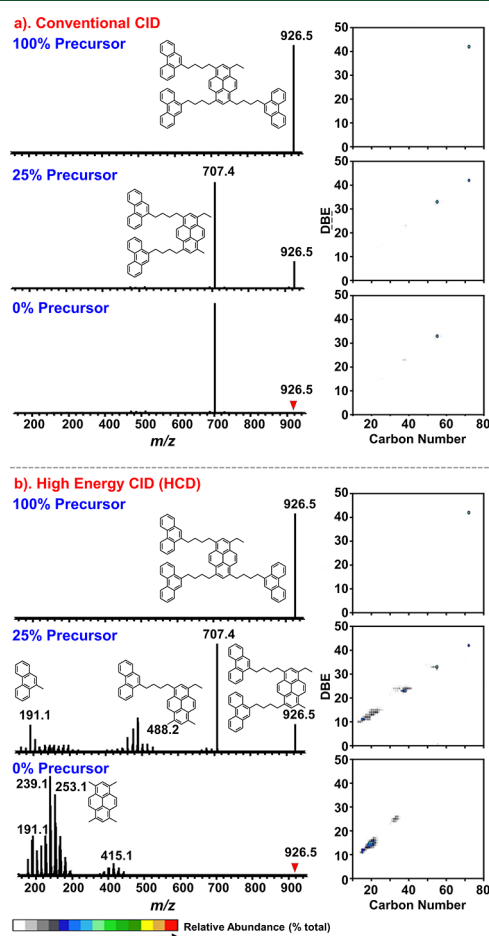


Figure 5. (a) CID and (b) HCD mass spectra and DBE versus carbon number plots for a 4-core archipelago model compound and its fragment products.⁸⁷ The results highlight the limited/partial fragmentation by CID, even for a precursor relative abundance of 0%, as only loss of one core, DBE = 10, is evident. Conversely, HCD enables complete fragmentation, producing abundant fragments with DBE values between 10 and 17. [Reproduced with permission from ref 87. Copyright 2018, American Chemical Society, Washington, DC.]

displays the mass spectra and DBE versus carbon number plots for precursor ions and fragments for an alkyl-bridged, four-core compound with DBE = 42. The results demonstrate that CID (Figure 5a) yields partial fragmentation: the highest collision energy (0% precursor remaining) yields an abundant fragment with DBE = 32. Conversely, HCD (Figure 5b) facilitates the total dissociation of the alkyl bridges, which produces abundant fragments with DBE values of 10 and 12, consistent with the aromaticity (DBE values) of the individual cores.

Recent Advances in Complex Mixture Analysis.

Recent works that employ exhaustive sample preparation, advanced precursor ion isolation, and infrared multiphoton dissociation coupled to (+) APPI FT-ICR MS demonstrate that asphaltene consist of a structural continuum of single-core and multicore compounds.^{66,88} The dominance of one structural motif over the other is sample-dependent and seems to correlate with asphaltene behavior in thermal cracking.⁸⁹ Despite the extensive evidence for the coexistence of island

and archipelago motifs in petroleum, including results for geologically diverse samples and model compounds, published by several research groups,^{64,66,87,90–92} questions have been raised about the possible misinterpretation of MS data. For instance, it has been suggested that asphaltene aggregation in atmospheric pressure ionization (e.g., ESI, APPI) could be the reason behind the detection of archipelago artifacts:⁷⁹ “the large (asphaltene) aggregate could be acting somewhat similar to bulk asphaltene; it is known that bulk decomposition of island model compounds can result in the synthesis of archipelago compounds.” In this scenario, concerns regarding MS data misinterpretation include, but are not limited to, the inability to determine if the precursor ions are asphaltene monomolecules (monomers) or aggregates. Thus, a concurrent loss of carbon number and DBE would hypothetically arise from the dissociation of asphaltene dimers, trimers, and tetramers, instead of covalent bond fragmentation.

In the following section, we review the principles of mass spectrometry applied to the compositional and structural characterization of ultracomplex mixtures. Sample ultracomplexity, selective ionization, and isolation of precursor ions for samples that feature a wide DBE range are addressed by ultrahigh-resolution mass spectrometry, sample fractionation, and advanced precursor ion isolation, followed by fragmentation under ultrahigh vacuum (no/extremely low possibility for addition-type reactions). We present a comprehensive series of controlled experiments to demonstrate that selective ionization is inherent to petroleum ultracomplexity, and compositional changes upon gas-phase fragmentation result from covalent bond cleavage rather than dissociation of asphaltene clusters/aggregates. Furthermore, an extensive literature search highlights that petroleum characterization by MS requires separations, because of the lack of an ion source capable of ionizing all petroleum compounds with no bias. The lessons learned during a decade-long assessment of asphaltene by FT-ICR MS can be applied to understand the molecular composition of other complex mixtures of environmental and energy interest, including weathered oil from spills,^{93,94} natural/dissolved organic matter,^{95,96} alternative fuels derived from thermal cracking of algae/wood/plastic materials,^{97,98} and organic aerosols.^{99,100}

■ A COMPREHENSIVE ANALYTICAL APPROACH TO UNDERSTAND ULTRACOMPLEX MIXTURES: THE ASPHALTENE CASE STUDY

Need for Ultrahigh-Resolution Mass Spectrometry.

Crude petroleum is perhaps the most complex natural mixture, and thus, its confident, precise mass spectral characterization demands ultrahigh mass accuracy and unprecedented resolving power. Among all petroleum fractions, asphaltene exhibit the highest hydrogen deficiency and heteroatom content, which dramatically increase their compositional complexity observed in mass spectrometry studies.¹⁰¹

As early as 1967, the need for high resolution to accomplish a comprehensive mass spectral characterization of high-boiling petroleum fractions was recognized. Teeter et al.¹⁰² reported the first multicomponent group-type analysis of high-boiling distillates by use of an electric sector/double-focusing mass spectrometer, with a resolving power of ~5000 at m/z 250. The authors recognized the limitations for resolving and identifying sulfur-containing compounds in fractions with a boiling point higher than 426 °C. They hypothesized that eventually, the development of mass analyzers with much

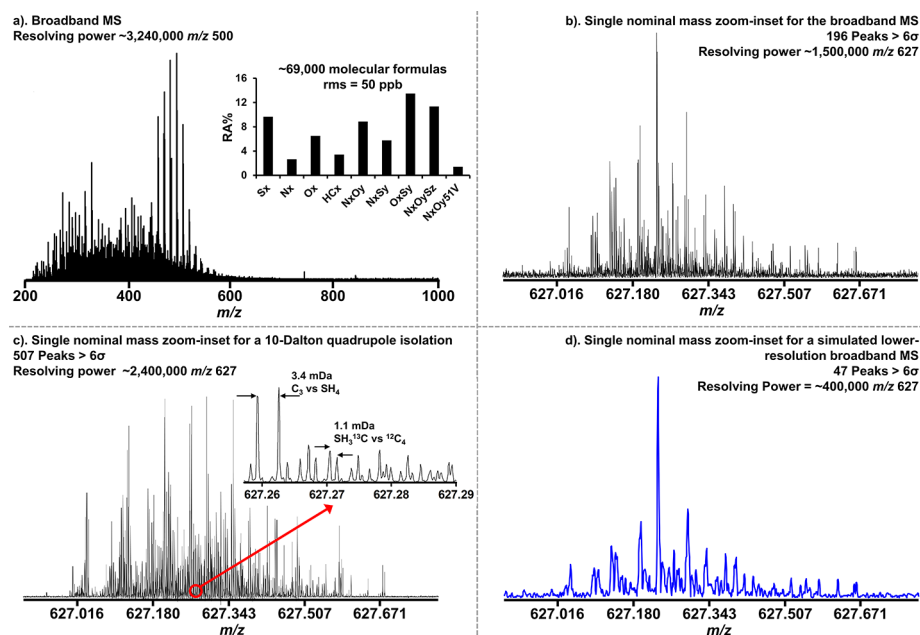


Figure 6. (a) Molecular weight distribution or broadband mass spectrum by (+) APPI 21 T FT-ICR MS of the interlaboratory sample known as PetroPhase 2017 asphaltene. The bar graph represents the heteroatom class distribution and suggests enrichment in S-containing compounds. (b) Inset showing an expanded view, relative to mass, from the broadband mass spectrum at a single nominal mass at m/z 627, which presents a remarkable spectral complexity with 196 peaks ($>6\sigma$). (c) Inset showing an expanded view, relative to mass, from a 10-Dalton quadrupole isolation. Segmented data collection enables the detection of ~ 2.6 -fold peaks; further zooming reveals abundant 1.1 mDa mass splits. (d) Simulated lower-resolution MS results, with a resolving power of $\sim 400\,000$ at m/z 627, much higher than LTQ, TOF, and conventional Orbitrap mass spectrometers, commonly used in asphaltene studies. The results suggest a dramatic decrease in the number of detected/resolved peaks.

higher resolution would reveal the totality of petroleum species, with no need for prior fractionation by silica gel chromatography or equivalent methods. In other words, at the time it was believed that ultrahigh-resolving power alone was the unique requirement for the complete MS characterization of petroleum.

In 1974, Marshall and Comisarow introduced FT-ICR MS,¹⁰³ which is the highest performance MS technique, in terms of resolution and mass accuracy.^{104,105} It was not until the late 1990s that high-field FT-ICR MS was used to access the molecular complexity of petroleum; the achieved resolution was $>100\,000$ at m/z 400. Rodgers and Marshall first reported that heavy petroleum was composed of heteroatom-containing (N, O, S) hydrocarbons with more than $\sim 20\,000$ unique molecular formulas ($C_xH_nN_mO_pS_q$).¹⁰⁶ The original studies performed at the NHMFL led to the term “Petroleomics”, coined by Dr. Carol L. Nilsson in a hallway conversation at the MagLab,⁴³ and first reported in 2003 in the Petroleum Chemistry Symposium led by Marshall and Rodgers at the Pittsburgh Conference on Analytical Chemistry and Applied Spectroscopy.¹⁰⁷ The authors emphasized that the key features that enabled the field of petroleomics were the unique capability of FT-ICR MS to resolve high m/z (>500) species that differ in elemental composition by, i.e., C_3 vs SH_4 (separated by 0.0034 Da) and $SH_3^{13}C$ vs $^{12}C_4$ (separated by 0.0011 Da).¹⁰⁸ Between 2005 and 2015, reports by Schrader,¹⁰⁹ Barrow,¹¹⁰ Witt,¹¹¹ Romão,¹¹² Shi,¹¹³ Zimmerman,¹¹⁴ Cho,¹¹⁵ Qian,¹¹⁶ and many other authors^{117–122} also demonstrated that any attempt to understand the elemental composition of individual petroleum molecules and their structure requires the ultrahigh resolving power exclusively offered by FT-ICR MS.

Arabian heavy asphaltene were first comprehensively analyzed via (+) APPI FT-ICR MS in 2013 by McKenna et al.¹²³ The authors defined the asphaltene compositional range and demonstrated the increased molecular complexity of asphaltene relative to maltenes. Asphaltene were shown to be enriched in compounds with higher DBE values (>20), consistent with the classical view of asphaltene chemistry. However, the average H:C ratios derived from (+) APPI FT-ICR MS ranged between 0.82 and 0.89,¹²³ far below the values typically found by combustion elemental analysis (~ 1.10).^{60,124,125} It was suspected that ionization bias was the reason behind the discrepancy, because APPI could disproportionately ionize highly aromatic species. Furthermore, it was hypothesized that aggregation could potentially remove compounds with higher H:C ratios. Thus, nonaggregated highly aromatic/alkyl-deficient species remain molecularly dispersed and are efficiently ionized by APPI and detected by FT-ICR MS analysis. Other studies by Rogel,^{126,127} Combariza,^{54,128} Cho,¹²⁹ and Zimmerman,¹³⁰ also demonstrate that mass spectrometric analysis of whole asphaltene samples enables the preferential detection of hydrogen-deficient molecules.

In 2017, TOTAL released the interlaboratory sample known as “PetroPhase 2017 Asphaltene”, prepared by the Combariza Group following a preparation procedure focused on decreasing the content of coprecipitated/occluded maltenic material.^{128,131} The cleaning process is pivotal to access asphaltene compounds by APPI, given the increased ionization efficiency of maltenes relative to asphaltene.⁶⁶ Figure 6a presents the molecular weight distribution of PetroPhase 2017 asphaltene accessed by (+) APPI 21 T FT-ICR MS.¹³² The achieved resolving power at m/z 500 was $\sim 3\,240\,000$; the

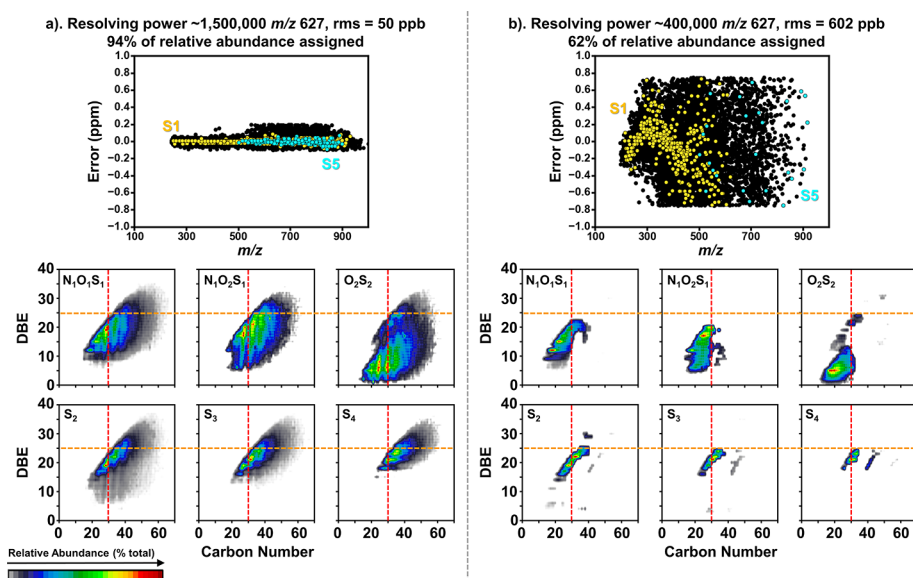


Figure 7. Error distribution for molecular formula assignments and DBE vs carbon number plots for selected sulfur-containing compounds for (a) ultrahigh-resolution MS characterization of PetroPhase 2017 asphaltenes [(+) APPI 21 T FTICR MS], and (b) simulated lower-resolution MS.

ultrahigh mass accuracy enabled the assignment of $\sim 65\,000$ unique molecular formulas with a root-mean-square (RMS) error of ~ 50 ppb. The assigned formulas can be sorted into heteroatom groups (e.g., the group S_x comprises the species with one [S_1 class], two [S_2 class], three [S_3 class], etc., S atoms). The bar graph in Figure 6a shows the heteroatom group distribution and suggests that PetroPhase 2017 asphaltenes contain abundant S-containing molecules (i.e., S_x , O_xS_y , $N_xO_yS_z$). Moreover, the results suggest that more than $\sim 90\%$ of the detected compounds contain at least one heteroatom and the prominent peaks between $m/z \sim 450$ – 650 correspond to vanadyl porphyrins (group $N_xO_yS_zV_1$). Figure 6b displays an expanded-view inset at a single nominal mass at m/z 627, which contains 196 peaks ($>6\sigma$) and resolving power of 1 500 000. The results were the first to highlight the remarkable molecular complexity of petroleum asphaltenes.¹³²

Mass Isolation Increases Resolving Power Requirements. The selection of ions prior to fragmentation methods such as CID, via a quadrupole mass filter, is necessary for structural analyses. PetroPhase 2017 asphaltenes were subjected to a 10 Da-wide quadrupole isolation (m/z 622–632). Figure 6c presents a single-nominal-mass zoom inset at m/z 627 for the isolation window. Approximately 2.6-fold more peaks were detected in the mass isolated region, proving that segmented data acquisition reveals increased sample complexity, as previously shown by Marshall¹³³ and Barrow et al.¹³⁴ A closer look at this nominal mass exposes several peaks separated by 1.1 mDa, which reveals the ultrahigh compositional complexity and confirms the need for remarkable instrument performance. The reason behind the significant increase in the number of detected peaks lies in the ion dynamics inside the ICR cell. The number of species trapped in an ICR cell is usually limited to roughly 10^6 charges to prevent distortion of orbiting ion packets, which leads to peak shifting, broadening, coalescence, and other phenomena that decrease instrument performance. In the FT-ICR MS analysis of a given sample that contains tens of thousands of different elemental compositions, the signals from many ions may fall below the signal-to-noise threshold for peak detection (6σ

RMS noise). When the ICR cell is filled with ions with narrower m/z ranges, the total ion current is shared by fewer species; thus, the signal-to-noise ratio is drastically improved, and the number of detected peaks per nominal mass increases. Therefore, the results demonstrate that structural studies demand much higher resolving power than routine broadband MS characterization. Figure 6d features simulated results for lower-resolution mass spectrometry. The simulated mass spectrum is obtained by truncating the time domain data points collected for the mass spectrum presented in Figure 6a. The resolving power for the simulated mass spectrum is $\sim 400\,000$ at m/z 627, which is much higher than the resolution achieved by linear trap quadrupole (LTQ), time-of-flight (TOF), and comparable to the highest performance, commercially available Orbitrap mass spectrometers, typically used in asphaltene studies that support the dominance of single-core motifs in petroleum.^{135–137} Figure 6d demonstrates that a resolution of $\sim 400\,000$ allows for the detection of only 47 peaks. Thus, conclusions derived from molecular and structural characterization via lower performance mass analyzers are likely incomplete. Below, it is demonstrated that ultrahigh-resolution MS is not the only requirement for the accurate understanding of complex mixtures; separations and advanced precursor ion isolation/fragmentation methods are also critical.

Figure 7 compares the molecular assignments achieved by ultrahigh-resolution MS (broadband 21 T FT-ICR MS, resolving power $\approx 1\,500\,000$ at m/z 627) and simulated lower-resolution MS of the same data (resolving power $\approx 400\,000$ at m/z 627). It is clear that HRMS (Figure 7a) enables a superior understanding of the molecular composition: the assigned species represent 94% of the ion abundance, and the error distribution is centered at ~ 0 ppm, with an RMS error of ~ 50 ppb. Conversely, simulated low-resolution MS (Figure 7b) accounts for only 62% of the assigned abundance, with a nonuniform error trend (across m/z) and an RMS error of ~ 602 ppb, which undermines the reliability of the data and decreases confidence in molecular formula assignments. Figure 7 also presents the DBE vs carbon number plots for sulfur-containing classes. The HRMS results (Figure 7a, bottom)

indicate that PetroPhase 2017 asphaltenes span a wide range of DBE values (~ 7 – 35), consistent with the presence of highly aromatic compounds (S_{3-4} classes) and “unexpected” low DBE $N_xO_yS_z/O_xS_y$ species. Clearly, low-resolution MS (Figure 7b, bottom) cannot access high-DBE (<25)/high carbon number compounds (<30). Thus, given the ultrahigh compositional complexity of petroleum asphaltenes, no definitive compositional/structural conclusions can be drawn from low-resolution MS studies.^{138,139} It is important to highlight that, in the early days of petroleomics, it was suggested that ultrahigh resolving power was the unique requirement to reveal the complete composition of heavy petroleum by MS.^{140,141} Below, it is demonstrated that the lack of a “universal” ion source, capable of unbiased ionization of the individual molecules within a complex mixture, makes the use of fractionation methods prior to MS analyses necessary.

The results summarized in Figure 7 demonstrate that the complex nature of asphaltenes necessitates the use of ultrahigh resolution mass spectrometry, or high-field FT-ICR MS, which provides high resolving power, mass accuracy, and sensitivity that enables insight into previously unseen asphaltene molecular features; however, the technique remains limited by selective ionization.

Selective Ionization. The lack of a “universal” ion source, capable of ionizing chemical mixtures without bias, demands separations to access the composition of complex mixtures. Advances in soft ionization methods, i.e., electrospray ionization (ESI), atmospheric pressure photoionization (APPI), atmospheric pressure chemical ionization (APCI), and matrix-assisted laser desorption/ionization (MALDI), developed between the 1980s and 2000s, have opened MS to nonvolatile and labile analytes such as proteins, carbohydrates, lipids, and heavy petroleum fractions, enabling the fields of, e.g., proteomics,¹⁴² glycomics,¹⁴³ lipidomics,¹⁴⁴ and petroleomics.¹⁰¹ Despite improved ionization methods, the characterization of complex mixtures is still limited by selective ionization, because there is not a commercially available ion source that can fully volatilize and ionize all compounds without bias. For instance, ESI enables the ion production for acidic/basic species, in which ionization efficiency relies, in part, on the specific acidity/basicity of the analytes.¹⁴⁵ Conversely, APPI facilitates the ionization of compounds with π electrons, such as polycyclic aromatic hydrocarbons with or without heteroatoms within the core structure.¹⁴⁶ On the other hand, APCI is better suited to ionize saturated hydrocarbons.^{139,147} It is important to point out that the amount and abundance of detected compounds in complex mixture MS characterization is not only affected by selective ionization. The sensitivity of the instrument (limitations in dynamic range) is also a shortcoming that has been investigated by segmented data acquisition, as reported by Marshall¹³³ and Barrow et al.¹³⁴

Evidence for Selective Ionization of Mixtures of Petroleum Model Compounds by Commercially Available Ion Sources. *Atmospheric Pressure Photoionization (APPI).* In APPI, liquid samples are vaporized by heated nebulizing gas, such as nitrogen. At atmospheric pressure, gas-phase neutrals are photoionized, usually by ~ 10 eV photons from a krypton lamp. The analyte molecules are ionized by two main pathways: direct photoionization, which produces radical cations ($M^+ \bullet$) or gas-phase reactions that lead to protonation/deprotonation ($[M+H]^+/[M-H]^-$). Purcell et al.¹⁴⁸ investigated the ionization of equimolar mixtures of pyridinic/

pyrrolic petroleum model compounds and found trends in ion abundance that suggested nonuniform ionization. The authors concluded that the most aromatic pyrrolic compound (a dibenzocarbazole derivative, 5-ring aromatic) was present at a higher ion abundance (radical cation) than carbazole (3-ring aromatic), which suggests that structures with a higher ring number can stabilize radical cations more efficiently, and thus, exhibit increased ionization efficiency in APPI. In another work, Kauppila et al.¹⁴⁹ tracked the ionization behavior of naphthalene model compounds substituted with a wide diversity of functional groups (e.g., ketone, carboxylic acid, phenol). The ionization energies (IEs) for all the studied molecules were much lower than that of the dopant (toluene), and, thus, it was expected unbiased ionization; instead, the authors found a correlation between ion abundance and analyte IE.

Electrospray Ionization (ESI). ESI is achieved by applying a strong electric field (~ 2.5 – 4.0 kV) to a liquid sample that flows through a capillary tube with, typically, a micrometric internal diameter. Ions are preformed in solution before their transfer to the gas phase. It is well-known that ESI selectively ionizes acidic or basic species as negative or positive ions; the ionization is improved by the use of a modifier (e.g., ammonium hydroxide or formic acid) that facilitates proton transfer reactions.¹⁵⁰ Kiontke et al.¹⁵¹ investigated the ionization trends of 56 nitrogen-containing model compounds by (+) ESI. The model mixtures included aromatic amines and pyridines. Over a wide pH range, the authors found a correlation between ion abundance and compound basicity. Moreover, the authors found that the boiling point and the vapor pressure of the model compounds disproportionately affected the ion abundance at acidic pH: the nonpolar/highly volatile species exhibited enhanced ionization as a function of decreased pH. In another study, Krueve et al.¹⁵² investigated the ion production, for (–) ESI, of mixtures of 63 model compounds containing phenol, carboxylic acid, and amide functionalities. The authors proposed an ionization efficiency predictive model dependent on molecular properties such as charge delocalization, polarizability, hydrogen bond acidity/basicity, and surface area.

Atmospheric Pressure Chemical Ionization (APCI). In APCI, liquid samples are vaporized by heated nebulization; gas-phase neutrals are then ionized by a corona discharge, which produces radical cations and protonated/deprotonated compounds. Rebane et al.¹⁵³ proposed an ionization efficiency scale for positive-ion APCI for a set of 40 model compounds, including pyridines, aromatic/aliphatic/heterocyclic amines, tetra-alkylammonium salts, and other species not easily ionized by ESI, such as saturated hydrocarbons. The authors concluded that polarizable compounds with high surface area and hydrophobic species have much higher ionization efficiencies in APCI.

Two-Step Laser Desorption Ionization Mass Spectrometry (L^2MS). It has been suggested that L^2MS is an ionization method with minimal or no bias in the ionization of mixtures of asphaltene model compounds and petroleum samples.^{154,155} According to the authors, the advantage of L^2MS lies in the temporal and spatial separation of the sample desorption and ionization steps. First, an infrared laser desorbs the sample and produces a low-density cloud of gas-phase neutrals. The authors have suggested that the desorption process involves rapid heating (10^8 °C/s), which suppresses covalent bond fragmentation. Second, a UV laser of 157 nm facilitates

nonresonant single-photon ionization, which has been suggested to be almost equally efficient for a wide range of model compounds and presents only up to a 4-fold variation in ion production efficiency.^{155–157}

The authors demonstrated with selected model compounds, caffeic acid and L-tryptophan, that single-photon ionization (SPI, 157 nm) L²MS is superior to multiphoton ionization L²MS (266 nm) and surface-assisted laser desorption ionization (SALDI), since SPI L²MS decreases fragmentation and prevents adducts and aggregates.¹⁵⁷ However, the results remain controversial for widely reported asphaltene model compounds. For instance, in the SPI L²MS analysis of an equimolar mixture of island model compounds, only 8 out of 13 species revealed the molecular ion (radical cation) or quasi-molecular ion (protonated molecules) with a relative abundance (peak area, PA) of 100%, which indicates the absence of fragmentation.^{65,137,157,158} The authors suggested that all the species were detected within a factor of 2 of ion abundance, which indicates almost uniform ionization. However, fragmentation issues were recognized: in cases where fragmentation occurred, the reported PA (or ion abundance) was calculated as the sum of the PA of the molecular/quasi-molecular ion peak plus the PA of its fragment peaks.⁶⁵ Furthermore, extensive fragmentation and decreased ion production were more prevalent for archipelago model compounds: none of the tested archipelagos revealed a 100% relative abundance for the molecular/quasi-molecular ion, and 4 out of 10 species presented a normalized ion abundance of <30%.

In another report, the authors suggested that SPI L²MS enables the detection of mixtures of asphaltenes and model compounds with almost equal sensitivity.¹⁵⁹ UG8 asphaltenes and a porphine model compound (Por 734) were mixed in a molar ratio of 2:1. Figure 8a presents the SPI L²MS spectrum of the mixture. The authors indicated that the normalized peak areas (bar graph to the right) demonstrate that asphaltenes and the standard compound were detected with almost equal sensitivity, with an abundance ratio of ~2.5:1, consistent with their concentration in the mixture. However, it is essential to highlight that these studies were performed with a time-of-flight (TOF) mass spectrometer, with a typical resolving power of ~5000–10 000 at m/z 400,¹⁶⁰ and thus, the calculated ion abundance for a particular analyte (Por 734), within a complex mixture (asphaltenes), is likely inaccurate.

It is widely documented that SPI L²MS supports the dominance of island motifs in petroleum asphaltenes.^{65,154,161} The authors have shown that the increase of the ionization laser power causes minimal or no fragmentation of island model compounds, whereas archipelago standards produce abundant fragments.¹⁵⁵ The authors have suggested that asphaltene samples have behavior consistent with island model compounds, because the increase of the ionization laser energy causes no variations in the detected MWD. However, Figure 8b reveals that BG5 asphaltenes produce a bimodal MWD in SPI L²MS (also evident in Figure 8a). The abundance of the low mass distribution (m/z ~150–400) increases concurrent with the ionization laser energy, which suggests abundant fragmentation. It is critical to note that 1–5-ring alkyl-substituted aromatics have molecular weights between m/z 150–400.¹⁶² Their production in Tandem-MS of highly aromatic asphaltene samples is possible only if archipelago motifs exist.

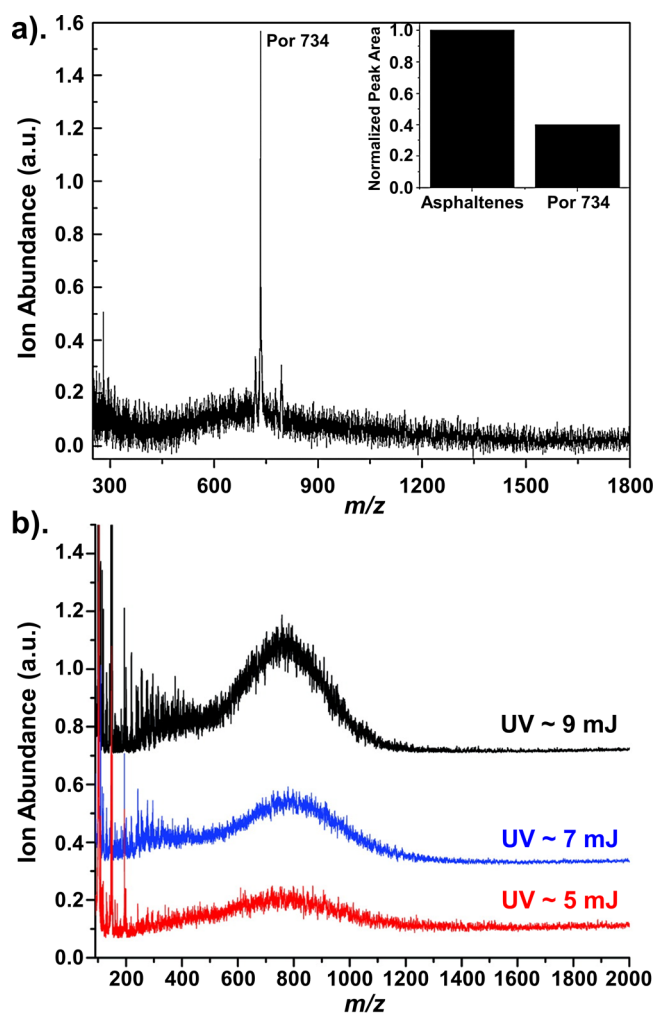


Figure 8. (a) SPI L²MS mass spectrum of crude oil asphaltenes mixed with a porphine model compound (Por 734) in a molar ratio of 2:1; the results include the normalized peak areas. [Reproduced with permission from ref 159. Copyright 2012, American Chemical Society, Washington, DC.] (b) L²MS spectra of BG5 asphaltene powder recorded at different ionization pulse energies. It has been suggested there is no change in MWD. [Reproduced with permission from ref 155. Copyright 2018, American Chemical Society, Washington, DC.]

Several reports indicate that the L²MS method involves single-photon ionization and, therefore, ion abundance linearly increases as a function of increasing laser energy,^{137,154} which is accurate in the absence of fragmentation. However, the results shown in Figure 8b, as well as other reports,^{157,158,163} suggest that the abundance for the low MWD has increases faster than linear (“superlinear”), which indicates that ionization is not the only cause for the observed ion abundance trends. This result is strong evidence for fragmentation: it is likely that singly charged high- m/z molecular ions yield fragments with remarkably similar (if not isobaric) masses, resulting in the superlinear ion signal increase. In other words, the low- m/z fragment ions may be generated from multiple precursors. Moreover, readers should consider that 157-nm lasers are routinely used to fragment ions (ultraviolet photon dissociation, UVPD), and there is insufficient experimental evidence to prove that these lasers do not cause fragmentation in L²MS of complex mixtures. The per photon energy of the

157-nm laser exceeds the energy required for bond dissociation of nearly all common diatomic bonds (C–C, C–N, C–O, etc.), which is the entire basis of UVPD in modern mass spectrometry. Whether there is enough energy post-ionization to induce bond dissociation in L²MS remains an open question. However, the reported results indicate that the excess of energy is enough to cause fragmentation, which has been admitted for multicore model compounds.^{65,137,157,158}

The Ionization Method of Choice for Heavy Petroleum and Asphaltenes. It is evident that simple mixtures of model compounds (<100 components) suffer selective ionization when analyzed by the most common commercially available ionization methods. Furthermore, custom-built ion sources, such as L²MS, are also affected by biased ionization and can produce fragmentation of archipelago motifs. Hyphenation of the ion sources does not overcome selective ionization. For instance, Kondyli et al.¹⁶⁴ combined ESI/APPI, ESI/APCI, and APPI/APCI for the MS analysis of a light crude oil. For ESI combinations, the authors directed the ESI spray into the UV photon beam of the APPI lamp or the corona discharge of the APCI source. The authors found that hyphenating different ionization methods can lead to higher ion suppression effects or no significant increase in the number of the detected species.¹⁶⁴

Therefore, it is essential to select an ionization method for optimal access to heavy petroleum and asphaltene samples. Huba et al.¹⁶⁵ investigated the ionization behavior of a wide range of petroleum standards (e.g., naphthenic acids, 2–7 ring PAHs, nitrogen/sulfur-containing PAHs, furans, phenols) by positive/negative ion APPI, ESI, and APCI. The authors concluded that APPI revealed lower ion suppression effects than ESI and APCI and allowed the ionization of the broadest range of model compounds. Furthermore, characterization of asphaltene model compounds by (+) APPI 9.4 T FT-ICR MS revealed that single- and multicore compounds are not fragmented during the desorption and ionization steps.⁶⁶ Therefore, the majority of asphaltene studies and control experiments discussed below are based on APPI. However, it is important to consider that the boiling-point upper limit for APPI is unknown, but is hypothesized to be >1300 °F.

First, it is critical to review the general instrumental components of the 9.4 T FT-ICR mass spectrometer routinely used at the NHMFL to characterize heavy petroleum and asphaltenes. The general configuration of the mass spectrometer is shown in Figure 9.¹⁶⁶ After ionization, the ions are transported from atmosphere to vacuum through a heated metal capillary (HMC) to a tube lens/skimmer, after which they are collected by a quadrupole ion guide (quadrupole 1). A mass-selective quadrupole is placed between quadrupole 1 and an accumulation octopole, so that mass selection can be performed outside the ICR cell. The accumulation octopole has tilted wire electrodes to improve ion ejection, and an auxiliary radio-frequency electric field is applied to minimize TOF mass discrimination ion transfer to the ICR cell. Quadrupole ion guides (transfer quadrupoles) transfer ions through the magnetic field gradient to a custom-built dynamically harmonized 9.4 T ICR cell,¹⁶⁷ which, for absorption mode broadband mass spectra, enables a routine resolving power of ~1 700 000 at m/z 400 and ~1 100 000 at m/z 627.

Infrared multiphoton dissociation (IRMPD) is performed once the ions are trapped in the ICR cell (<10⁻¹⁰ Torr); IRMPD is performed via irradiation with a CO₂ laser (λ = 10.6

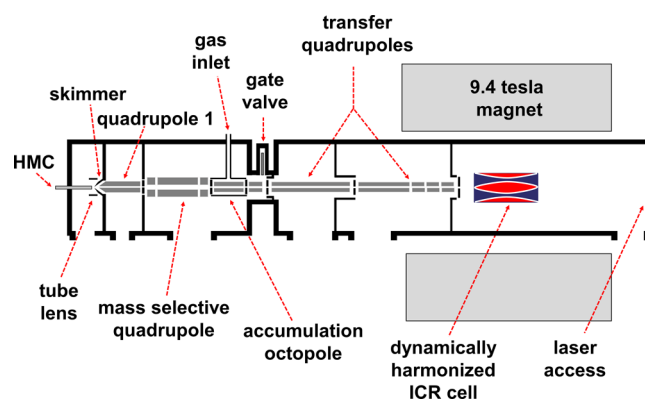


Figure 9. General configuration of the 9.4 T FT-ICR mass spectrometer routinely used for heavy petroleum characterization at the National High Magnetic Field Laboratory.

μm). Ion excitation and detection are performed with the same electrodes, with an angular extent of 120°. High mass resolving power, mass accuracy, and sensitivity are ensured by selectively signal-averaging mass spectra with approximately the same number of ions. This process is accomplished by calculation of the total ion current across a desired m/z range, and signal-averaging only those values that fall within a predetermined optimal range.

The accumulation octopole serves as an ion trap; it can be filled with ions for accumulation periods ranging between 5 and 20 000 ms. Samples that ionize efficiently by positive-ion APPI, e.g., aromatic petroleum fractions, PAHs, and purified vanadyl porphyrins, require accumulation periods between ~1–10 ms to reach a target ion number optimal for data collection. Conversely, samples with limited ionization such as vacuum residues and asphaltenes may require ~100-fold longer accumulation periods, even as high as 10 000 ms for some samples. Thus, the accumulation period reflects the ion production efficiency for monomeric ions (petroleum “monomolecules”/nonaggregated species) produced via APPI, and detected by FT-ICR MS. It is important to highlight that mass spectrometry detection, in the asphaltene NHMFL’s studies, is tuned between m/z 90 and m/z 1500, and the extent of production of “charged aggregates”, with much higher molecular weights, is unknown. Thus, to facilitate comparison of samples, monomer ion yield (MIY) was defined as a parameter inversely proportional to the accumulation period (eq 1), in milliseconds (ms), required to reach an optimal number of ions.

$$\text{MIY} = \frac{1}{\text{accumulation period (ms)}} \times 1000 \quad (1)$$

MIY is proposed as a measure of the production efficiency of nonaggregated asphaltene ions (“monomers”) in APPI as detected by mass spectrometry. The concept is not related to ionization cross-section,¹³⁷ which, in mass spectrometry, is frequently used to describe an area through which electrons must travel to efficiently interact with gas-phase neutrals and cause ionization (as in electron impact ionization). Instead, monomer ion yield is an indirect measure of the amount of monomeric charged species produced by APPI.⁶⁶ Current studies are focused on using automatic gain control (AGC) to normalize MIY measures for a wide set of asphaltene samples and petroleum fractions.

Selective Ionization of Petroleum Solubility Fractions by (+) APPI. Figure 10a presents isoabundance contour plots of

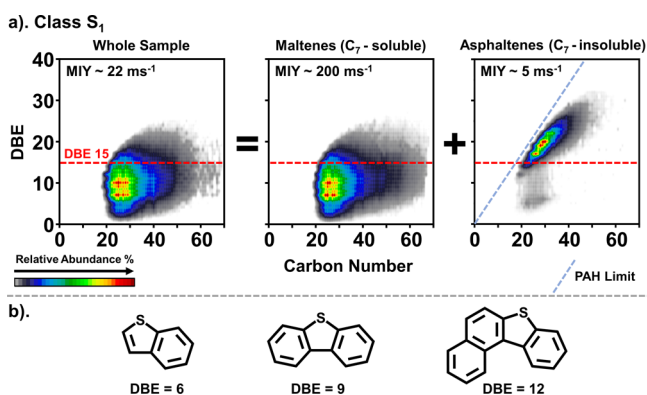


Figure 10. (a) Isoabundance color-contoured plots of DBE (DBE = number of rings plus double bonds to carbon) vs carbon number for the S_1 class derived from (+) APPI 9.4 T FT-ICR MS analyses of a South American vacuum residue and its maltene (~ 58.0 wt %) and asphaltene (~ 42.0 wt %) fractions. The entire vacuum residue is the sum of maltenes and asphaltenes. Monomer ion yield (MIY) values are included. (b) Likely structures for S_1 stable aromatic cores.

DBE vs carbon number for the S_1 class, derived from the (+) APPI 9.4 T FT-ICR MS characterization of a whole vacuum residue (left), and its heptane-soluble (middle)/heptane-insoluble (right) fractions. The plots highlight the monomer ion yield (MIY) for the three samples. Importantly, the whole vacuum residue contains a high concentration of asphaltenes (heptane-insoluble material, ~ 42.0 wt %). The entire sample (left plot) reveals a compositional range with abundant S_1 compounds with DBE values below 15 and carbon numbers between 20 and 60. The presence of abundant homologous series with DBEs of 6, 9, and 12 suggest the dominance of geologically stable core structures such as alkyl-substituted benzothiophenes, dibenzothiophenes, and benzonaphthothiophenes (structures shown in Figure 10b). Homologous series with intermediate DBE values (e.g., 7, 10) likely have peripheral cycloalkyl groups. The separation of the sample by solubility in heptane yields maltenes (nC_7 -soluble) and asphaltenes (nC_7 -insoluble), which exposes dramatic molecular-level differences. Specifically, maltenes resemble the compositional range of the entire sample and require a shorter accumulation period (5 ms, $MIY \approx 200 \text{ ms}^{-1}$) to reach the target ion number optimal for data collection. For comparison, the entire vacuum residue required an accumulation period of 45 ms ($MIY \approx 22 \text{ ms}^{-1}$). In contrast, asphaltenes, which consist of ~ 42 wt % of the entire sample, reveal a complementary compositional range to maltenes: with a similar carbon number range but a high relative abundance of species with DBE > 15 that are clustered close to the polycyclic aromatic hydrocarbon (PAH) limit. This compositional boundary (PAH limit) represents the highest possible DBE value, at a given carbon number, for planar/near planar petroleum molecules.^{168–170} DBE values above this limit contain nonplanar aromatic cores (fullerene-like compounds) that are most likely absent in naturally occurring petroleum.^{171,172} The analyzed asphaltenes required an accumulation period ~ 40 -fold longer than for maltenes (200 ms, $MIY \approx 5 \text{ ms}^{-1}$); therefore, the characterization of the entire sample preferentially reveals maltenic compounds (despite containing

~ 42 wt % asphaltenes), because asphaltenes are more difficult to ionize by APPI.

Asphaltenes are not the only compound family that exhibits a disproportional bias in ionization. Carboxylic acids, pyridinic nitrogen-containing species, and interfacial material, among other petroleum fractions, also exhibit a wide range of ionization efficiencies that limit their mass spectral characterization via ESI and APPI. For instance, Rowland et al.¹⁷³ developed a solid-phase extraction to extend the characterization of petroleum carboxylic acids by (–) ESI FT-ICR MS, because of selective ionization of low-molecular-weight acids. The separation is based on the strong adsorption of carboxylic acids on aminopropyl silica gel ($\text{SiO}_2\text{-C}_3\text{-NH}_2$). After the elution of nonacidic compounds, the acids are extracted with an elutropic gradient starting with a hydrophilic solvent mixture (MeOH/ H_2O) spiked with formic acid. The hydrophobicity is increased by sequential addition of dichloromethane, enabling the stepwise elution of acidic species with a higher content of carbon atoms (increasing molecular weight). The authors demonstrated that when acids are desorbed in a single step, without fractionation by hydrophobicity, the molecular composition, as revealed by FT-ICR MS, suggests the dominance of acids with carbon numbers between 20 and 50 and DBE < 15 . Conversely, when the acids are sequentially eluted by hydrophobicity, it is possible to access compounds with carbon numbers up to 90 and DBE up to 23. Along similar lines, Romão et al.¹⁷⁴ reported the fractionation of pyridinic nitrogen-containing species based on their adsorption onto an acidic stationary phase and elution with a hydrophobicity gradient. In another work, Clingenpeel et al.¹⁷⁵ extracted the interfacial material (IM) from bitumen oil and concluded that FT-ICR MS characterization of the acidic compounds of the entire IM sample preferentially revealed monocarboxylic acids with carbon numbers < 40 and DBE < 15 , whereas fractionation by hydrophobicity exposed both monocarboxylic and dicarboxylic species with up to 70 carbon atoms and DBE ≈ 25 .

Selective Ionization within Asphaltene Samples. Figure 11 presents the combined compositional range for all compound classes for exhaustively cleaned nC_7 asphaltenes isolated from several oils:¹³¹ South American medium/heavy, Venezuelan heavy, Maya (Gulf of Mexico), Wyoming Deposit (Wyoming, USA), Arabian heavy, and Athabasca/Mackay bitumen oils. The data are derived from (+) APPI 9.4 T FT-ICR MS characterization. The left plots in each panel present the compositional range in terms of DBE vs carbon number, whereas the graphs to the right display H:C ratio vs carbon number. In both types of plots, the color scale represents the relative abundance, which is normalized separately for each sample.

The modified Yen model contends that petroleum asphaltenes consist of highly aromatic/alkyl-deficient compounds, with an average ring number of ~ 7 , which is equivalent to DBE ~ 20 (highlighted by a black dashed line in the DBE plots) and consistent with the structure shown in Figure 11 (left panel, lower side).^{48,176,177} Coronene, a 7-ring structure with DBE = 19, is also included for reference in the DBE vs carbon number plot for Wyoming deposit asphaltenes. The results indicate that asphaltene samples are composed of both low and high DBE species. Out of eight samples, only South American medium and Wyoming Deposit asphaltenes present a compositional range uniquely dominated by compounds that feature high DBE (> 19) and limited alkyl

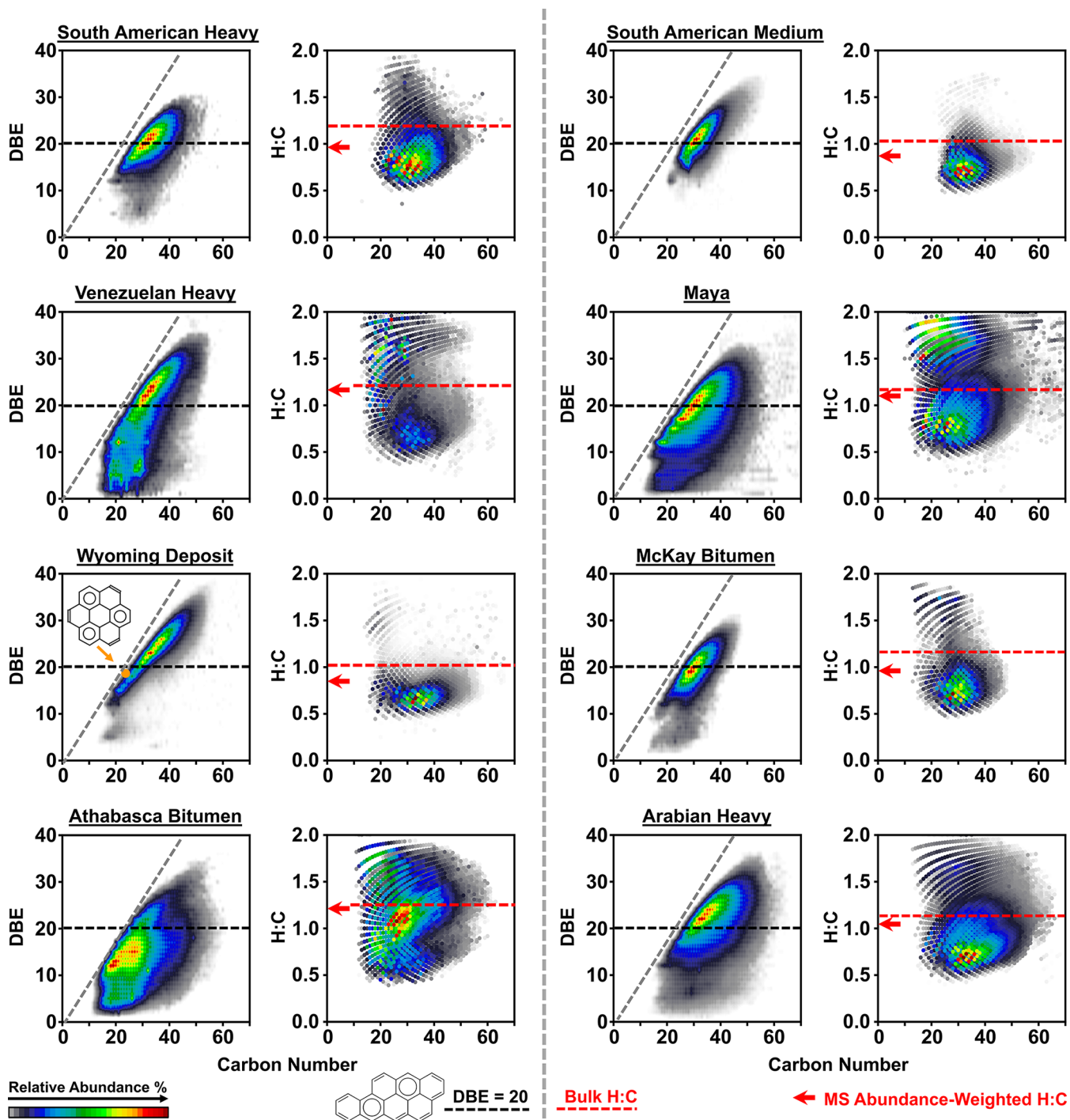


Figure 11. Combined compositional range for the most abundant compound classes ($RA > 0.15\%$) for nC_7 asphaltenes from different geological origins. Vanadyl porphyrins ($N_4O_1V_1$ class) were excluded from the graphs. In each panel, the plots on the left present the DBE and carbon number. The graphs to the right feature the H:C ratios; abundance-weighted (MS-derived), and bulk H:C ratios (combustion elemental analysis) are highlighted by a red arrow and a red dashed line.

substitution, which is evident by the presence of short homologous series (species with equal DBE but varying content of CH_2 units). The remaining samples, in particular Maya, Athabasca bitumen, and Venezuelan heavy asphaltenes, present abundant low-DBE compounds that are inconsistent with the “classical” view of asphaltene composition. Such high-quality, highly sample-dependent asphaltene mass spectra are currently routine and are in stark contrast to those obtained in past analyses. Thus, it is important to note that these

asphaltene samples were exhaustively extracted with nC_7 to decrease the concentration of occluded/coprecipitated maltenes (now standard practice), which is crucial for the detection of asphaltenes by APPI-MS.¹³¹

Regardless of the presence of “atypical” compounds with low aromaticity, all asphaltene samples present a high relative abundance of molecules clustered close to the PAH limit (gray dashed line), which suggests abundant species with a high hydrogen deficiency. Figure 11 (plots to the right in each

panel) also presents the abundance weighted (AW) H:C ratios determined by mass spectrometry (red arrows) and the H:C ratios derived from combustion elemental analysis (red dashed lines). The AW H:C ratios derived from mass spectrometry are calculated by eq 2, in which $H:C_i$ is the H:C ratio for each detected ion, RA_i is the abundance for which it was detected, and RA is the sum of the abundances for all detected ions.

$$AW\ H:C = \frac{\sum_{i=1}^n H:C_i \times RA_i}{\sum_{i=1}^n RA} \quad (2)$$

From FT-ICR MS data, it is also possible to obtain the abundance-weighted carbon number, DBE, and other atomic ratios. Generally, the results indicate that MS-derived H:C ratios are significantly lower than bulk values. For instance, South American heavy asphaltene have a bulk H:C ratio of ~ 1.18 , whereas the MS-derived value is ~ 0.98 . The difference is also evident for Wyoming deposit asphaltene, with a bulk H:C ratio of 1.03 and a MS-derived value of 0.79. Other samples such as Athabasca bitumen and Venezuelan heavy asphaltene feature small differences between bulk and MS-derived results. Generally, the discrepancy for the H:C ratios suggests selective ionization of hydrogen-deficient compounds in APPI, as reported by McKenna et al.¹²³

The use of an alternate ion source, such as L²MS, does not appear to solve such hydrogen-deficient bias in asphaltene ionization, as observed in APPI. Figure 12 presents an

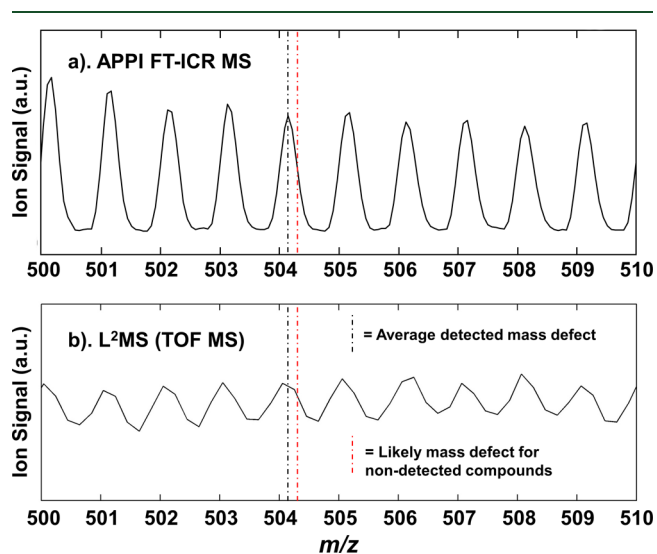


Figure 12. Expanded-view inset for mass spectra of UG8 asphaltene accessed by (a) positive-ion APPI FT-ICR MS (truncated time-domain data to match the resolving power of TOF-MS) and (b) L²MS TOF-MS. The black dashed line highlights the average mass defect accessed by both ion sources; the red dashed line indicates the likely average mass defect for undetected compounds (H:C = 1.1).

expanded-view inset between m/z 500–510 for the mass spectra of UG8 asphaltene obtained by positive-ion APPI FT-ICR MS and L²MS (with a TOF mass analyzer). The FT-ICR MS time domain data points were truncated to match the TOF-MS resolution. First, readers should consider that the exact mass of ¹²C is 12.000000 Da, whereas the exact mass of ¹H is 1.007825 Da. Thus, hydrogen-enriched compounds (lower DBE/highly alkyl-substituted) have exact masses with increased mass defect (i.e., the difference between the exact mass and the nearest integer mass, 0.007825 for ¹H).¹⁰¹ In

Figure 12, the black dashed line highlights the average mass defect (<0.20000) of the detected species and indicates that L²MS and APPI yield similar results; it strongly suggests that both methods preferentially ionize hydrogen-deficient compounds (H:C < 0.90). The red dashed line is the expected mass defect for these asphaltene species (H:C = 1.1), which should match that of elemental analysis. The use of multiple ionization methods to analyze complex petroleum solubility fractions have made great strides in overcoming selective ionization. However, ionization challenges still exist, but can be lessened, to some extent, by incorporating the use of separation/fractionation techniques. Thus, the following section discusses the use of separations to mitigate the effects of selective ionization.

Fractionation of Asphaltene by Aggregation and Molecular Types To Improve MS Analysis. It has been widely reported that separations extend the characterization of petroleum compounds by atmospheric pressure ionization (e.g., ESI, APPI) coupled to FT-ICR MS.^{109,129,178} Recently, an extrography separation was specifically developed to extend the characterization of petroleum asphaltene.¹⁶² The separation involves the adsorption of the samples on silica gel at low analyte mass loading (≤ 1 wt %, i.e., ≤ 10 mg of asphaltene per gram of SiO₂).¹⁶² It is hypothesized that low mass loading facilitates the adsorption of approximately a monolayer/bilayer of nanoaggregates on the surface silanol groups, improving the fractionation selectivity. In the short version of the separation, the dry mixture of asphaltene and silica gel is sequentially extracted with acetone, Hep/Tol (1:1), and Tol/THF/MeOH (5:5:1) by use of a Soxhlet apparatus; each extraction period lasts 24 h and is conducted under a nitrogen atmosphere. Although the solvent series seems unorthodox, it enables the initial extraction of highly aromatic/pericondensed structures with a high ion production efficiency of nonaggregated asphaltene species (or high MIY), leaving behind the compounds that are more difficult to ionize. Acetone is a polar solvent, but its predominant intermolecular interactions are dipole–dipole, which facilitates the extraction of alkyl-deficient PAHs and abundant vanadyl porphyrins, as suggested by Buenrostro-Gonzalez et al.¹⁷⁹ The second solvent mixture, Hep/Tol, assists the isolation of alkyl-aromatic compounds that are not easily removed by acetone. Finally, Tol/THF/MeOH promotes the extraction of asphaltene compounds that interact strongly with the silanol groups of silica gel via the disruption of hydrogen bonding. That fraction contains abundant asphaltene species enriched with polarizable functionalities, which are more difficult to ionize by APPI due to self-association.¹⁶² Figure 13a presents monomer ion yields (MIY) for geologically diverse whole asphaltene samples and their corresponding extrography fractions. Figure 13b presents the gravimetric yields, for the extrography separation, in a ternary diagram. Each coordinate axis corresponds to one extrography fraction: acetone, Hep/Tol, and Tol/THF/MeOH + unrecovered material. Note that asphaltene experience strong, and in many cases, irreversible adsorption onto mineral surfaces.^{180–184} Therefore, the mass recovery for the reported extrography separation is typically between 88 wt % and 98 wt %.^{89,162}

In Figure 13a, trends in MIY indicate that acetone species produce up to ~ 110 -fold more “monomeric” ions than the whole asphaltene and Tol/THF/MeOH fractions. The results highlight the wide range of ionization efficiencies that asphaltene molecules exhibited by APPI. It also reveals that

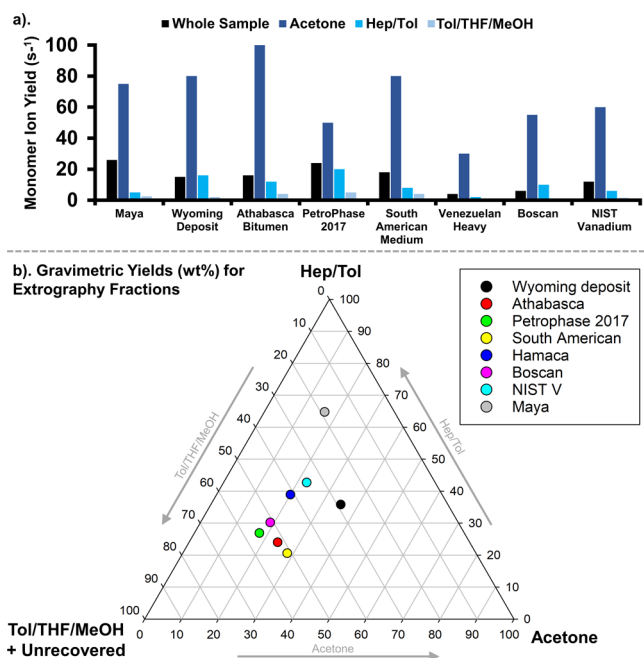


Figure 13. (a) Monomer ion yield for geologically diverse asphaltene samples and their extrography fractions. (b) Gravimetric results for the extrography separation. Each coordinate axis represents one extrography fraction: acetone, Hep/Tol, and Tol/THF/MeOH + unrecovered material.

APPI-MS characterization of whole asphaltenes preferentially reveals the compounds concentrated in the acetone fraction. Furthermore, the trend in which the samples “cluster” in the ternary plot (Figure 13b) suggests that Wyoming deposit, Maya, and Athabasca bitumen asphaltenes have a contrasting composition: the acetone fraction is abundant for Wyoming deposit asphaltenes (~ 37 wt%), whereas Athabasca bitumen and Maya samples reveal abundant Tol/THF/MeOH (~ 52 wt%) and Hep/Tol (~ 65 wt%) fractions. The following section focuses on these three compositionally diverse asphaltenes, which are well-known for their different behavior in thermal cracking/hydroconversion.^{59,185}

Figure 14 presents the combined isoabundance-contoured plots of DBE versus carbon number for all compound classes, except vanadyl porphyrins, for whole asphaltenes from Wyoming deposit, Athabasca bitumen, and Maya crude oils and their extrography fractions (acetone, Hep/Tol, and Tol/THF/MeOH). Hydrocarbons and only N-/O-containing classes have been combined in the leftmost plots in each panel (e.g., HC, N_1 , N_2 , O_1 , O_2 , N_1O_1). The plots to the right feature all sulfur-containing species (e.g., S_1 , S_2 , N_1S_1 , O_1S_1 , $N_1O_1S_1$). Sulfur-containing compounds are plotted separately because several works have shown their distinctive compositional trends and a possible correlation with the tendency of asphaltene samples to stabilize emulsions.^{186–188}

Again, it is critical to point out that the widespread notion that petroleum asphaltenes are primarily single aromatic cores of ~ 7 fused aromatic rings would suggest that the mass spectral data would contain dominant DBE values between ~ 19 and

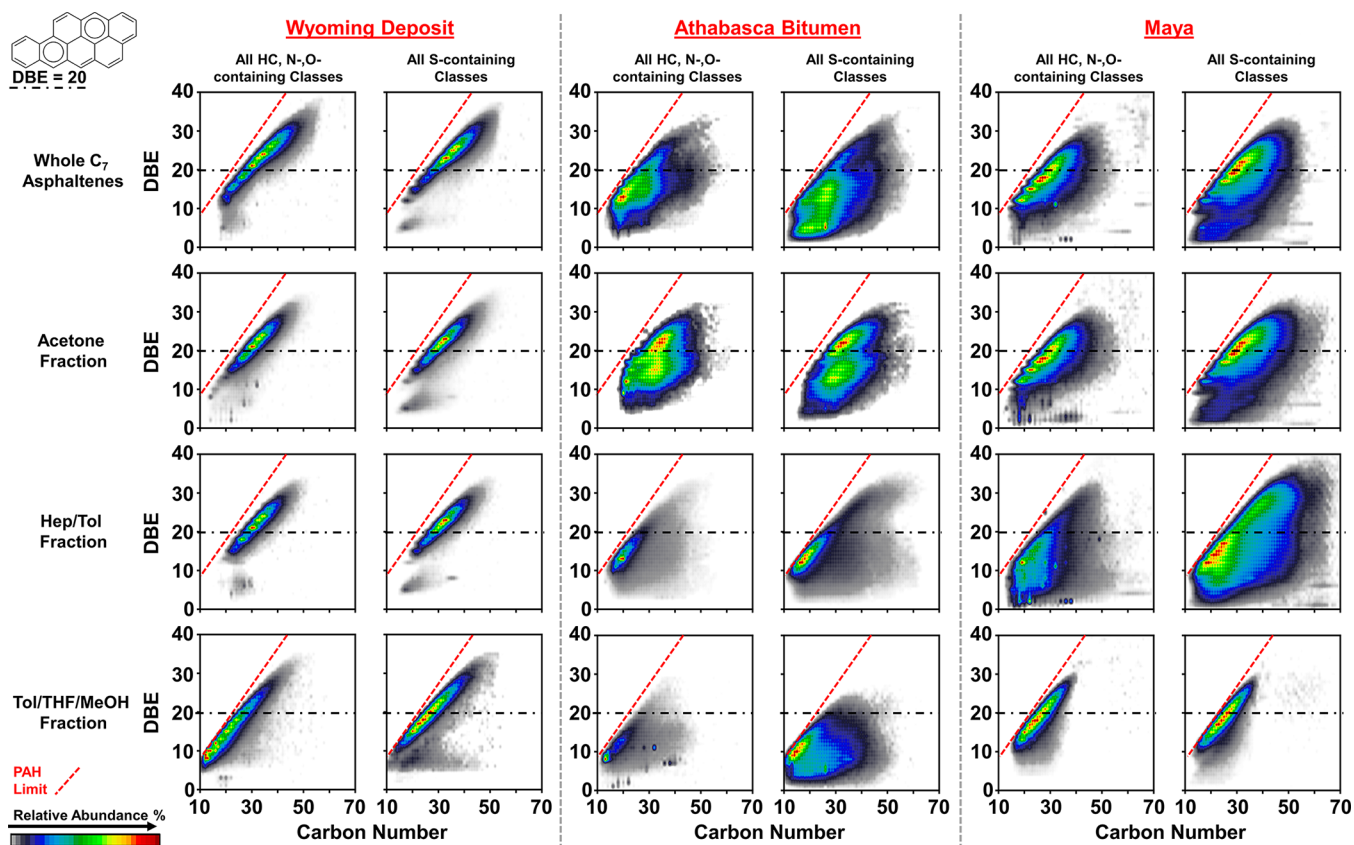


Figure 14. Combined isoabundance color-contoured plots of DBE vs carbon number for HC and nitrogen-/oxygen-containing species and sulfur-containing compounds. Data are derived from (+) APPI 9.4 T FT-ICR MS characterization of whole nC_7 asphaltenes and their extrography fractions. Samples were selected from geologically diverse origins: Wyoming deposit, Athabasca bitumen, and Maya.

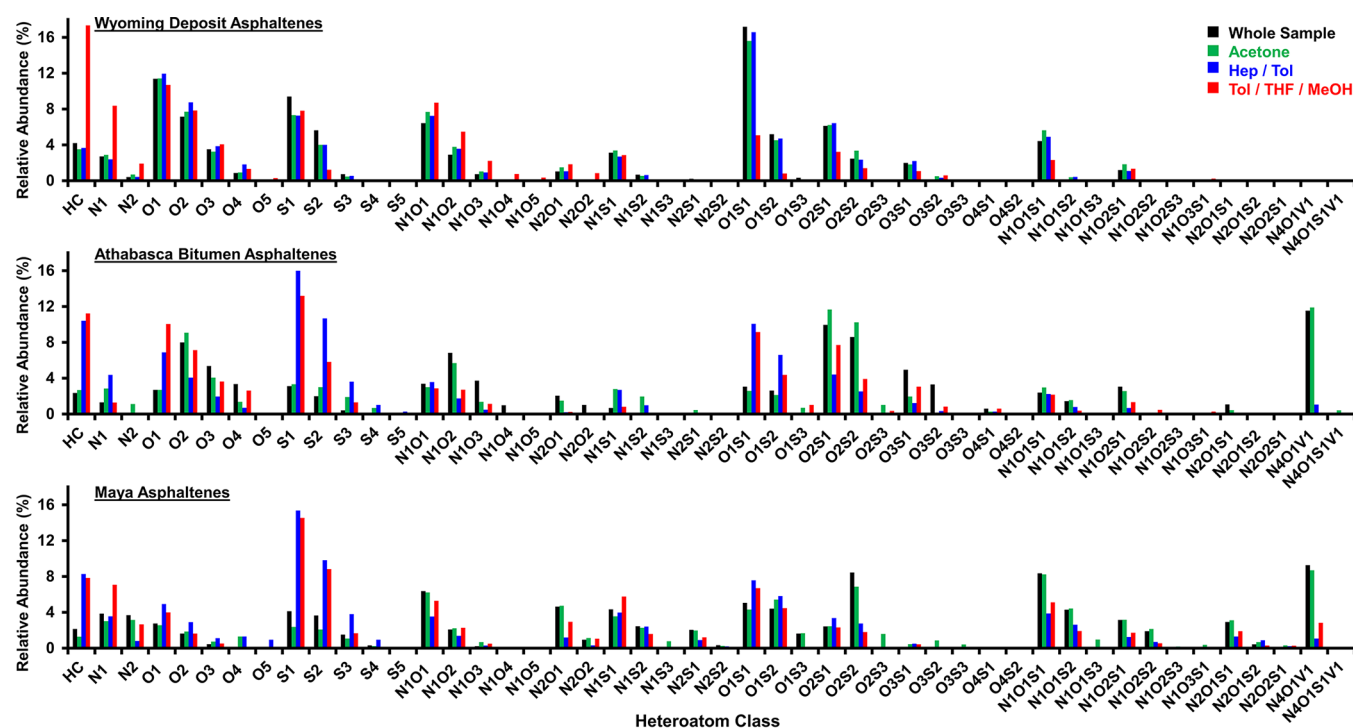


Figure 15. Heteroatom class distribution, derived from (+) APPI 9.4 T FT-ICR MS, for whole asphaltenes and extrography fractions for Wyoming deposit, Athabasca bitumen, and Maya crude oil.

21.^{176,177} However, (+) APPI FT-ICR MS results for whole nC_7 asphaltenes (top row, Figure 14) indicate that only the composition of the Wyoming sample is consistent with this “classical” view of asphaltene structure. Conversely, Athabasca bitumen and Maya samples reveal abundant nitrogen-, oxygen-, and sulfur-containing compounds with low DBE values (DBE < 10), which suggests abundant, high heteroatom-containing species that contain three or fewer aromatic rings.

The results reveal that the whole and all extrography fractions of the Wyoming deposit asphaltenes consist of abundant highly aromatic species clustered close to the PAH line, with limited content of alkyl-side chains (short homologous series, narrow x -axis width). Only the Tol/THF/MeOH fraction reveals lower-carbon numbers and smaller fused aromatic cores (DBE \approx 7–20). Thus, the composition of Wyoming deposit asphaltenes is consistent with the notion that asphaltenes comprise abundant highly aromatic/condensed molecules. Indeed, Juyal et al.¹⁸⁵ reported that Wyoming deposit asphaltenes produce \sim 69 wt % residue in thermogravimetric analysis (TGA). The authors indicated that the TGA residue of other asphaltene samples from diverse origins is notably lower (ranges between 38–49 wt %).¹⁸⁹ The Wyoming sample behavior is consistent with a high content of large/fused aromatic cores with limited substitution by pendant ring groups (dominance of island motifs). Furthermore, Juyal and Rueda-Velasquez et al.^{58,185} reported the amount of products (coke vs distillable fractions) from Wyoming deposit and Athabasca bitumen asphaltenes cracked under favorable hydrogenation conditions. Wyoming asphaltenes yielded >30 wt % coke and only \sim 25 wt % distillable products with boiling points of <538 °C. In contrast, Athabasca bitumen asphaltenes produced <5 wt % coke and \sim 60 wt % distillates.

Moreover, Figure 14 confirms that C_7 asphaltenes suffer from selective ionization by APPI. For all samples, the acetone

fractions, with the highest MIY (data shown in Figure 13), exhibit a compositional range similar to the whole samples. However, the Hep/Tol fractions from Athabasca bitumen and Maya asphaltenes feature species with lower carbon numbers and decreased DBE values. The Maya Hep/Tol fraction reveals sulfur-containing compounds with “atypical” DBEs between 2 and 15 and carbon numbers between 20 and 60. Similar sulfur-containing molecular formulas were found in the Tol/THF/MeOH fraction from Athabasca bitumen asphaltenes. The fact that low-DBE compounds were isolated in the last extrography fraction from Athabasca bitumen, which employs the sole protic-solvent mixture used in the separation (Tol/THF/MeOH), suggests that hydrogen bonding is the dominant intermolecular force in their solubility/extractability behavior. The molecular composition of Athabasca bitumen asphaltenes suggests the existence of abundant compounds with low aromaticity, suitable to produce distillable products in thermal cracking/hydroconversion. These samples feature a high heteroatom content, as shown in Figure 15, which presents the heteroatom class distribution for whole asphaltenes and their extrography fractions. Thus, low-DBE asphaltenes are nC_7 -insoluble, likely because their higher heteroatom content promotes heteroatom-based intermolecular/intramolecular interactions. Figure 15 demonstrates that the extrography separation, coupled with APPI FT-ICR MS, not only increases the compositional range coverage, in terms of DBE and carbon number, but also facilitates the detection of additional heteroatom classes (e.g., S_4 and S_5 classes detected for Athabasca bitumen acetone and Hep/Tol fractions). Furthermore, Figure 15 confirms the existence of asphaltene molecules with up to 4–5 heteroatoms (e.g., S_4 , S_5 , O_2S_2 , $N_1O_2S_2$ classes). However, data interpretation should be done with caution, because the extent of selective ionization, and its effect on MS-derived atomic ratios, is not fully understood. Furthermore, Figure 15 clearly highlights that the HC class is

detected in all subfractions in lower abundance than heteroatom-containing compounds. The presence of these nonpolar species is intriguing, in particular for the Tol/THF/MeOH fraction. Moreover, it is not possible to determine if the detected abundance reflects their molar concentration within the fraction. We hypothesize that the presence of HC compounds in polar extrography fractions could be attributed to remnant occluded maltenes that are only exposed upon extrography fractionation, or possible fragmentation in the APPI source, of polar/thermally labile compounds, likely with acidic functionalities located in peripheral side groups.

Note that some asphaltenes such as PetroPhase 2017 (data presented in Figure 7a) reveal highly aromatic S_{2-4} molecules. However, when oxygen is incorporated (e.g., O_2S_2 class), the compositional range shifts to abundant low DBE compounds. It has been reported that the predominant ionization of such species as protonated molecules, rather than radical cations,¹⁹⁰ indicates that hydrogen bonding is a prevalent intermolecular force. Collectively, the results shown in Figures 7, 14, and 15 support Boduszynski's hypotheses regarding the existence of petroleum asphaltene compounds with low DBE (<10), high alkyl-chain content (up to 40–50 carbon atoms), and several heteroatoms.

Figure 16 presents the H:C ratios for a diverse set of asphaltene samples, determined by combustion elemental

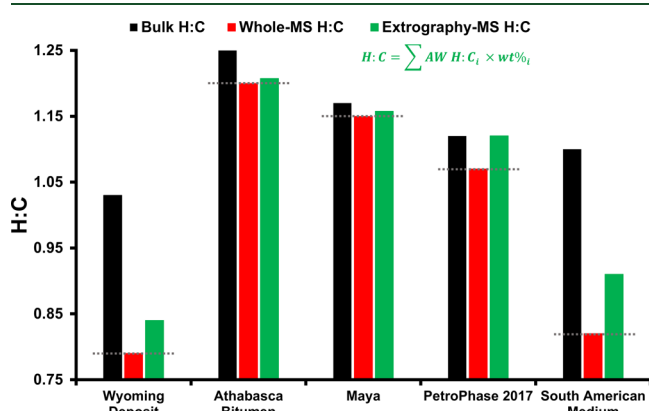


Figure 16. Bulk H:C ratios (black bars) and MS-derived (abundance-weighted (AW)) H:C ratios for whole samples (red bars) and the combined extrography fractions (green bars) for Wyoming deposit, Athabasca bitumen, Maya, PetroPhase 2017, and South American medium asphaltenes.

analysis (black bars) and (+) APPI FT-ICR MS characterization of whole asphaltenes (red bars) and their extrography fractions (green bars). As discussed earlier, the H:C ratios derived from the APPI-MS characterization of whole samples are consistently much lower than the bulk values because APPI ionizes hydrogen-deficient (higher DBE) compounds preferentially. However, the higher H:C values that result from the abundance-weighted (AW) sum of the MS-derived H:C ratios of the extrography fractions, determined by eq 3 (also shown in Figure 16), suggest that the extrography separation, to some extent, mitigates selective ionization. Separate APPI-MS characterization of asphaltene fractions enables the access to compounds with much higher H:C ratios that offset the high hydrogen deficiency of the preferentially ionized species in the analysis of whole asphaltenes. The improvement is more prominent for Wyoming deposit and South American Medium asphaltenes. However, it is critical to consider that individual

extrography fractions are still ultracomplex mixtures. Unquestionably, their APPI-MS characterization is still limited by selective ionization, which has been demonstrated by GPC with online FT-ICR MS detection, as discussed further in a later section.¹⁹¹

$$H:C = \sum AW H:C_i \times wt\%_i \quad (3)$$

The results shown in Figures 13–16 imply that APPI-MS analyses of whole asphaltene samples preferentially reveal the species that are isolated by acetone extraction. It has been hypothesized that combined effects of ionization energy and aggregation could be the reason behind selective ionization.⁴³ Direct aggregation measurements have not been performed for asphaltene extrography fractions; however, their elution behavior in GPC and their precipitation trends in Hep/Tol mixtures are well-documented. Figure 17a presents the GPC

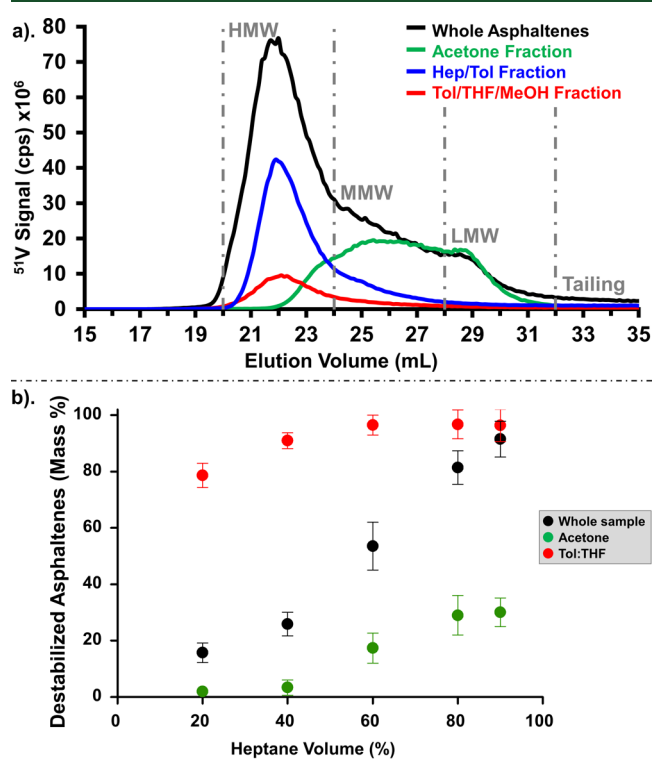


Figure 17. (a) Nanoaggregate size distributions for PetroPhase 2017 asphaltenes and its extrography fractions, as determined by GPC ^{51}V -ICP MS. [Reproduced with permission from ref 191. Copyright 2020, American Chemical Society, Washington, DC.] (b) Precipitation behavior in Hep/Tol for whole PetroPhase 2017 asphaltenes and its acetone and Tol/THF fractions. [Reproduced with permission from ref 162. Copyright 2018, American Chemical Society, Washington, DC.]

chromatograms, obtained by ^{51}V inductive-coupled plasma mass spectrometry (ICP-MS) detection, for whole PetroPhase 2017 asphaltenes and its extrography fractions.¹⁹¹ As reported by Putman and Bouysiere et al.,^{192–194} this approach enables a semiquantitative determination of ^{51}V -containing nanoaggregate size distributions. Whether or not GPC reflects the real aggregation of petroleum samples is another subject of debate. For instance, Muller et al.^{195,196} investigated the GPC elution trends of several crude oils and analyzed the collected GPC fractions by off-line FT-ICR MS. The authors concluded that aggregated/early eluting fractions were mainly comprised of

~1–3 fused aromatic rings with extensive content of alkyl side chains. Conversely, the nonaggregated/late-eluting fractions featured bigger aromatic cores of ~5–9 fused rings, with limited alkyl substitution. Therefore, possible “non-size” effects (i.e., strong adsorption on the GPC column) were hypothesized. Nevertheless, GPC is routinely used to compare the “nanoaggregate” size distribution of vacuum residues/asphaltenes^{197,198} and herein, provides invaluable insight into the aggregation tendencies of asphaltene extrography fractions, their precipitation trends with heptane titration, and ionization efficiencies.

In Figure 17a, the elution ranges are highlighted by gray dashed lines and were established based on the MWD of polystyrene standards (i.e., high molecular weight, >10 000 Da; medium molecular weight, ~1000–10 000 Da; low molecular weight, <1000 Da). The elution regions are as follows:^{193,199} high molecular weight (HMW, 20–24 mL elution volume), medium molecular weight (MMW, 24–28 mL), and low molecular weight (LMW, 28–32 mL), plus a “tailing” fraction (>32 mL). Figure 17a indicates that the whole sample (black) comprises a diverse population of ⁵¹V-containing aggregates: ~59%, 27%, and 10% of the total integrated area of the GPC chromatogram correspond to high-, medium-, and low-molecular-weight aggregates, plus ~3% for the tailing region. It is hypothesized that tailing and LMW species are free/disaggregated molecules.

The GPC elution profiles for the fractions indicate that the extrography separation yields asphaltene cuts with unique aggregation behavior. The acetone fraction, which has been shown to contain abundant highly aromatic asphaltenes with dominant single-core structure, features a MIY of ~50 s⁻¹ in APPI and mainly reveals MMW (~61%) and LMW (~25%) vanadium-containing compounds.^{89,162} Conversely, Hep/Tol and Tol/THF/MeOH mostly elute as HMW aggregates (73/66%). These fractions were previously demonstrated to contain abundant archipelago motifs with lower DBE values, higher heteroatom content, and much lower MIY (~20/5 s⁻¹). Thus, the results suggest a link between nanoaggregate size distribution and the production efficiency of nonaggregated ions in APPI (MIY). Note that collection of the GPC subfractions (e.g., HMW from acetone) followed by solvent evaporation, redissolution in tetrahydrofuran (a “good” asphaltene solvent), and reinjection of the prepared solution into the GPC instrument, reveals a nanoaggregate distribution consistent with HMW species, suggesting a high nanoaggregate stability.²⁰⁰

Figure 17b presents the precipitation behavior of the samples in Hep/Tol. The whole PetroPhase 2017 asphaltene sample and its acetone and Tol/THF extrography fractions were dispersed in toluene and then titrated with heptane.¹⁶² Gravimetric measurements indicate that only ~22 wt % of the acetone fraction precipitates when 90% of heptane is added. Conversely, the whole sample and the Tol/THF fraction exhibit precipitation of ~91 and 96 wt %. Similar trends have been reported by Giraldo-Davila et al.,¹²⁸ who fractionated asphaltenes by thin-layer chromatography on SiO₂ plates and traced the stability of the fractions by near-infrared scattering measurements. The authors found that toluene solutions prepared with the most polarizable asphaltene TLC fractions (e.g., noneluted and eluted with protic solvent mixtures), revealed stronger precipitation trends when titrated with heptane.

“Classical” Asphaltenes Are, After all, Very Uncommon. Most of the asphaltene samples analyzed by (+) APPI FT-ICR MS at the NHMFL present abundant “atypical” compounds with low DBE and moderate/high heteroatom content. Reports by Romão,¹¹² Rogel,¹²⁶ Chacón-Patiño,¹⁵¹ Ballard,²⁰¹ McKenna,²⁰² and Giraldo-Davila,²⁰³ have demonstrated the existence of such atypical species. However, concerns have been raised regarding the true solubility nature of these low-DBE compounds: specifically, if such species are entrained/occluded maltenes that remain after exhaustive cleaning with heptane by standard or modified methods,^{131,204} and Soxhlet extraction (i.e., first extraction steps with acetone and Hep/Tol in the extrography method for asphaltene fractionation).

Separations are necessary to determine whether the chemistry of low-DBE species with high heteroatom content is consistent with asphaltene solubility behavior. The wet silica method, designed for the isolation of interfacial material, has been successfully used for separating petroleum fractions that reveal abundant low-DBE (<20) heteroatom-rich compounds in APPI/ESI FT-ICR MS. These fractions are well-known to stabilize water-in-oil emulsions. The wet silica method uses water-saturated silica gel that contains ~26 water monolayers.^{205,206} Petroleum or asphaltene samples are mixed with the wet material, resulting in a slurry that is packed in a glass column and washed with a hydrophobic solvent (e.g., heptane, Hep/Tol, or toluene) to extract noninterfacially active compounds. Subsequently, the interfacial material, among several water layers, is desorbed by a protic solvent mixture (e.g., toluene/methanol or tetrahydrofuran/methanol). Interfacially active material from whole Athabasca bitumen asphaltenes and its acetone and Tol/THF/MeOH fractions has been extracted and studied by (+) APPI FT-ICR MS and GPC.²⁰⁷

Figure 18a presents isoabundance-contoured plots of DBE vs carbon number for S_xO_y classes for the interfacial material from whole Athabasca bitumen C₇ asphaltenes. The results suggest that interfacially active asphaltenes comprise abundant species with DBE < 10 and carbon numbers of <40. However, readers should consider that IM mass spectral analysis is still affected by selective ionization.¹⁷⁵ For the detected species, the compositional range suggests abundant molecules with less than five fused aromatic rings (DBE < 15). From all the plotted classes, only O₁S₁ hints at a few species consistent with classical asphaltene chemistry, with DBE values of >20 and close to the PAH limit. Compounds with high S and O content, e.g., O₃S₃, reveal abundant homologous series with remarkably low DBE values. Solubility tests in Hep/Tol indicate that IM from asphaltenes matches the asphaltene solubility definition, as it is *n*C₇-insoluble and toluene-soluble. Therefore, its molecular aggregation must be ruled by heteroatom-based interactions rather than π -stacking. Figure 18b presents the heteroatom class distribution of the IM; the abundance of radical cations (M^{•+}) and protonated molecules ([M + H]⁺) is highlighted in orange and yellow. The results demonstrate the existence of molecules with up to seven heteroatoms (e.g., O₄S₃ and O₅S₂ classes). Those compounds were not detected by the APPI-MS analysis of whole asphaltenes or extrography fractions, likely because of the combined effects of selective ionization and low IM concentration (~8 wt %).

The bars in Figure 18b present the abundance of detected radical cations (orange, M^{•+}) and protonated molecules (yellow, [M + H]⁺). Globally, the IM fraction yielded ~68%

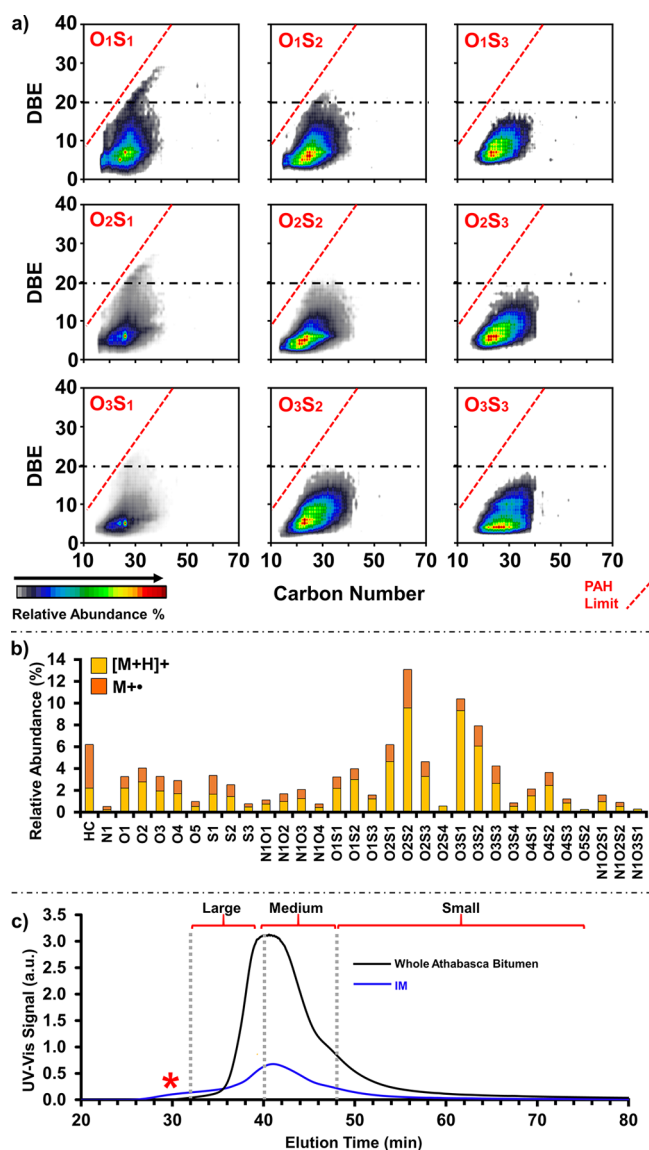


Figure 18. (a) Compositional range for selected compound classes of interfacial material (IM) extracted from Athabasca bitumen asphaltene; (b) heteroatom class distribution for IM and whole asphaltene (included for comparison); (c) GPC elution behavior, as detected by UV-vis spectroscopy for IM and whole asphaltene.

of protonated molecules versus 38% of radical cations. Thus, the results suggest that IM contains abundant heteroatom-rich O_xS_y species that ionize predominantly via protonation and feature low DBE values. Several works demonstrate a direct correlation between analyte tendency to produce protonated molecules (proton affinities in the gas phase) and the capability to hydrogen bond in solution.^{208–210} For instance, sulfoxides [R–S(=O)–R'] are weak bases that have a tendency to produce protonated molecules.²¹¹ Furthermore, Figure 18c presents the GPC UV-vis chromatogram for whole Athabasca bitumen nC₇ asphaltene and its IM. The results suggest that higher amounts of larger nanoaggregates are present for the IM, which elute prior to the large aggregates of the whole asphaltene sample. Collectively, the results support the existence of heteroatom-rich/low DBE compounds that fit into the solubility definition of asphaltene, because their high heteroatom content promotes multiple intermolecular interactions per molecule, which results in a strong aggregation

tendency (extremely high molecular weight, red asterisk) as detected by GPC.¹⁹⁰

Readers should consider that regardless of exhaustive asphaltene cleaning and multiple separation steps, sample analysis is still hindered by selective ionization in APPI. In other words, it is difficult to determine the extent to which observed ions reflect the actual composition of the analyzed samples. For instance, Clingenpeel et al.¹⁷⁵ fractionated IM from whole Athabasca bitumen by solid-phase extraction with aminopropyl silica gel and a hydrophobicity elutropic gradient. The authors found that the (–) ESI FT-ICR MS characterization of the whole IM preferentially revealed heteroatom-rich compounds with DBE values of <10 and carbon numbers between 10 and 40. As expected, the fractionation increased the compositional space coverage: highly hydrophobic fractions revealed ~39 000 new molecular formulas with carbon numbers between 40 and 60 and DBE values of 3–20, still low enough aromaticity to fit into the classical structural definition of asphaltene. The authors suspected that ion suppression effects remain, despite the fractionation by carbon number.

Up to this point, it has been highlighted how molecular-level characterization of asphaltene can be improved with the use of extrography separation methods, which help to overcome, to some extent, selective ionization. This improved access to previously undetected species has enabled progress for structural characterization. Without separations, asphaltene structure has been misrepresented as island-dominant. The following section summarizes the advances in the structural analysis of asphaltene via gas-phase fragmentation, or tandem MS.

Advanced Precursor Ion Isolation and Tandem-MS: Gas-Phase Fragmentation in Ultrahigh Vacuum by Infrared Multiphoton Dissociation. The preferential ionization of highly aromatic/alkyl-deficient asphaltene by APPI has profound implications on how asphaltene has been understood by tandem MS. Therefore, a comprehensive understanding of asphaltene structure via mass spectrometry can only be achieved by analyzing asphaltene fractions.

The general configuration of the 9.4 T FT-ICR mass spectrometer, presented in Figure 9, highlights the mass-selective quadrupole used for precursor ion isolation; that process is performed under mild vacuum (~2 × 10^{–4} Torr). Ions are then transferred to the ICR cell in which fragmentation is performed by IRMPD in ultrahigh vacuum (<10^{–10} Torr). A CO₂ laser (10.4 μm) directs a beam of infrared photons to the center of the ICR cell. The ions trapped at the center of the cell eventually absorb multiple photons, resulting in increased internal energy, and ultimately dissociation if enough energy is absorbed to break covalent bonds. The amount of energy is a function of laser power and irradiation period, which are tunable.²¹² The resulting fragment ions are then analyzed by typical ICR excitation and detection.

Figure 19 presents the common fragmentation pathways of petroleum compounds. An extrography fraction from North American asphaltene was subjected to gas-phase fragmentation by IRMPD. Precursor ions with *m/z* 454–458 reveal two main fragmentation pathways: dealkylation, highlighted by the blue arrow in the mass spectrum, and “bridge” dissociation products, highlighted by the green dashed line. Molecular formula assignment indicates that the fragments from dealkylation keep the same DBE range of the precursor ions and

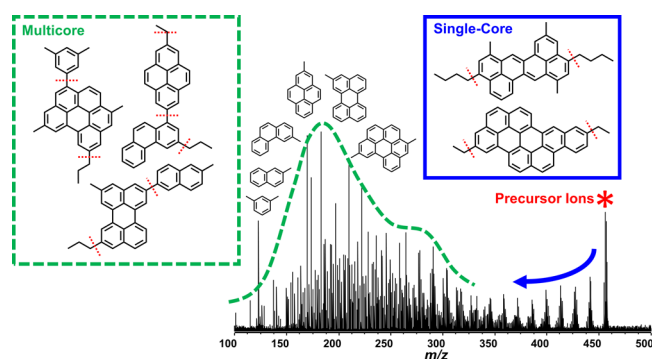


Figure 19. Fragmentation pathways for petroleum compounds determined by infrared multiphoton dissociation followed by FT-ICR MS characterization.

experience only a decrease in carbon number due to the cleavage of alkyl side chains, consistent with single-core motifs (island). The fragments from bridge dissociation are characteristic of multicore motifs (archipelago), as they feature lower carbon numbers and lower DBEs than the precursor ions. Indeed, the low molecular weight distribution ($m/z \sim 120\text{--}350$), highlighted by the green dashed line, is comprised mainly of 1–5-ring alkyl-substituted aromatics, whose production is possible only if archipelago structures exist. Studies on model compounds demonstrate that large aromatic cores (e.g., coronene) cannot produce lower-ring number species upon IRMPD, even when higher fragmentation energies are provided via extended irradiation periods. Instead, higher IRMPD energies cause hydrogen loss, which increases the DBE.²¹³ Figure 19 is not intended to address the nature of the archipelago bridges, e.g., aryl–aryl versus alkyl-chains. That is the topic of ongoing research and future reports.

Questions have been raised regarding the limitations and possible misinterpretation of recently published data derived from APPI IRMPD FT-ICR MS.^{79,214} For instance, it has been suggested that (1) the selected precursor ions are aggregates, rather than asphaltene monomolecules, and that those aggregates in MS could behave similarly to bulk asphaltenes in thermal cracking and produce archipelago artifacts.⁷⁹ (2) Moreover, a concurrent loss of DBE and carbon number in IRMPD could result from aggregate dissociation, rather than covalent bond fragmentation. We consider the published results from IRMPD FT-ICR MS reflect, to some extent, the actual composition/structure of the samples, because:

- The hundreds of isolated ions span a molecular weight range between $m/z \sim 350\text{--}650$, far below the demonstrated mass for dimers/multimers and bigger aggregates.²¹⁵
- Fragmentation of the samples is performed in ultrahigh vacuum ($<10^{-10}$ Torr), in which secondary reactions are highly unlikely compared to the bulk phase (thermal cracking).
- The energy required for the dissociation of noncovalent ion clusters is significantly lower than that for fragmentation of covalent bonds.²¹⁶ Under these low irradiation energy (dissociation) conditions, petroleum model compounds and asphaltene samples yield neither dissociation nor fragment products; thus, ion clusters are not present.²¹⁶
- Under the same MS experimental conditions, different samples reveal a different fragmentation behavior. The

results are consistent with known asphaltene properties.⁸⁹

- Naturally occurring internal standards reveal a fragmentation behavior consistent with their known molecular structure.⁸⁹

Different Samples Reveal Different Fragmentation Behaviors. Under the same experimental conditions (e.g., sample vaporization/ionization, IRMPD energy, and FT-ICR MS excitation/detection), different samples display different fragmentation behaviors. Figure 20a presents the positive-ion

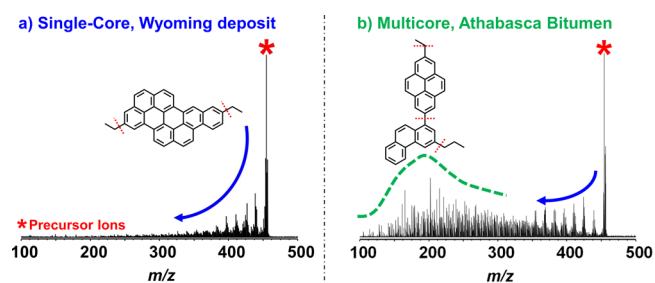


Figure 20. Fragmentation behavior for whole (a) Wyoming deposit and (b) Athabasca bitumen C_7 asphaltenes. [Reproduced with permission from ref 89. Copyright 2018, American Chemical Society, Washington, DC.]

APPI IRMPD FT-ICR MS of precursor ions with $m/z 454\text{--}457$ for whole Wyoming deposit and Athabasca bitumen nC_7 asphaltenes. Wyoming deposit predominantly reveals the dealkylation pattern, which indicates the dominance of single-core compounds; that finding is consistent with the tendency of Wyoming deposit asphaltenes to produce significant amounts of coke in thermal cracking and hydro-conversion processes.^{58,185} Conversely, Athabasca bitumen asphaltenes (Figure 20b), which are known to yield much higher amounts of distillable products,¹⁸⁵ reveal a fragmentation pattern consistent with a mixture of single-core (blue arrow) and abundant multicore motifs (low MWD, green dashed line).

Furthermore, the gravimetric yields for the extrography separation of these two samples (shown in Figure 13) indicates that Wyoming deposit is enriched in the acetone fraction (~ 37 wt %) and contains only $\sim 28\%$ of Tol/THF/MeOH, whereas Athabasca bitumen comprises ~ 24 wt % of acetone-extracted compounds and ~ 52 wt % of Tol/THF/MeOH. The IRMPD fragmentation behavior of the extrography fractions, reported elsewhere,⁸⁹ demonstrates that the acetone-extracted compounds from asphaltenes of different geological origins comprise abundant single-core motifs. In contrast, Hep/Tol and Tol/THF/MeOH fractions feature increased amounts of multicore species. Collectively, the gravimetric results for the extrography separation, the compositional range of the samples (Figure 14), and the IRMPD behavior of the whole samples support the documented behavior of Wyoming deposit and Athabasca bitumen asphaltenes in thermal cracking and hydroconversion processes.

Fragmentation of Naturally Occurring Internal Standards. Asphaltenes are known to contain high amounts of metal porphyrins (e.g., vanadyl and nickel).^{217–219} Figure 21a presents the broadband mass spectra for Athabasca bitumen nC_7 asphaltenes. The abundant species between $m/z 470\text{--}650$ correspond to vanadyl porphyrins, or $N_4O_1V_1$ class, with a compositional range (Figure 21a, right side) that indicates

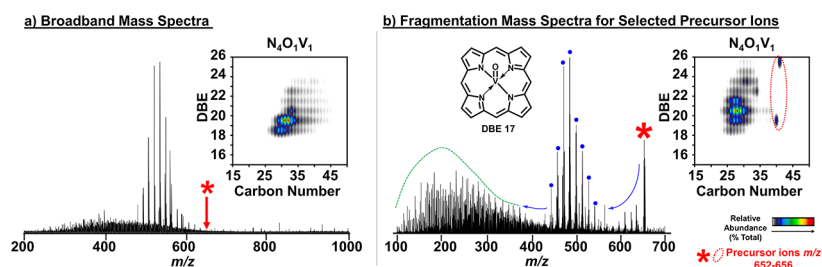


Figure 21. (a) (+) APPI FT-ICR broadband mass spectrum for the acetone fraction from Athabasca bitumen asphaltenes. The DBE vs carbon number plot to the right highlights the compositional range of vanadyl porphyrins ($N_4O_1V_1$ class). (b) Fragmentation of precursor ions with m/z 652–656, which reveals both dealkylation and the production of the low MWD. The DBE vs carbon number plot to the right features the compositional range of $N_4O_1V_1$ precursor ions and their IRMPD fragments. [Reproduced with permission from ref 89. Copyright 2018, American Chemical Society, Washington, DC.]

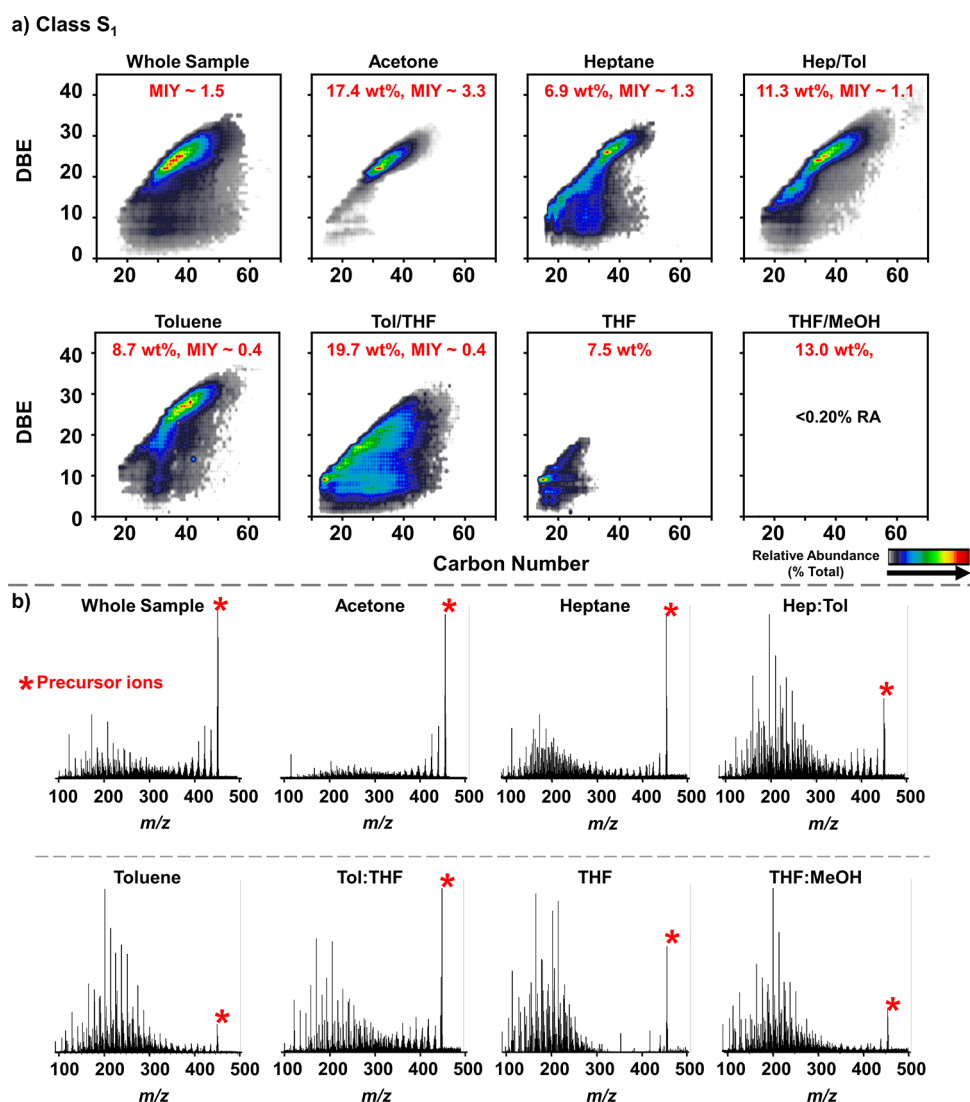


Figure 22. Molecular composition of South American medium C_7 asphaltenes determined by (+) APPI FT-ICR MS: (a) DBE vs carbon number plots for the S_1 class and (b) fragmentation spectra of precursor ions with m/z 454–457. Each DBE plot includes the gravimetric yield for the extrography separation (wt %) and the monomer ion yield (MIY). [Reproduced with permission from ref 162. Copyright 2018, American Chemical Society, Washington, DC.]

abundant species with DBE values between 18 and 24, and carbon numbers between 25 and 45. Precursor ions were isolated at m/z 652–656 (highlighted with the red asterisk) and fragmented by IRMPD. Figure 21b features the fragmentation spectrum for the selected precursor ions,

revealing dealkylation (blue arrow/marks) and the low molecular weight distribution indicative of archipelago-derived fragments (green dashed line). It is important to keep in mind that the selected precursor ions span a wide assortment of compound classes (e.g., HC, S_1 , O_2 , $N_4O_1V_1$), but here, we

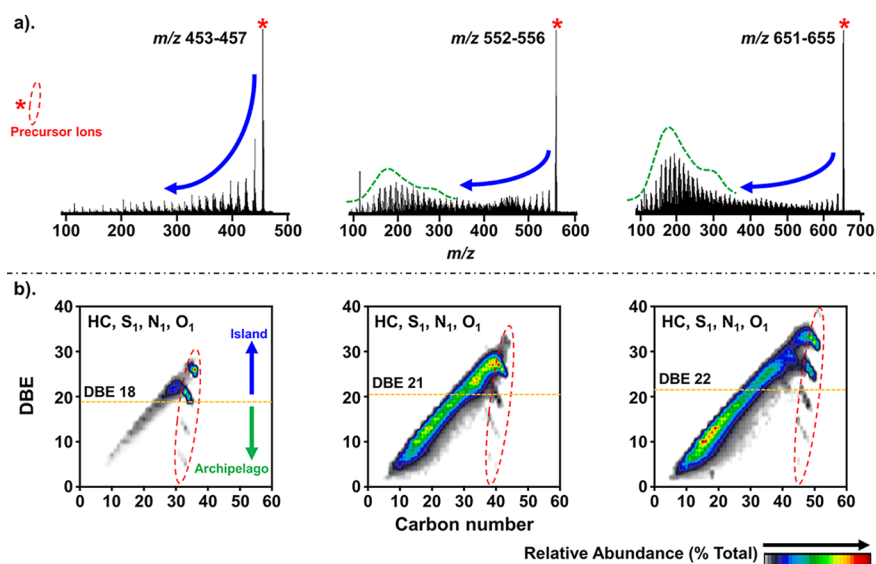


Figure 23. (a) Fragmentation spectra and (b) combined DBE vs carbon number plots, for HC and monoheteroatomic classes, for fragments and precursor ions isolated at m/z 453–457 (left), 552–556 (middle), and 651–655 (right). [Reproduced with permission from ref 162. Copyright 2018, American Chemical Society, Washington, DC.]

focus on vanadyl porphyrins, whose precursors span a DBE range between 19 and 26 with carbon numbers of 40–41 (red dashed circle, far right). After dissociation, dealkylation fragments are clearly evident. The fragments preserve the DBE range of the precursors, which proves that the tetrapyrrole core of vanadyl porphyrins, which is a single-core structure of DBE 17,⁸⁶ remains intact upon fragmentation. Higher DBE values correspond to vanadyl porphyrins with fused exocyclic naphthenic or aromatic rings (single-core), as reported elsewhere.^{47,220–222} The results demonstrate that the proposed methodology yields structural data consistent with known structural motifs in petroleum (in this case, known island-dominant porphyrins), reinforcing the validity of the reported results for asphaltene samples.

For several years, it was believed that MS data supported the dominance of single-core structures in petroleum asphaltenes. However, many of those reports did not meet the requirements for the accurate characterization of complex mixtures. Specifically, the studies that concluded that asphaltenes comprised mostly single-core species were performed using low-resolution mass spectrometry (i.e., time-of-flight/ion trap mass analyzers with resolving power below 20 000 at m/z 400), unsuitable fragmentation methods for total dissociation (e.g., low-energy CID), and performed on whole asphaltene samples, where MS characterization is disproportionately affected by selective ionization.^{223–225} Figure 22 demonstrates that APPI-MS/tandem-MS analysis of whole asphaltene samples leads to misleading conclusions. Figure 22a features the DBE vs carbon number plots for the S_1 class for whole PetroPhase 2017 asphaltenes and its extrography fractions prepared by the extended version of the separation method.¹⁶² Gravimetric yields (wt %) and MIY are included. Figure 22b presents the fragmentation spectra for precursor ions with m/z 454–457 for all of the samples.¹⁶²

Figure 22a demonstrates that APPI MS characterization of whole asphaltene samples supports the dominance of highly aromatic compounds, as the compositional range of the whole sample features abundant species with DBE values of >20. The acetone fraction is enriched with high DBE compounds, close

to the PAH limit. However, the extrography separation exposes molecules that feature much lower MIY and an “atypical” compositional range (or low DBE). Figure 22b demonstrates that whole PetroPhase 2017 asphaltenes reveal a mixture of island and archipelago species. The acetone fraction, which features the highest ionization efficiency in APPI, comprises abundant island motifs: the dealkylation fragmentation pathway is more evident/abundant. As the elutropic gradient progresses from heptane to Tol/THF and THF/MeOH, the fragmentation spectra reveal higher abundances of archipelago-derived fragments. The results demonstrate that archipelago motifs concentrate in the extrography fractions with decreased MIY in APPI, therefore, their observation, in whole sample analysis, is hampered by selective ionization. Separations facilitate their detection by APPI FT-ICR MS.

The Amount of Multicore Motifs Is Not Uniform across the Entire MWD. Accurate structural characterization of asphaltene samples requires isolation and fragmentation of precursor ions across the entire MWD, because the island-to-archipelago ratio decreases as a function of increasing m/z .^{90,162,226} Figure 23a (right side) displays the fragmentation spectra of precursor ions with m/z 454–457 for the acetone fraction from South American medium nC_7 asphaltenes. The compositional range of precursor (circled in red) and fragment ions is shown in the rightmost plot in Figure 23b. We have grouped the compositional range of hydrocarbons (HC) and monoheteroatomic classes (S_1 , N_1 , O_1), for precursor and fragment ions, into one DBE vs carbon number plot. The results indicate that the dominant structural motif is island/single-core, as the predominant fragmentation pathway is dealkylation (mass spectrum, blue arrow). In the DBE vs carbon number plots, an orange dashed line highlights the “island compositional boundary”, defined as the abundance-weighted average of DBE values for the precursor ions minus the weighted standard deviation.¹⁶² IRMPD fragments with DBE values below this compositional boundary are produced via dissociation of multicore motifs, because those structures lose both carbon number and DBE. Figure 23b indicates that most of the fragments, from precursors with m/z 453–457, are

derived from island structural motifs as they have DBE values above the compositional boundary.

An increase of ~ 100 Da (middle spectrum/DBE plot) reveals higher amounts of archipelago species. The fragmentation spectrum of precursor ions with m/z 552–556 shows dealkylation (blue arrow) and the low MWD (green dashed line), which suggest a mixture of island and archipelago structures. The compositional range for precursor and fragment ions demonstrates that the proportion of fragments, above and below the compositional boundary, is $\sim 1:1$. Finally, precursor ions with m/z 651–655 feature increased amounts of archipelago motifs. The fragmentation spectrum displays the low MWD (green dotted line) with a much higher relative abundance than that of the dealkylation fragmentation (blue arrow). Furthermore, the abundance of fragments below the island compositional boundary is much higher. The results indicate that the acetone fraction (island dominant), from an asphaltene sample with predominant island motifs (South American medium asphaltenes), consists of abundant archipelago motifs at high m/z .¹⁶² We hypothesize the existence of a carbon number limit in which the molecules cannot support more carbon atoms within a single-core and remain soluble in organic solvents such as toluene and THF; when additional carbons are incorporated as 1–4 ring aromatics pendant groups, the range of solubility is extended. For example, kerogen, the precursor to petroleum, is insoluble in normal organic solvents, in part because it has no apparent limit in carbon number (MW).²²⁷ In solubility terms, asphaltenes are considered as intermediate species between kerogen and maltenes.²²⁸ Thus, there is likely a carbon number limit, for each given structural motif, which may correlate with solubility properties.

Characterization of Fossil Fuel Samples with Wide DBE Range. Figures 11 and 14, as well as several reports from other authors, demonstrate the existence of asphaltene samples with a wide DBE range.^{114,126,229} Low DBE species (DBE <12) are not usually considered asphaltenes because they present 4 or less fused aromatic rings. However, the reported “atypical” samples match the solubility behavior of asphaltenes (heptane-insoluble/toluene-soluble), because their high heteroatom content promotes multiple intermolecular interactions per molecule, which likely results in the production of supramolecular networks.

Experimental evidence for the existence of supramolecular networks in asphaltene deposits was reported by Acevedo et al.,²³⁰ who performed multistep characterization of whole asphaltenes and their extrography fractions by quartz crystal resonator (QCR) sensor, (+) APPI FT-ICR MS, GPC ICP-MS, and AFM. Toluene solutions of the samples were titrated with heptane, and their flocculation behavior was traced by QCR. Aggregates, deposited on the QCR sensor, were characterized by AFM. FT-ICR MS, QCR, and AFM results are presented in Figure 24 and help to visualize the compositional range (Figure 24a), the deposition trends as measured by QCR sensor (Figure 24b), and the aggregates' topography (Figure 24c) for one of the reported asphaltene samples and its extrography fractions.²³⁰ The acetone fraction, shown to contain abundant island motifs for abundant compounds with high DBE values (APPI FT-ICR MS characterization), produced lower amounts of deposited material than Tol/THF/MeOH (enriched with archipelago, low-DBE species). The combined DBE vs carbon number plots, for HC/O-/N-containing molecules (Figure 24a, upper

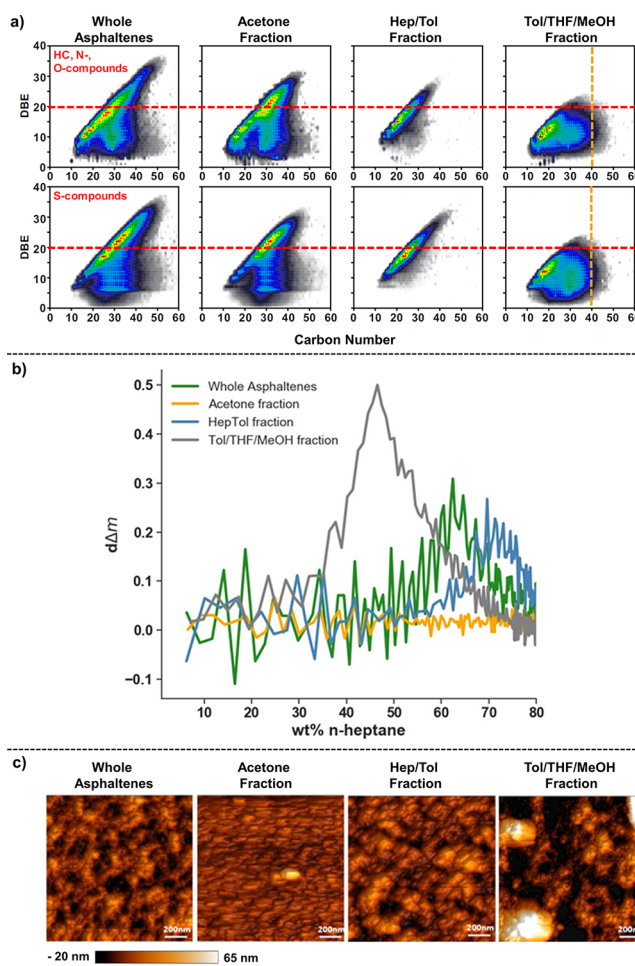


Figure 24. (a) Combined DBE vs carbon number plots for HC/N₁/O₁-containing compounds and sulfur-containing species, for whole asphaltenes and their extrography fractions. (b) Deposition behavior as measured by a quartz crystal resonator (QCR) sensor. (c) AFM characterization of deposited whole asphaltenes and extrography fractions. [Reproduced with permission from ref 230. Copyright 2020, American Chemical Society, Washington, DC.]

row) and sulfur-containing species (Figure 24a, lower row), indicate that acetone features a wide DBE range, with abundant molecules with DBE values of >20 (red dashed line), whereas Tol/THF/MeOH mostly consists of low DBE species (<15). Figure 24b presents the QCR results: derivation of the deposited mass ($d\Delta m$) on the quartz surface vs the amount of added heptane. The results demonstrate that the acetone and Hep/Tol fractions, which are more aromatic, have a tendency to deposit less material than Tol/THF/MeOH.

With regard to the topography of the deposits, Figure 24c indicates that the acetone fraction presented an organized aggregate structure with regular deposition and the smallest size ($\varnothing \approx 50$ nm), whereas whole asphaltenes and the Tol/THF/MeOH fraction featured a layer of aggregates with irregular shape, and the largest aggregates ($\varnothing \approx 120$ nm). Hep/Tol aggregates presented an intermediate behavior, with less organized/bigger structures than those from acetone, but with a more regular deposition pattern than Tol/THF/MeOH. Collectively, the results demonstrate that asphaltene species with “atypical” composition (Tol/THF/MeOH, FT-ICR MS) exhibit stronger deposition trends (QCR results), and produce less spatially organized macroaggregates that point to the

existence of supramolecular asphaltene networks, similar to the structures proposed by Gray et al.¹⁴ In Gray's model, asphaltenes contain abundant compounds with moderate/low ring number, single-core and multicore molecular structure, and several heteroatoms, which can interact with several asphaltene neighboring molecules by various intermolecular interactions: e.g., π -stacking, hydrogen bonding, acid/base associations, and van der Waals (vdW) forces between hydrophobic moieties, whose synergistic effect likely translates to strong aggregation.^{14,39} On the other hand, the acetone fraction, more aromatic, revealed a much weaker deposition and produced organized aggregates that point to predominant π -stacking interactions.²³⁰

The structural characterization of samples with a wide DBE range, via tandem MS, is challenging, because even a single Dalton isolation window contains precursor ions with DBE values from ~ 2 to 40. For instance, Wittrig et al.²³¹ reported the structural characterization of petroleum ring (ARC) fractions by isolation of precursor ions within 1 Da isolation windows (single Dalton isolation). The authors performed subsequent CID FT-ICR MS. The fractionation process, reported elsewhere,²³² separates petroleum into fractions with a distinctive number of aromatic rings. Figure 25 (upper panel) presents the mass spectra zoom (inset), prior to fragmentation, for the isolated precursor ions for each ARC fraction at m/z 670. Generally, complexity and heteroatom content increase as a function of ARC fraction number: ARC4+ contains more isobaric ions per nominal mass with diverse "hydrogen deficiency" or Z number. Equation 4 presents the correlation between Z and DBE, in which n is the number of N atoms.^{233,234} Assuming no N atoms, the precursor ions feature a DBE range from ~ 9 to 30. CID produces abundant fragments with DBE values that remain in the range of the precursors (Figure 25b), and a few products with slightly lower DBE. Therefore, the results are not conclusive for the presence of archipelago species, as it is difficult to determine if the high DBE precursors yield low DBE fragments, which is the basis to confirm the existence of multicore motifs. This shortcoming is solved by performing precursor ion isolation via stored waveform Fourier transform (SWIFT).⁸⁸

$$Z = -2(\text{DBE}) + n + 2 \quad (4)$$

Figure 26 presents the structural analysis of coal n_{C-7} -insoluble material. Soluble compounds were isolated from Illinois coal via Soxhlet extraction with Tol/THF/MeOH for 5 days. Subsequently, n_{C-7} -insoluble species were precipitated by heptane addition, and studied by FT-ICR MS.⁸⁸ Figure 26 presents a quadrupole isolation (Figure 26a), which is compared with the use of a mult notch SWIFT^{235,236} waveform (in addition to quadrupole isolation, Figure 26b). The mass-selective quadrupole (shown in Figure 9) was used to isolate precursor ions at $m/z \sim 460$ (Figure 26a, 4 Da window). The isolated precursors feature mass defects from ~ 0.0500 to 0.4000 Da, which translates into a wide range of DBE values, as noted by the DBE versus carbon number plot for monoheteroatomic precursor ions (N_1 , O_1 , S_1 , circled in red). Upon IRMPD, the fragmentation mass spectrum (Figure 26a, right side) features the low MWD (m/z 120–300, green dashed line) and the dealkylation fragmentation with similar abundances. The compositional range for precursors and fragments, combined in the same plot (Figure 26a, right side) demonstrates the production of high- and low-DBE fragments. However, since the quadrupole-isolated precursor ions span

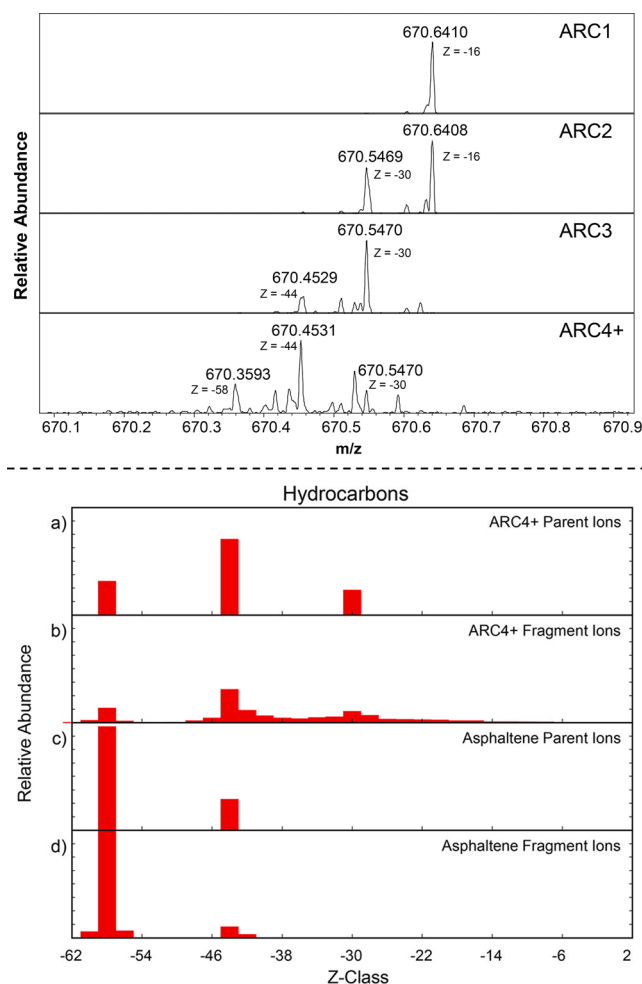


Figure 25. Upper panel: mass spectra (inset shows an expanded view) for single Dalton isolation of precursor ions for aromatic ring fractions from petroleum (ARC). Lower panel: relative abundance vs. hydrogen deficiency (Z number) for precursor ions and CID fragments for ARC4+ and asphaltenes. [Reproduced with permission from ref 231. Copyright 2017, American Chemical Society, Washington, DC.]

both low and high DBE values, it is impossible to determine whether or not the high DBE precursors yield low DBE fragments. This question can be answered by applying a mult notch SWIFT waveform (highlighted in purple, Figure 26b) to the quadrupole isolated ions once they are trapped inside the ICR cell. In this case, the application of the SWIFT waveform enables the isolation of ions with low mass defect/high DBE (mass defect < 0.250000 , DBE > 16) through the ejection of ions with higher mass defects that lie outside of the window (high SWIFT excitation amplitude). Therefore, only ions within a 4-Da isolation window with a mass defect of < 0.25000 Da remained in the ICR cell prior to IRMPD. The compositional range for the SWIFT-isolated precursor ions demonstrates the efficacy of the method, because only high-DBE precursors remain for subsequent IRMPD. The fragmentation mass spectrum of the high DBE species reveals both dealkylation (blue arrow) and the low MWD with reduced relative abundance, suggesting that high DBE precursors are a mixture of island and archipelago motifs. Therefore, the isolation and fragmentation method provide unambiguous evidence for the existence of archipelago motifs

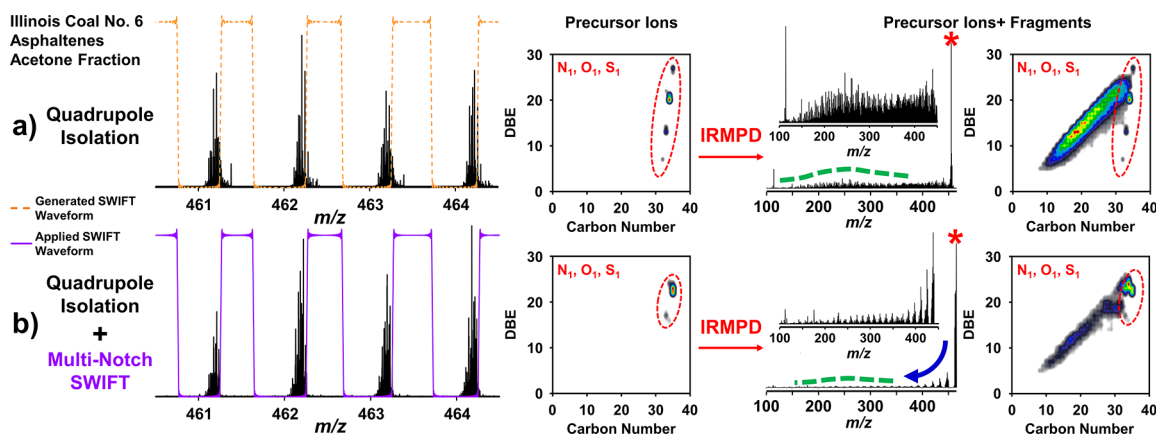


Figure 26. Structural characterization of coal asphaltenes performed by isolation of precursor ions via (a) mass-selective quadrupole with subsequent IRMPD, and (b) mass-selective quadrupole followed by application of a multinotch SWIFT waveform with subsequent IRMPD. [Reproduced with permission from ref 88. Copyright 2020, American Chemical Society, Washington, DC.]

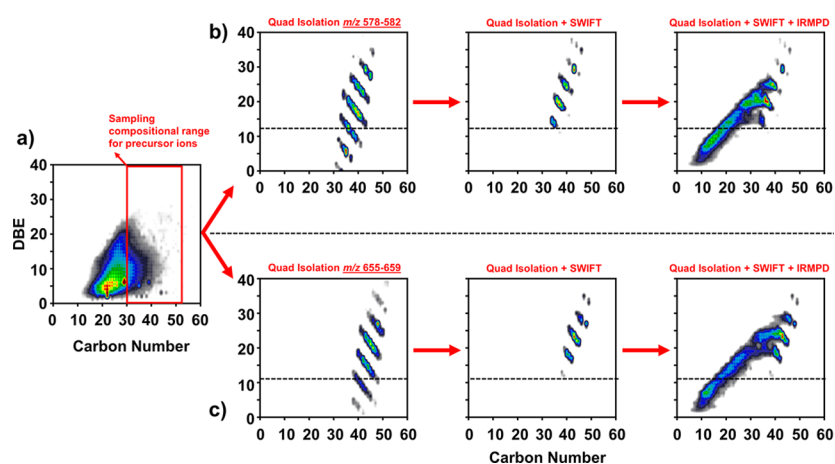


Figure 27. (a) Combined DBE vs carbon number plot for all compound classes for the interfacial material (IM) from the acetone fraction for Athabasca bitumen asphaltenes. The plot is obtained from the molecular formulas assigned to the peaks detected in the (+) APPI FT-ICR broadband mass spectrum. (b, c) Compositional range for precursor ions isolated by a mass-selective quadrupole (left) and mass-selective quadrupole + SWIFT multinotch (middle), and high DBE precursors plus their IRMPD fragments (right).

in Tol/THF/MeOH-soluble/*n*C₇-insoluble coal compounds, which, as stated above, present a compositional range with wide DBE range. The results are consistent with the existence of multicore motifs and their role in coal processability.²³⁷

Structural Characterization of Interfacially Active Asphaltenes. Figure 27 presents the structural characterization of high-*m/z* interfacially active asphaltenes extracted from the acetone fraction from Athabasca bitumen asphaltenes. The analysis was performed by (+) APPI FT-ICR MS and IRMPD.²⁰⁷ Figure 27a features the combined DBE vs carbon number plots for all the detected classes for the broadband mass spectra. As previously discussed, the IM from acetone Athabasca bitumen asphaltenes reveals an atypical compositional range, with abundant molecules with DBE values between ~2–25 and carbon numbers up to ~45. The sample is heteroatom-rich, because it presents abundant polyheteroatomic classes such as O₃S₂, O₄S₂, N₁O₃S₁; the heteroatom class distribution is shown in Figure 28. Furthermore, the red box in the DBE plot of Figure 27a highlights the compositional range for the precursor ions selected for IRMPD FT-ICR MS. In Figures 27b and 27c, the DBE vs carbon number plots to the left present the molecular composition for all the precursor ions isolated by the mass-selective quadrupole. The diagonals

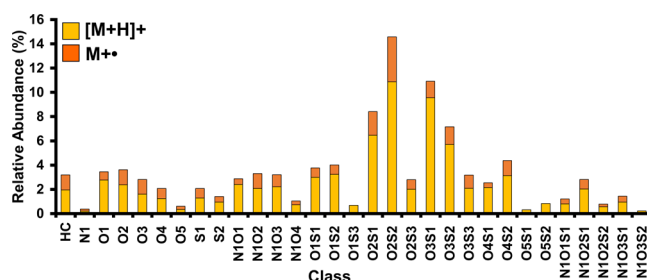


Figure 28. Heteroatom class distribution for the IM extracted from the acetone fraction from Athabasca bitumen asphaltenes. Data derived from (+) APPI 9.4 T FT-ICR MS. Radical cations and protonated molecules are highlighted in orange and yellow.

result from the high molecular complexity of the selected ions within a 4 Da isolation window, as they span different degrees of heteroatom content, carbon number, and mass defect (DBE/hydrogen deficiency). In this case, the precursor ions have DBE values from 1 to 40 and carbon numbers between 30–50. Many of those ions are not evident in the compositional range of the sample (Figure 27a, broadband mass spectrum), because of limitations in dynamic range. Segmented data acquisition, through a mass-selective quadrupole

pole, helps to mitigate this shortcoming, because the number of trapped charges inside the ICR cell, usually limited to $\sim 1 \times 10^6$, is distributed over fewer ions, which dramatically improves the signal-to-noise (S/N) ratio of the mass-isolated segment. Therefore, the quadrupole-isolated segments reveal compounds that are not easily detected in the broadband mass spectrum, because of their low S/N. The application of a multinotch SWIFT waveform ejects low DBE precursor ions (< 12) outside the ICR cell; thus, only high DBE precursors remain for IRMPD, as shown in the middle plots in Figures 27a and 27b. Finally, the plots to the right feature the molecular composition of the precursor ions and their IRMPD fragments. The abundant production of fragment ions with DBEs ≤ 12 demonstrates that interfacially active asphaltenes comprise abundant multicore motifs (archipelago) of 1–4-ring cores, as well as island structures that lose only carbon number during IRMPD.

Figure 28 presents the heteroatom class distribution for the IM extracted from the acetone fraction from Athabasca bitumen asphaltenes. The results indicate that $\sim 75\%$ of the produced ions are protonated molecules $[M + H]^+$, which points to dominant hydrogen bonding interactions in solution.¹⁹⁰ Furthermore, the sample contains abundant molecules with 4–7 heteroatoms, e.g., O_2S_2 , O_3S_1 , O_3S_3 , and O_5S_2 classes. Thus, compositional and structural data revealed by FT-ICR MS support the hypothesis that asphaltenes are a complex mixture of single-core and multicore motifs, with high and low DBE values, with up to seven heteroatoms per molecule, whose strong aggregation likely results from cooperative effects of several intermolecular forces, including hydrogen bonding, π -stacking, acid/base, and vdW interactions.

Collectively, FT-ICR MS results highlight that asphaltenes are an ultracomplex mixture of components that are insoluble in *n*-alkanes due to their polarity, ultrahigh aromaticity, and/or aggregation. The mixture includes island and archipelago structures in proportions currently unknown. However, it is clear that some samples are depleted in island motifs (e.g., Athabasca bitumen asphaltenes) and reveal abundant amounts of archipelago species with molecular weights from m/z 350 to m/z 700, and DBE (or aromaticity) from 10 to 40. The archipelago structures are enriched in heteroatomic groups. Nanoaggregation appears to occur extensively with archipelago structures, suggesting that it is driven by polar interactions. The least-soluble asphaltenes appear to be composed mainly of the more-polar asphaltenes, the molecular composition of which suggests that they are a mixture of high-DBE archipelagos (DBE > 20) and low-DBE species. Interfacially active asphaltenes also consist of the more-polar compounds. Hence, the results indicate that both the least-soluble and the interfacial asphaltenes are dominated by self-associating polar archipelago structures. However, the species responsible for strong aggregation tendencies are a significant limitation in asphaltene analysis, as shown in the following section via gel permeation chromatography coupled to FT-ICR MS.

Mass Spectrometry Coupled to GPC. *Gel Permeation Chromatography.* Advances in soft ionization methods, MS instrumentation, and MS data analysis for complex mixtures have enabled the coupling of chromatographic separations and high-resolution mass spectrometry.^{238–242} Development of high-field FT-ICR MS is central for data collection for complex mixture separation on a chromatographic time scale, e.g., as a function of elution in high-performance liquid chromatography

(HPLC). It is important to consider that, in FT-ICR MS, mass resolving power improves linearly, and dynamic range (S/N), charge capacity before peak coalescence, and mass accuracy improve quadratically with the magnetic field strength.²⁴³ For instance, Smith et al.^{244,245} reported the comparison between 9.4 and 21 T FT-ICR MS characterization of several complex mixtures, including Suwanee river fulvic acid standard, Gulf of Mexico crude oil from Macondo well, an asphalt volcano, and Canadian bitumen. For direct infusion experiments, it was demonstrated that 21 T FT-ICR MS yielded more than a 2-fold improvement for root-mean-square (RMS) assignment error, relative to 9.4 T FT-ICR MS. The results demonstrated that 21 T FT-ICR MS characterization consistently revealed greater numbers of assigned molecular formulas for a wide diversity of samples, ionized by different methods, e.g., APPI/ESI, positive/negative-ion modes. Generally, 21 T FT-ICR MS yielded mass-resolving powers superior to 2 700 000 at m/z 400, facilitating the resolution of mass differences of 0.53 mDa at $m/z > 600$ (molecular formulas differing in $H_8S_1^{34}S$ vs C_5N_1 content).²⁴⁵

Recently, Putman et al.¹⁹⁴ demonstrated that the 21 T FT-ICR mass spectrometer at the NHMFL is uniquely suited for online detection of chromatographic separations of complex mixtures. High magnetic field enables larger ion populations to be analyzed for each spectrum (single scan), for higher dynamic range, and enables a mass resolving power of $> 1\,600\,000$ at m/z 400 (3.1 s transient duration) and $> 2\,500\,000$ at m/z 400 (6.2 s transient duration). These features make possible MS data collection with chromatographic resolution while maintaining a high mass accuracy (RMS < 0.150 ppm). Figure 29a presents a single transient mass spectrum for the HPLC APPI 21 T FT-ICR MS analysis of an Arabian heavy distillate.²⁴⁶ The HPLC method was an aromatic ring separation that provided six major elution ranges: saturates, 1-ring, 2-ring, 3-ring, 4-ring, 5-ring plus “polar” compounds, and sulfides as shown in the extracted ion chromatogram (Figure 29b).²⁴⁷ Figure 29a presents the single transient result at a retention time of 27 min from the 2-ring elution range, collected with a 6.2 s transient length. The results demonstrate that a single-scan absorption-mode mass spectrum enables the assignment of 6451 molecular formulas with an RMS error of 0.120 ppm, a base peak signal-to-noise ratio of 855, and a resolving power of 3 200 000 at m/z 400. The mass expanded-view inset at m/z 683 accounts for the remarkable instrument performance. Therefore, the 21 T FT-ICR mass spectrometer is particularly well-suited for data collection, as a function of sample elution from LC separations, because the exceptional data quality obtained in a single scan avoids the need for coaddition of tens to hundreds of scans, which is required in direct infusion 9.4 T FT-ICR MS studies.

Recent reports demonstrate the successful coupling of asphaltene GPC fractionation and online (+) APPI 21 T FT-ICR MS detection.^{191,194} For example, compositional trends for vanadium-containing compounds in asphaltene GPC fractions were qualitatively accessed by (+) APPI 21 T FT-ICR MS. Semiquantitative results were obtained by ^{51}V -ICP-MS detection and used to hypothesize the “amount” of species accessed by APPI-MS. Figure 30 (upper panel) presents the GPC chromatograms obtained by ^{51}V -ICP-MS (black) and (+) APPI 21 T FT-ICR MS (total ion current, TIC), for whole PetroPhase 2017 asphaltenes. Semiquantitative results (ICP) indicate that most of the sample ($\sim 59\%$ integrated chromatogram area) consists of high-molecular-

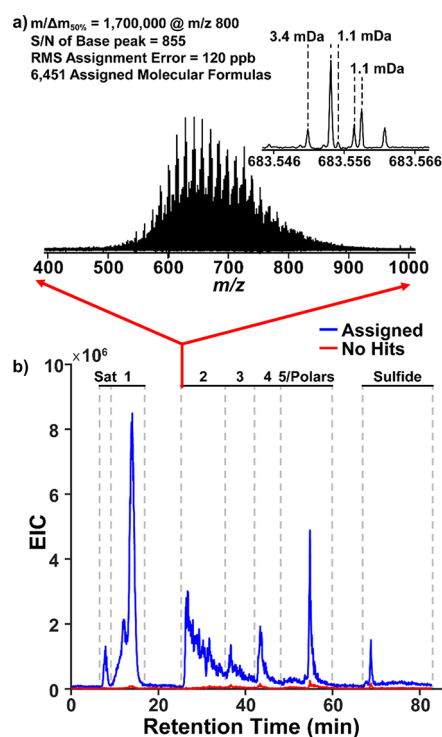


Figure 29. (a) Single transient mass spectrum from HPLC coupled to (+) APPI 21 T FT-ICR MS analysis of an Arabian heavy distillate. The data correspond to the data collected at 27 min (2-ring fraction). (b) Extracted ion chromatogram of molecular formula assignments and no hits. The dotted lines indicate the various fractions and highlight the elution points where the fractions should be collected for direct infusion experiments. [Reproduced with permission from ref 246. Copyright 2021, American Chemical Society, Washington, DC.]

weight (HMW) compounds. However, the ion current, as detected by (+) APPI FT-ICR MS (TIC), is maximum for the medium-molecular-weight (MMW) species, displaced toward the lower-molecular-weight (LMW) elution range.

It is essential to consider that the front end of the 21 T FT-ICR mass spectrometer is equipped with automatic gain control (AGC), a linear ion trap that performs a brief scan to determine the instantaneous number of charges. That measurement is used to determine the accumulation period (ion injection times (ITs)) required to meet the user-defined AGC target (number of charges optimal for data collection).^{248,249} For instance, in the study reported by Chacón-Patiño et al.,¹⁹¹ the AGC target was 1×10^6 charges. Figure 30 (lower panel) presents the accumulation period (ITs, blue), as a function of the elution volume. The ITs maxed out for HMW nanoaggregates and the elution regions with extremely low or no ^{51}V content (<20 mL and tailing). The monomer ion yield trend is highlighted in orange, calculated by eq 1, and consistent with the TIC. The results suggest an inverse correlation between the production efficiency of monomeric ions, MIY, and nanoaggregate size as determined by GPC. The extrography fractions for PetroPhase 2017 asphaltenes revealed trends remarkably similar to the whole sample: semi-quantitative results demonstrated a much higher content of HMW and MMW species; however, most of the ions detected by APPI-MS were produced from the LMW elution range. The intersection areas between the ICP-MS and FT-ICR MS chromatograms were used to hypothesize the fraction of species detected by (+) APPI FT-ICR MS. It was suggested

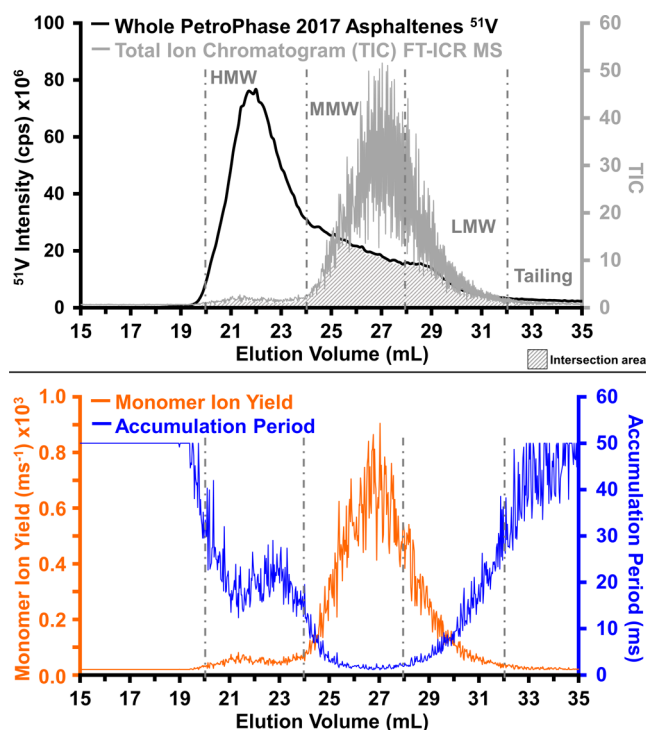


Figure 30. (Upper panel) GPC chromatograms for whole PetroPhase 2017 asphaltenes obtained by ^{51}V ICP-MS detection (black) and (+) APPI 21 T FT-ICR MS (gray). (Lower panel) ion injection time or accumulation period (ms) required to hit the AGC target of 1×10^6 charges (blue) and MIY (orange) calculated by eq 1; data derived from (+) APPI 21 T FT-ICR MS. [Reproduced with permission from ref 191. Copyright 2020, American Chemical Society, Washington, DC.]

the access extended to only $\sim 6\%$ – 37% of the sample, which proves that asphaltene analysis by APPI-MS remains highly limited, even with multiple fractionation steps, i.e., GPC separation of extrography fractions.

Compositional Trends as a Function of GPC Nanoaggregate Size. Figure 31 presents the extracted ion chromatogram (XIC), i.e., relative abundance as a function of elution time, for vanadyl porphyrins ($\text{N}_4\text{O}_1^{51}\text{V1}$ class) for PetroPhase 2017 asphaltenes obtained by GPC (+) APPI 21 T FT-ICR MS. The abundance-weighted H:C ratio as a function of elution time is plotted in red with the y -axis inverted. Figure 31 also presents the DBE vs carbon number plots for $\text{N}_4\text{O}_1^{51}\text{V}$ species detected at four specific elution times. The results indicate that the earliest-eluting vanadyl porphyrins (highly aggregated) are hydrogen-rich, with an abundance-weighted H:C ratio of ~ 1.25 . The displayed compositional ranges suggest that highly aggregated $\text{N}_4\text{O}_1^{51}\text{V}_1$ species (leftmost DBE vs carbon number plot) span the most extended carbon number range, which translates to a greater content of CH_2 units or longer homologous series. Carbon number range and H:C ratio decrease as a function of decreasing nanoaggregate size. The authors found, for a wide diversity of compound classes (e.g., S_1 , S_2 , $\text{N}_1\text{O}_2\text{S}_1$, O_1S_1 , N_1O_1), a direct correlation between a larger nanoaggregate size (early eluting species) and lower aromaticity/higher content of CH_2 moieties. Global and local compositional trends are consistent with several reports by Muller et al.,^{195,196} and they suggest that interactions between aliphatic moieties and aromatic cores (π -stacking) are

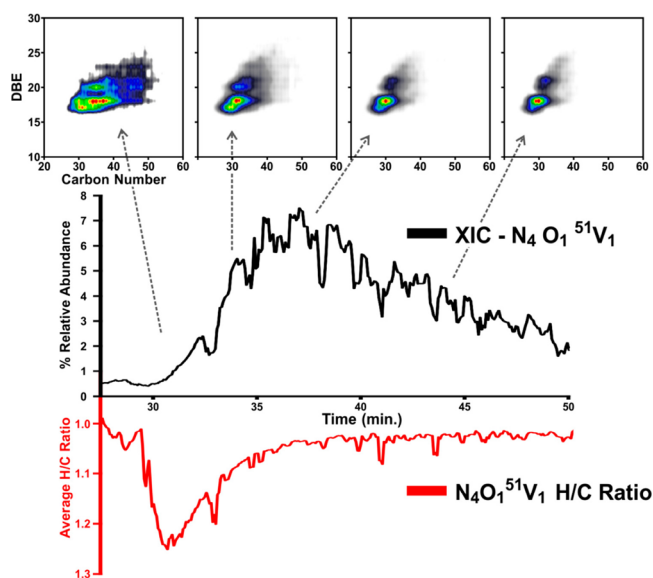


Figure 31. Extracted ion chromatogram (XIC) and DBE vs carbon number plots for the $N_4O_1^{51}V_1$ class (top) from the GPC APPI 21 T FT-ICR MS analysis of whole PetroPhase 2017 asphaltenes. The inverted chromatogram shows the average H/C ratio as a function of elution time (red). [Reproduced with permission from ref 250. Copyright 2020, American Chemical Society, Washington, DC.]

central intermolecular forces in the nanoaggregation of heteroatom-containing asphaltene molecules.

Figure 32 presents the compositional trends for sulfur-containing compounds for the GPC elution ranges for the acetone extrography fraction from PetroPhase 2017 asphaltenes. Figure 32a features the GPC ^{32}S ICP-MS chromatogram, along with the ion chromatograms (APPI FT-ICR MS) for S-containing heteroatomic groups: S_x , S_xO_y , and N_xO_ySz . For example, the group S_x includes S_1 , S_2 , S_3 , S_4 , and S_5 classes. The ion chromatograms of Figure 32a indicate that medium-/low-molecular-weight aggregates (MMW/LMW) exhibited the highest abundance of sulfur-containing species by (+) APPI FT-ICR MS. However, semiquantitative results demonstrate that nanoaggregation hampers MS detection, because ^{32}S ICP-MS shows much higher amounts of sulfur-containing molecules in the high-molecular-weight (HMW) elution range. Figure 32b presents the combined compositional range for sulfur-containing species detected for all of the spectra for each elution range. In other words, the molecular formulas used to make the DBE vs carbon number plots result from coadding all the spectra collected for each of the elution regions (HMW, MMW, LMW, and tailing GPC regions). Abundance-weighted H:C ratios are included and suggest that detectable species from sizable/larger aggregates have H:C ratios up to ~ 1.16 . Such compounds exhibit longer homologous series and low DBE values, which fits in the compositional range characteristic of interfacial material (HMW/MMW, group S_xO_y , DBE < 15). Conversely, less-aggregated/free molecules (LMW/tailing) feature much lower H:C ratios (0.61–0.74), abundant compounds with DBE values of >20, and shorter homologous series with a high relative abundance of ions close to the PAH limit, indicating the prevalence of highly aromatic/pericondensed asphaltenes.

It is essential to consider that ICP-MS data indicates that aggregated material is not fully detected by FT-ICR MS. The detected ions are possibly unbound molecules on the surface of

the nanoaggregates that are readily ionized. Therefore, it is likely that the MS-derived H:C ratios are not representative of aggregates. Given the significantly low H:C ratios for the LMW and tailing subfractions, we hypothesize HMW and MMW species are highly enriched in saturated moieties; therefore, their increased H:C ratios would offset the low values detected for LMW/tailing.

GPC FT-ICR MS results are consistent with several works that suggest that London forces between aliphatic moieties might be central in asphaltene aggregation.^{251–253} For instance, the self-aggregation nature of model asphaltene compounds, with varying content of aliphatic chains and heteroatomic functionalities, was tested by molecular dynamics simulations.²⁵⁴ The authors observed a direct correlation between increased dissociation energy and higher contents of aliphatic chains and heteroatoms. The authors concluded that the solubility behavior of petroleum asphaltenes should be ruled by a delicate balance between π -stacking (aromatic core size), heteroatom-based interactions (content of polarizable functionalities), and London forces between aliphatic side chains (entanglement of long aliphatic chains).

The results demonstrate that limitations for asphaltene MS analysis, posed by nanoaggregation, can be revealed with ICP-MS analysis of GPC fractions, which suggests the existence of two major types of chemistries: (a) the disaggregated fractions reveal a composition consistent with classical asphaltenes (highly aromatic, alkyl-depleted, and low-moderate heteroatom content), which preferentially ionizes over the (b) aggregated fractions (atypical low DBE values, higher alkyl-chain content, high levels of heteroatoms). The difficulty in vaporization/ionization of the aggregated asphaltene fractions suggests the use of thermal analysis to assist their molecular interrogation.

Thermal Analysis Coupled to FT-ICR MS. In addition to direct infusion high-resolution mass spectrometry and/or sophisticated fractionation combined with chromatographic attempts, the chemical nature of asphaltenes can also be approached by thermal analysis techniques, which are particularly useful for fractions with extremely low volatility/strong aggregation tendency.^{130,255} Here, an aliquot of the sample material, typically an amount of a few micrograms up to several milligrams, is thermally treated by a defined temperature protocol or heated to a specific set temperature. The highly viscous or solid asphaltenes can directly be analyzed with almost no sample preparation. The thermal decomposition of asphaltenes is strongly linked to the unwanted formation of coke and deposits in petroleum refining. Consequently, thermal analysis of asphaltenes has received increased attention in the last decades.

Generally, asphaltenes undergo three main pathways during thermal treatment, schematically presented in Figures 33a and 33b.²⁵⁶ The evaporation process can be separated into two phases: the desorption and pyrolysis phase. Nonevaporable material remains as a residue. Typically, predominant desorption is observed up to 300 °C, while pyrolysis starts between 300 °C and 350 °C.²⁵⁷ During the desorption phase, smaller, low-molecular-weight molecules are intactly evaporated, as a function of their boiling points. In the pyrolysis phase, high-molecular-weight compounds are thermally cracked.¹¹⁴ Species composed of several building blocks, i.e., archipelago, are likely cracked at their aliphatic bridges.^{54,258} Compounds containing one highly aromatic core, i.e., island, are known to cleave their alkyl side chains during thermal degradation. If the pyrolysis fragments are evaporable, they will

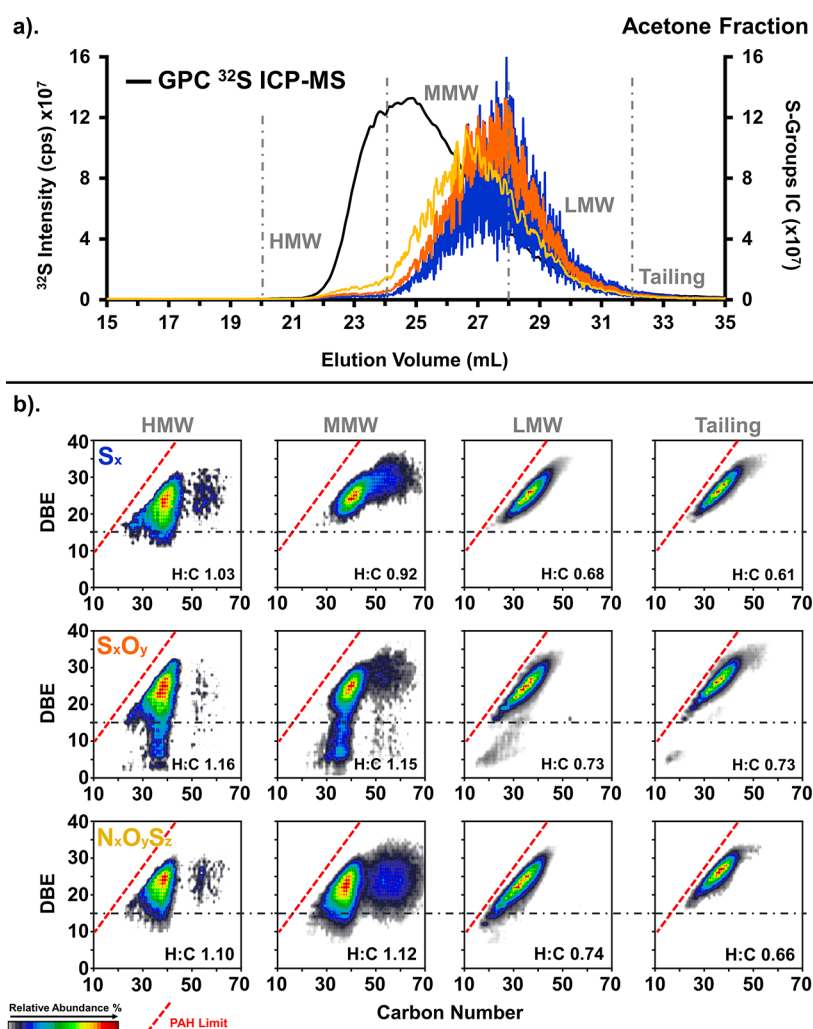


Figure 32. (a) GPC ^{32}S ICP-MS and APPI 21 T FT-ICR MS-derived ion chromatograms for sulfur-containing groups for the acetone fraction from PetroPhase 2017 asphaltenes. (b) Combined DBE vs carbon number plots for S_x , S_xO_y , and $\text{N}_x\text{O}_y\text{S}_z$ groups for each elution range. [Reproduced with permission from ref 191. Copyright 2020, American Chemical Society, Washington, DC.]

be detected during evolved gas analysis; otherwise, highly aromatized compounds remain as coke in the residue.^{259,260}

Evolved gas analysis (EGA) from the thermal analysis of complex mixtures is performed with various analytical methods.²⁶¹ With respect to the extreme molecular complexity of asphaltenes or petroleum fractions in general, FT-ICR MS detection is most often favored. From an instrumental perspective, this process is frequently achieved by hyphenation of an external thermobalance or thermogravimetry (TG) unit to mass spectrometric detection or by the usage of a direct inlet probe (DIP) evaporating the material directly inside the ion source of the mass spectrometer, either at atmospheric pressure or under vacuum conditions.^{262–271} Moreover, pyrolysis gas chromatography mass spectrometry (Py-GCMS) might also be assigned to this group, but that will not be discussed here.

Thermogravimetry (TG) enables tracking the mass loss directly as a function of temperature or heating period. For petroleum-derived material, thermogravimetric analysis (TGA) is frequently applied to determine bulk parameters such as mass loss or coke yield.^{114,130,270} Because of its temperature profile, the thermal analysis process can be seen as a separation method, reducing the complexity of the spectra compared to

direct infusion.^{263,265,272–275} A recent report discusses the evolved gas pattern of various heavy oil fractions and corresponding asphaltene fractions ($n\text{C}_5\text{--C}_7$).¹¹⁴ High-energy collision-induced dissociation was deployed to study the dominant core structural motifs after dealkylation. Asphaltenes are known to aggregate even at low concentrations, and maltenic compounds can be occluded by asphaltenes in pores or via polar interactions. It could be shown that poorly heptane-extracted asphaltenes contain a variety of occluded species, which are partially released from the aggregates at lower temperatures in the desorption phase up to 300 °C.^{114,256} The chemical signature (compound class distribution and DBE pattern) and abundance of this occluded material differs strongly, depending on the precipitation solvent and the pyrolysis pattern of the asphaltenes at higher temperatures.

Occluded compounds can significantly distort the chemical characterization of asphaltenes, e.g., by causing strong matrix effects and ion suppression in mass spectrometric analysis. Consequently, increased efforts were made to generate “cleaned” heptane-extracted asphaltene fractions provided for thermal analysis–mass spectrometry in the interlaboratory study for the PetroPhase 2017 conference. That material was

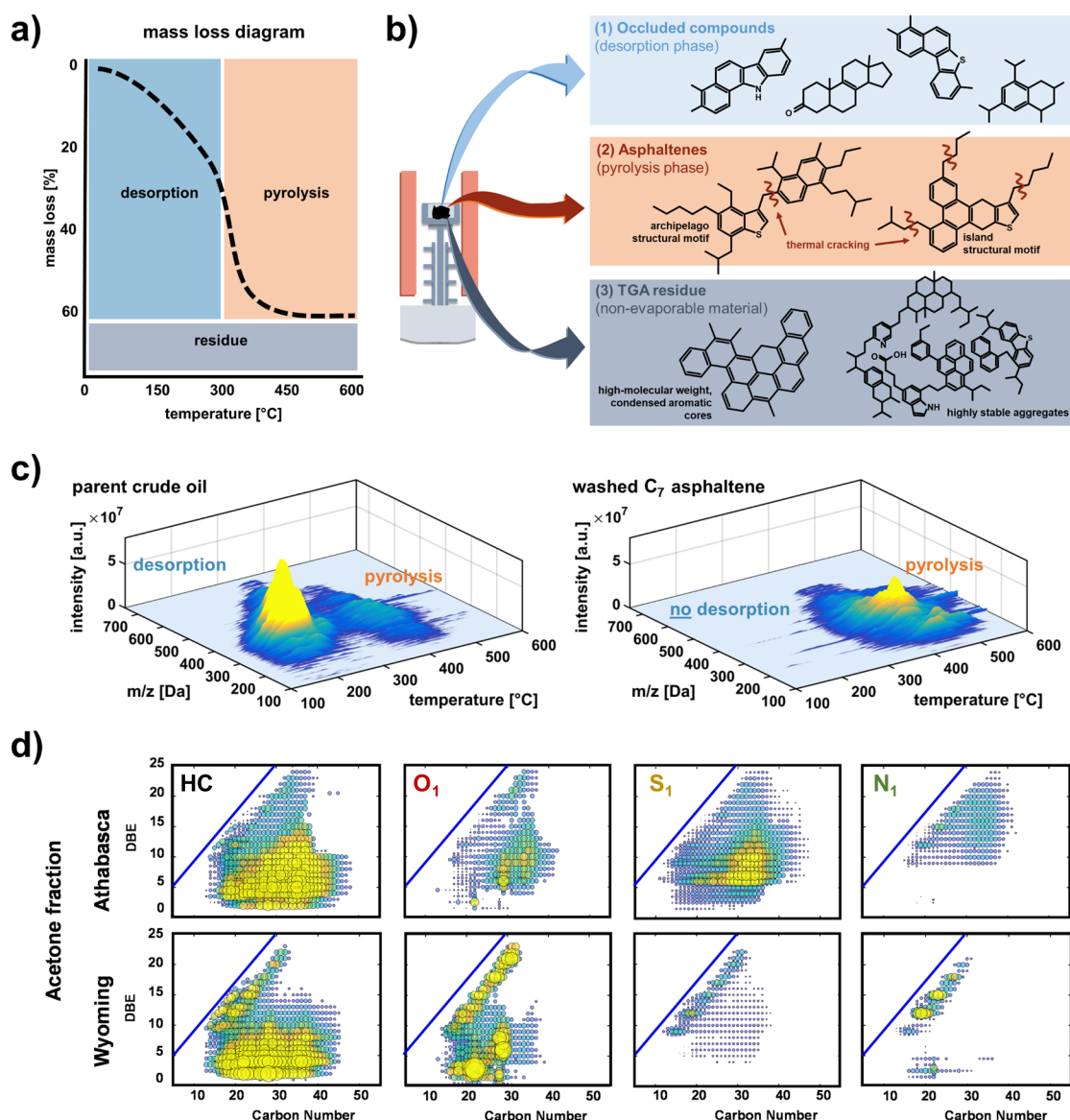


Figure 33. Compilation of thermal analysis mass spectrometry of asphaltenes. (a) Characteristic mass loss diagram obtained by thermogravimetry measurement of petroleum-derived material. (b) The three main reaction pathways petroleum-derived material undergoes during thermal analysis. Smaller components are intactly desorbed, whereas high-molecular-weight compounds are decomposed into smaller pyrolysis fragments. Nonevaporable material remains as coke in the residue. (c) Survey diagram of temperature versus m/z for the thermogravimetric high-resolution mass spectrometric analysis of a crude oil (left) and the exhaustively extracted nC_7 PetroPhase 2017 asphaltenes (right). (d) Compound class resolved carbon number vs DBE plots for the pyrolysis step for the acetone fraction from Wyoming deposit and Athabasca bitumen asphaltenes. The gas mixture evolved from thermogravimetric hyphenation was analyzed by atmospheric pressure chemical ionization coupled to ultrahigh-resolution mass spectrometry (TG APCI FT-ICR MS). The blue line indicates the planar aromatic limit. [Reproduced with permission from ref 256. Copyright 2021, American Chemical Society, Washington, DC.]

highly purified through repeated Soxhlet extraction with *n*-heptane.¹²⁸ No occluded compounds evaporating below ~ 300 °C were found (Figure 33c). TG FT-ICR MS, thermal analysis coupled to vacuum ionization time-of-flight mass spectrometry, and Pyr-GCMS did not reveal any considerable signals for temperatures associated with intact desorption. During the pyrolysis phase, starting at 300–350 °C, asphaltenes experience fragmentation of C–C or C–S bonds. At first glance, unusually low complexity is commonly exhibited by thermal analysis, because of pyrolytic cracking.^{43,54} If multicore asphaltenes, containing heteroatoms in different cores, are thermally cracked into smaller building blocks, the complexity of the compound classes and heteroatom number is reduced.

Single-core, multiheteroatom asphaltenes with high polarity and large aromatic moieties likely form coke instead of being evaporated. Nonetheless, the combination of this molecular pyrolysis pattern from the thermal analysis techniques, with additional information from field desorption/ionization mass spectrometry and elemental analysis, allowed one to propose an average molecular structure.

Consequently, the most recent study on TG FT-ICR MS of asphaltenes focused on the solubility fractions of island/single-core- (Wyoming) and archipelago/multicore-enriched (Athabasca) asphaltenes. Notably, the extrographic fractions exposed occluded materials released during the desorption phase (<300 °C), not observed during the analysis of whole asphaltenes. In

particular, the acetone fraction revealed a high abundant signal. Thus, it is indicated that highly occluded material is potentially bonded by polar interactions into cooperative aggregates formed by asphaltene molecules of different solubility fractions. During the fractionation process, these aggregates seem to partially be dispersed, enabling the release of smaller, occluded compounds during the desorption phase. The released occluded material differs in chemical composition as well as structure among the solubility fractions, depending on the geological origin of the asphaltene sample.

It could be shown that the island-type enriched sample revealed a significantly higher coke residue after pyrolysis than the archipelago-type enriched material. More importantly, the whole asphaltene yielded a higher residue than their solubility fractions. That result suggests cooperative aggregation between asphaltene molecules of different fractions. The aggregates were hypothesized to be highly thermally stable, which likely led to coke formation instead of thermal decomposition into smaller, evaporable pyrolysis products (see Figure 33b). In 2011, Gray et al. described that highly stable aggregates may survive the heating process and form coke instead of being thermally degraded into smaller, evaporable products.¹⁴ Moreover, the molecular fingerprint of the pyrolysis phase revealed a bimodal behavior, suggesting the presence of both structural motifs in each asphaltene. DBE vs carbon number plots of these patterns revealed specific compositional trends: compounds with high DBE values and short alkylation are likely to be originated from island-type asphaltenes by the cleavage of alkyl side chains from the single, highly aromatic core. In contrast, species with low DBE values and high carbon numbers likely derive from archipelago-type asphaltenes by the thermal decomposition of alkyl linkers bridging several aromatic cores. Notably, comparable characteristic shifts could be revealed for direct-infusion IRMPD FT-ICR MS. Thus, thermal analysis techniques serve as an additional complementary approach and supplement the results obtained by direct infusion high-resolution mass spectrometry. Combining the mass loss information with the molecular fingerprint visualized by DBE vs carbon number plots serves as a measure for the dominance of a structural motif.

With high-resolution mass spectrometric platforms now more frequently available, the usage of direct inlet probe (DIP) approaches for the chemical description of heavy petroleum fractions has become more accessible. Recently, bitumen, a heavy distillate fraction of petroleum containing considerable amounts of asphaltenes, was the focus of several studies. DIP measurements of various polymer-modified bitumen samples at atmospheric pressure enabled characterization of the highly complex aromatic hydrocarbon pattern aside from the thermal degradation of the polymeric additives. Moreover, DIP investigation of bitumen at reduced pressure made it possible to intactly evaporate even larger compounds than atmospheric-pressure DIP. Evaporation prior to thermal decomposition helped to distinguish the origin of various bitumen samples based on their molecular fingerprint. Electron ionization particularly allows one to trace the pattern of large PAHs. The authors believe that vacuum DIP can be a highly valuable concept for future asphaltene research. The use of thermal analysis supports the existence of both island and archipelago structural motifs for asphaltenes and can help predict/anticipate the dominance of one motif over the other, allowing for new insight into be gained about how asphaltene samples will behave during industrial processing such as pyrolysis.

■ CONCLUDING REMARKS AND FUTURE DIRECTIONS

The use of FT-ICR MS as a molecular-level elemental analyzer provides exceptional opportunities to understand the chemistry of ultracomplex mixtures. Ultrahigh mass accuracy, achieved only by high-field FT-ICR MS, enables the assignment of a unique molecular formula/elemental composition to each peak detected in a mass spectrum. However, the mass-spectrometry/petroleum community should consider a key limitation of the technique: the relative abundances observed in FT-ICR-MS are not fully representative of the molar composition of the samples, because of selective ionization. Regardless of this limitation, after studying asphaltenes for over 10 years, via ultrahigh-resolution mass spectroscopy assisted by separations and gas-phase fragmentation, we have learned a series of lessons that can be summarized as follows:

- First, “*in science, mistakes always precede the truth.*” Preliminary data published in the 2000s for an “asphaltene” sample, ionized by (+) ESI, fragmented by low-energy CID, and analyzed by FT-ICR MS, suggested the dominance of single-core motifs. Advances over the past decade have revealed that the resulting conclusions were misleading, because of coprecipitation of maltenic species, limitations from selective ionization, and the use of inefficient gas-phase fragmentation.
- Asphaltenes are ultracomplex mixtures. Some samples, such as Arabian heavy nC_7 asphaltenes (known as PetroPhase 2017) can expose up to ~ 200 peaks *per nominal mass* in broadband FT-ICR MS, and up to ~ 500 peaks if a mass-selective quadrupole is used to isolate precursor ions prior to fragmentation. Therefore, an ultrahigh mass resolving power ($<700\,000$ at $m/z\ 650$) is needed to understand asphaltene molecular composition. Analysis with lower-performance mass analyzers, offering a resolving power below $700\,000$ at $m/z\ 650$, are deceptive, because they enable limited access to the elemental compositions of thousands of ions in broadband and tandem-MS studies. It is critical to highlight that many reports that have supported the exclusive dominance of island motifs in petroleum asphaltenes are based on time-of-flight and linear trap quadrupole mass spectroscopy, whose performance makes possible the resolution of a few peaks per nominal mass (only $\sim 2-5$).
- Ultrahigh mass resolving power alone is insufficient to understand the molecular composition of asphaltenes. Petroleum polydispersity in terms of carbon number, aromaticity, heteroatom content, chemical functionality, molecular structure, aggregation, and solubility, results in a wide range of ionization efficiencies. Thus, asphaltenes, as well as other complex mixtures (e.g., organic aerosols, dissolved organic matter), suffer from selective ionization. The first indication of this effect was the different values between bulk H:C ratios and MS-derived results. Collective data suggest that APPI, LDI, and custom-built ion sources, e.g., L^2MS , are similarly biased toward the selective ionization of hydrogen-deficient asphaltene molecules.
- Separation methodologies based on, e.g., differential precipitation, chromatography, extrography, and/or chemical functionality are critical to access species that remain undetected during whole sample analysis.

Characterization of the extrography fractions reveals that island-enriched samples, i.e., acetone fraction, ionize up to ~50-fold more efficiently than archipelago-enriched fractions. Notably, the MS-derived H:C ratios that result from averaging the values for the extrography fractions are closer to the bulk H:C composition.

- Effective gas-phase fragmentation methods (high-energy CID, IRMPD) are required for understanding petroleum molecular structure. It is critical to highlight the need for measuring the elemental composition of the individual precursor ions and their fragments. Two general fragmentation pathways have been identified for petroleum species: (1) dealkylation, dominant for island motifs, in which the ions lose carbon number but remain with constant DBE; (2) fragmentation of covalent bridges between aromatic cores of archipelago species, which produces a low molecular weight distribution ($\sim 90 < m/z < 350$) of fragments with lower carbon number and DBE values than the precursor ions. Several controlled experiments indicate that the structural analysis of petroleum samples via APPI FT-ICR MS and IRMPD is accurate and reflects the molecular composition/structure of the samples. Notably, under the same experimental conditions, different samples reveal a different fragmentation behavior, e.g., Wyoming deposit and Athabasca bitumen asphaltenes, which appear to correlate with product yields from thermal cracking processes.
- Selective ionization has misled how the petroleum community understood, for years, the gas-phase fragmentation behavior of petroleum asphaltenes. For instance, whole South American medium asphaltenes reveal abundant island structures. The sample consists of ~28 wt % of acetone (island dominant) and ~50 wt % of Tol/THF/MeOH fraction (archipelago dominant), as determined by extrography separation. However, given the much higher ionization efficiency of the acetone species, archipelago motifs can be accessed only upon extrography fractionation.
- The ratio archipelago/island is dependent on the sample (e.g., Wyoming deposit vs Athabasca bitumen), extrography fraction (acetone vs Tol/THF/MeOH), and increases as a function of m/z .
- What precipitates with nC_7 is a complex mixture of highly aromatic compounds and low-DBE molecules. Archipelago species have been detected for precursor ions with a wide range of DBE values (15–40). Those low-DBE atypical species exhibit high heteroatom content (e.g., O_4S_2 class). Thus, their insolubility in nC_7 can be viewed as molecular insolubility, because of high dipolar constants (given the high heteroatom content) and/or nanoaggregate insolubility, as a result of strong aggregation. However, since mass spectrometry is not inherently quantitative, methods/validations are further required to support this conclusion.
- Aggregation limits asphaltene characterization by MS. Asphaltenes were analyzed by GPC coupled to online APPI FT-ICR MS detection. Most of the ions were produced from disaggregated GPC fractions, revealing a compositional range consistent with classical asphaltene chemistry: high aromaticity, limited alkyl substitution, and low heteroatom content. Conversely, detected ions from highly aggregated GPC fractions are likely “free”

molecules on the aggregates’ surface and reveal a compositional range featured by low aromaticity but high heteroatom content (up to 6–7 atoms per molecule). Thus, the results indicate that aggregation continues to challenge the existent MS instrumentation for asphaltenes characterization. Future work should focus on disaggregating the aggregated material prior to or during the ionization process.

Thus, the future of ultrahigh-resolution FT-ICR MS in petroleum/asphaltene science has come full circle, back to the same issue that was raised when it was first applied to asphaltenes in the 2000s, which was concisely summarized by Dr. Howard Freund when he asked, “how do you know what you’re not seeing”, at one of the early PetroPhase meetings. Although the lessons described herein expand our compositional knowledge of “heavy” high boiling petroleum species (asphaltenes included), strongly support the Boduszynski continuum model, expose both island and archipelago structural motifs, underscore the importance of heteroatom chemistry, and reveal the need for fractionation prior to mass spectral characterization, aggregation remains the primary obstacle for ultimate molecular characterization. Hence, future efforts to disrupt asphaltene (nano)aggregates to reveal the species within will be paramount. Regardless, no single analytical technique can address the structural and chemical complexity of asphaltenes and/or their unique aggregation behavior. The greatest insight to date has been gleaned from a diverse collection of methods that seek to disassemble the complexity based on both chemical and structural information provided by past research efforts. Chemical functionality targeted fractionation methods, like those proposed by Boduszynski, combined with the latest structurally targeted fractionation methods (extrography), provide potentially useful steps forward to correlate structure/chemistry to process behaviors/products and insight into the more efficient use of the “bottom of the barrel” for future energy and material science applications.

■ AUTHOR INFORMATION

Corresponding Authors

Martha L. Chacón-Patiño – National High Magnetic Field Laboratory, Florida State University, Tallahassee, Florida 32310, United States; International Joint Laboratory–iC2MC: Complex Matrices Molecular Characterization, TRTG, 76700 Harfleur, France; orcid.org/0000-0002-7273-5343; Email: chacon@magnet.fsu.edu

Ryan P. Rodgers – National High Magnetic Field Laboratory, Florida State University, Tallahassee, Florida 32310, United States; International Joint Laboratory–iC2MC: Complex Matrices Molecular Characterization, TRTG, 76700 Harfleur, France; Department of Chemistry and Biochemistry, Florida State University, Tallahassee, Florida 32306, United States; E2S UPPA, CNRS, IPREM, Institut des Sciences Analytiques et de Physico-chimie pour l’Environnement et les Matériaux, Université de Pau et des Pays de l’Adour, 64053 Pau, France; orcid.org/0000-0003-1302-2850; Email: rodgers@magnet.fsu.edu

Authors

Murray R. Gray – University of Alberta and Alberta Innovates, Calgary, AB T2L 2A6, Canada

Christopher Rüger – Joint Mass Spectrometry Centre (JMSC)/Chair of Analytical Chemistry, University of Rostock, 18059 Rostock, Germany; Department Life, Light & Matter (LLM), University of Rostock, 18051 Rostock, Germany; orcid.org/0000-0001-9634-9239

Donald F. Smith – National High Magnetic Field Laboratory, Florida State University, Tallahassee, Florida 32310, United States; orcid.org/0000-0003-3331-0526

Taylor J. Glattke – Department of Chemistry and Biochemistry, Florida State University, Tallahassee, Florida 32306, United States; orcid.org/0000-0003-2934-0749

Sydney F. Niles – Department of Chemistry and Biochemistry, Florida State University, Tallahassee, Florida 32306, United States; orcid.org/0000-0002-3487-6612

Anika Neumann – Joint Mass Spectrometry Centre (JMSC)/Chair of Analytical Chemistry, University of Rostock, 18059 Rostock, Germany; Department Life, Light & Matter (LLM), University of Rostock, 18051 Rostock, Germany; orcid.org/0000-0001-7256-3716

Chad R. Weisbrod – National High Magnetic Field Laboratory, Florida State University, Tallahassee, Florida 32310, United States; orcid.org/0000-0001-5324-4525

Andrew Yen – Ennova LLC, Stafford, Texas 77477, United States

Amy M. McKenna – National High Magnetic Field Laboratory, Florida State University, Tallahassee, Florida 32310, United States; orcid.org/0000-0001-7213-521X

Pierre Giusti – International Joint Laboratory–iC2MC: Complex Matrices Molecular Characterization, TRTG, 76700 Harfleur, France; TotalEnergies Refining and Chemicals, TotalEnergies Research and Technologies Gonfreville, 76700 Harfleur, France; orcid.org/0000-0002-9569-3158

Brice Bouyssiere – International Joint Laboratory–iC2MC: Complex Matrices Molecular Characterization, TRTG, 76700 Harfleur, France; E2S UPPA, CNRS, IPREM, Institut des Sciences Analytiques et de Physico-chimie pour l'Environnement et les Matériaux, Université de Pau et des Pays de l'Adour, 64053 Pau, France; orcid.org/0000-0001-5878-6067

Caroline Barrère-Mangote – International Joint Laboratory–iC2MC: Complex Matrices Molecular Characterization, TRTG, 76700 Harfleur, France; TotalEnergies Refining and Chemicals, TotalEnergies Research and Technologies Gonfreville, 76700 Harfleur, France

Harvey Yarranton – Department of Chemical and Petroleum Engineering, Schulich School of Engineering, University of Calgary, Calgary, Alberta T2N 1N4, Canada; orcid.org/0000-0002-7726-5061

Christopher L. Hendrickson – National High Magnetic Field Laboratory, Florida State University, Tallahassee, Florida 32310, United States; Department of Chemistry and Biochemistry, Florida State University, Tallahassee, Florida 32306, United States

Alan G. Marshall – National High Magnetic Field Laboratory, Florida State University, Tallahassee, Florida 32310, United States; Department of Chemistry and Biochemistry, Florida State University, Tallahassee, Florida 32306, United States; orcid.org/0000-0001-9375-2532

Complete contact information is available at:
<https://pubs.acs.org/10.1021/acs.energyfuels.1c02107>

Notes

The authors declare no competing financial interest.

Biographies

Dr. Martha L. Chacón-Patiño obtained her Ph.D. at Universidad Industrial de Santander, in Bucaramanga-Colombia, and she has been a member of the National High Magnetic Field Laboratory since 2016. Dr. Chacón-Patiño is an expert in analytical chemistry, with a focus on the characterization of complex organic mixtures by separations and ultrahigh-resolution mass spectrometry. In the last 10 years, she has explored the molecular composition of one of the most complex organic mixtures, the asphaltenes, and their role as precursors of emerging/water-soluble contaminants in the built environment.

Murray R. Gray is Professor Emeritus of Chemical Engineering at University of Alberta and Senior Technical Advisor at Alberta Innovates. He has over 30 years of research experience in the upgrading of heavy oil and oil sands bitumen. Gray obtained his Ph.D. in Chemical Engineering from the California Institute of Technology in 1984. He also holds a M. Eng. degree from the University of Calgary (1980) and a B.Sc. degree in Chemical Engineering from the University of Toronto (1978).

Christopher P. Rüger received his Ph.D. degree in 2018 with distinction (*summa cum laude*) from the University of Rostock, Germany. His research focuses on developing novel techniques in high-resolution mass spectrometry for complex mixtures analysis, particularly thermal analysis coupling and photoionization. During his Postdoc at the University of Rouen-Normandy (Prof. Afonso), he broadened his focus toward ion mobility spectrometry. Currently, he is group leader for high-resolution mass spectrometry and habilitation candidate at the University of Rostock.

Donald F. Smith received his Ph.D. from Florida State University in 2008, with a focus on FT-ICR MS instrumentation and complex mixture analysis. His research has focused on new instrumentation, ionization, and methods for high-resolution mass spectrometry. Currently, he manages the Proteomics, Metabolomics, and Mass Spectrometry facility at Montana State University in Bozeman, MT.

Taylor J. Glattke received her B.S. degree in chemistry from Spring Hill College in 2018. She began her Ph.D. in analytical chemistry at Florida State University under the mentorship of Dr. Alan Marshall and Dr. Ryan Rodgers in 2018 and earned her M.S. degree in May 2021. She currently works as a graduate student at the National High Magnetic Field Laboratory where she uses ultrahigh-resolution mass spectrometry to study photoproducts generated from the photo-oxidation of fossil-fuel-derived products and their impact on the environment and public health.

Dr. Sydney F. Niles obtained her B.S. degree in chemistry from the University of Michigan in 2016 and her Ph.D. degree in analytical chemistry from Florida State University in 2020. Her graduate research was conducted with advisors Dr. Alan Marshall and Dr. Ryan Rodgers at NHMFL and probed the molecular transformation of fossil fuels in the environment using FT-ICR MS. Currently, she is the lead scientist for the high-resolution mass spectrometry facility at Honeywell UOP, where she uses FT-ICR MS to improve and develop new refinery processes.

Anika Neumann received her Ph.D. degree in 2021 from the University of Rostock, Germany, working on thermal analysis high-resolution mass spectrometry on complex petrochemical materials in the working group of Prof. Ralf Zimmermann. She is currently performing a Postdoc in the same working group, studying the deposition behavior of fossil distillates and heating oils from

alternative feedstocks utilizing thermal analysis and gas chromatographic techniques.

Chad R. Weisbrod received a Ph.D. degree in 2013 from the University of Washington, working on FT-ICR MS instrumentation. He was a Visiting Scholar at the National High Magnetic Field Laboratory during the 21 T FT-ICR MS project. Chad also worked as a Senior Scientist at the Thermo Fisher Mass Spectrometry Research and Development team in San Jose, CA, with a focus on tandem MS and high-resolution analyzer development. He now is a member of the Research Faculty for the National High Magnetic Field Laboratory with a focus on instrumentation development.

Andrew Yen obtained his Ph.D. degree in Chemistry from the University of Michigan and is currently the Director of Chemical Services at ENNOVA LLC in Stafford, TX. He has more than 20 years of research and development experience in the areas of flow assurance and, oil sand and production chemistry. He has coauthored more than 50 papers.

Dr. Amy M. McKenna is an analytical environmental and petroleum chemist and Research Faculty III and manages the Ion Cyclotron Resonance user facility at the National High Magnetic Field Laboratory, an NSF-funded user laboratory. Since 2009, her research has focused on analytical method development for complex organic mixtures, such as petroleum, asphaltene, weathered oil, and natural organic matter that utilize FT-ICR mass spectrometry.

Dr. Pierre Giusti obtained his Ph.D. degree in analytical chemistry from the University of Pau and Pays de l'Adour in 2006. He is currently the manager of the Molecular Separation and Identification Service in the R&D department of TotalEnergies Refining & Chemicals. He is the cofounder of the International Laboratory on Complex Matrices Molecular Characterization (iC2MC) laboratory, and he also obtained the position of CNRS Research Director in January 2021. His research interests are the elemental and molecular analyses of complex matrices in the field of energy.

Brice Bouyssiere is a professor of analytical chemistry at the University of Pau and is one of the cofounders of the iC2MC Laboratory. After attending Chemical and Process Engineering School (ENSGTI) and obtaining a Ph.D. degree dealing with the speciation of mercury and arsenic in gas condensates at the University of Pau, he did postdoctoral work at the GKSS Geesthacht, Germany. His principal research interest is metal speciation in complex matrices.

Caroline Barrère-Mangote obtained her Ph.D. degree in MS and NMR at Aix-Marseille University in 2011. Then, she worked as a postdoc at Normandy University on the development of innovating analytical methods for polymers and petroleum samples by (IM)MS. Since 2014, she has been LC Laboratory Manager in the R&D department of TotalEnergies Refining & Chemicals. Her areas of research include fractionation and elemental speciation in petroleum samples, pyrolysis oils (plastic or bio), or biocrude.

Harvey Yarranton is a Professor of Chemical and Petroleum Engineering at the University of Calgary. He received his B.Sc. (1985) and Ph.D. (1997) degrees in Chemical Engineering from the University of Alberta. Between degrees, he worked for Dome Petroleum, Ltd. and Amoco Canada, Ltd. in reservoir, production, and operations engineering. His research interests include the phase behavior and properties of heavy oils and solvents, the fundamentals and treatment of water-in-oil emulsions, and oil sands extraction and froth treatment.

Christopher L. Hendrickson obtained a B.A. degree from the University of Northern Iowa (1990) and a Ph.D. degree in Analytical Chemistry from The University of Texas at Austin (1995). After that,

he was a postdoctoral researcher at the National High Magnetic Field Laboratory with Professor Alan G. Marshall. Dr. Hendrickson is currently Director of the Ion Cyclotron Resonance Program at the National High Magnetic Field Laboratory and Distinguished University Scholar at Florida State University in Tallahassee, FL.

Alan G. Marshall obtained his B.A. degree from Northwestern University in 1965 and a Ph.D. degree from Stanford University in 1970. After that, he spent 11 years at the University of British Columbia and 13 years at The Ohio State University; in 1993, he moved to Florida State University, where he is Lawton Professor of Chemistry and Biochemistry, and Chief Scientist for the NHMFL Ion Cyclotron Resonance Program. He coined Fourier transform inductively coupled resonance (ICR) mass spectrometry. His current research includes FT-ICR instrumentation development, complex mixture analysis, and mapping protein structures.

Ryan P. Rodgers received a B.S. degree in chemistry from the University of Florida, and a Ph.D. degree in analytical chemistry from Florida State University. After a postdoctoral appointment at Oak Ridge National Laboratory, he joined the Ion Cyclotron Resonance Program at the National High Magnetic Field Laboratory (Florida State University). He is currently a Research Faculty III, the Director of the Future Fuels Institute, an FSU Distinguished University Scholar, and a past Associate Editor of *Energy and Fuels*.

■ ACKNOWLEDGMENTS

This work was supported by the National Science Foundation Division of Chemistry (No. DMR-1644779), Florida State University, and the State of Florida. The authors thank Greg Blakney for help with data calibration and Yuri E. Corilo for PetroOrg software.

■ REFERENCES

- (1) Ruiz-Morales, Y.; Wu, X.; Mullins, O. C. Electronic Absorption Edge of Crude Oils and Asphaltene Analyzed by Molecular Orbital Calculations with Optical Spectroscopy. *Energy Fuels* **2007**, *21* (2), 944–952.
- (2) Herod, A. A. Limitations of Mass Spectrometric Methods for the Characterization of Polydisperse Materials. *Rapid Commun. Mass Spectrom.* **2010**, *24* (17), 2507–2519.
- (3) Akbarzadeh, K.; Zhang, D.; Creek, J.; Jamaluddin, A. J.; Marshall, A. G.; Rodgers, R. P.; Mullins, O. C. Asphaltene—Problematic but Rich in Potential. *Oilfield Rev.* **2007**, *19* (2), 22–43.
- (4) McKenna, A. M.; Blakney, G. T.; Xian, F.; Glaser, P. B.; Rodgers, R. P.; Marshall, A. G. Heavy Petroleum Composition. 2. Progression of the Boduszynski Model to the Limit of Distillation by Ultrahigh-Resolution FT-ICR Mass Spectrometry. *Energy Fuels* **2010**, *24* (5), 2939–2946.
- (5) Buenroostro-Gonzalez, E.; Groenzin, H.; Lira-Galeana, C.; Mullins, O. C. The Overriding Chemical Principles That Define Asphaltene. *Energy Fuels* **2001**, *15* (4), 972–978.
- (6) Groenzin, H.; Mullins, O. C. Asphaltene Molecular Size and Structure. *J. Phys. Chem. A* **1999**, *103* (50), 11237–11245.
- (7) Carbognani, L.; Espidel, J.; Izquierdo, A. Characterization of Asphaltene Deposits from Oil Production and Transportation Operations. In *Asphaltene and Asphalts, 2. Developments in Petroleum Science*; Elsevier BV: Amsterdam, 2000; Vol. 40, pp 335–362, DOI: 10.1016/S0376-7361(09)70284-5.
- (8) Boduszynski, M. M. Asphaltene in Petroleum Asphalts. Composition and Formation. In *Chemistry of Asphaltene*; Bunker, J. W., Li, N. C., Eds.; Advances in Chemistry, Vol. 195; American Chemical Society: Washington, DC, 1982; pp 119–135.
- (9) Storm, D. A.; DeCanio, S. J.; DeTar, M. M.; Nero, V. P. Upper Bound on Number Average Molecular Weight of Asphaltene. *Fuel* **1990**, *69* (6), 735–738.

- (10) Acevedo, S.; Gutierrez, L. B.; Negrin, G.; Pereira, J. C.; Mendez, B.; Delolme, F.; Dessalces, G.; Broseta, D. Molecular Weight of Petroleum Asphaltene: A Comparison between Mass Spectrometry and Vapor Pressure Osmometry. *Energy Fuels* **2005**, *19* (4), 1548–1560.
- (11) Long, R. B. The Concept of Asphaltene. In *Chemistry of Asphaltene*; Advances in Chemistry, Vol. 195; American Chemical Society: Washington, DC, 2012, pp 17–27, DOI: 10.1021/ba-1981-0195.ch002.
- (12) Mullins, O. C. The Asphaltene. *Annu. Rev. Anal. Chem.* **2011**, *4*, 393–418.
- (13) Mullins, O. C.; Martínez-Haya, B.; Marshall, A. G. Contrasting Perspective on Asphaltene Molecular Weight. This Comment vs the Overview of A. A. Herod, K. D. Bartle, and R. Kandiyoti. *Energy Fuels* **2008**, *22* (3), 1765–1773.
- (14) Gray, M.; Tykwinski, R.; Stryker, J.; Tan, X. Supramolecular Assembly Model for Aggregation of Petroleum Asphaltene. *Energy Fuels* **2011**, *25*, 3125–3134.
- (15) Putman, J. C.; Moulian, R.; Barrère-Mangote, C.; Rodgers, R. P.; Bouyssié, B.; Giusti, P.; Marshall, A. G. Probing Aggregation Tendencies in Asphaltene by Gel Permeation Chromatography. Part 1: Online Inductively Coupled Plasma Mass Spectrometry and Offline Fourier Transform Ion Cyclotron Resonance Mass Spectrometry. *Energy Fuels* **2020**, *34* (7), 8308–8315.
- (16) Lang, I.; Vavreka, P. Standardization of VPO Asphaltene Molecular Weight. *Fuel* **1981**, *60* (12), 1176–1177.
- (17) Acevedo, S.; Mendez, B.; Rojas, A.; Layrisse, I.; Rivas, H. Asphaltene and Resins from the Orinoco Basin. *Fuel* **1985**, *64*, 1741–1747.
- (18) Ali, M. F.; Saleem, M. Asphaltene in Saudi Arabian Heavy Crude Oil Solubility and Molecular Weights In. *Fuel Sci. Technol. Int.* **1988**, *6* (5), 541–556.
- (19) Altgelt, K. H. Gel Permeation Chromatography of Asphalts and Asphaltene. Part I. Fractionation Procedure. *Makromol. Chem.* **1965**, *88* (1), 75–89.
- (20) Altgelt, K. H. Fractionation of Asphaltene by Gel Permeation Chromatography. *J. Appl. Polym. Sci.* **1965**, *9* (0), 3389–3393.
- (21) Selucky, M. L.; Kim, S. S.; Skinner, F.; Strausz, O. P. Structure-Related Properties of Athabasca Asphaltene and Resins as Indicated by Chromatographic Separation. In *Chemistry of Asphaltene*; Bunger, J. W., Li, N. C., Eds.; Advances in Chemistry, Vol. 195; American Chemical Society: Washington, DC, 1982; pp 83–118.
- (22) Koots, J. A.; Speight, J. G. Relation of Petroleum Resins to Asphaltene. *Fuel* **1975**, *54* (3), 179–184.
- (23) Boduszynski, M. M. Composition of Heavy Petroleum. Molecular Weight, Hydrogen Deficiency, and Heteroatom Concentration as a Function of Atmospheric Equivalent Boiling Point up to 1400 °F (760 °C). *Energy Fuels* **1987**, *1* (1), 2–11.
- (24) McKenna, A. M.; Purcell, J. M.; Rodgers, R. P.; Marshall, A. G. Heavy Petroleum Composition. 1. Exhaustive Compositional Analysis of Athabasca Bitumen HVGO Distillates by Fourier Transform Ion Cyclotron Resonance Mass Spectrometry: A Definitive Test of the Boduszynski Model. *Energy Fuels* **2010**, *24* (5), 2929–2938.
- (25) Murgich, J. Intermolecular Forces in Aggregates of Asphaltene and Resins. *Pet. Sci. Technol.* **2002**, *20*, 983–997.
- (26) Bissada, K. K. A.; Tan, J.; Szymczyk, E.; Darnell, M.; Mei, M. Group-Type Characterization of Crude Oil and Bitumen. Part I: Enhanced Separation and Quantification of Saturates, Aromatics, Resins and Asphaltene (SARA). *Org. Geochem.* **2016**, *95*, 21–28.
- (27) Speight, J. G.; Long, R. B.; Trowbridge, T. D. On the Definition of Asphaltene. *Am. Chem. Soc., Div. Pet. Chem., Prepr.* **1982**, *27* (3), 268–275.
- (28) Boduszynski, M. M.; McKay, J. F.; Latham, D. R. Asphaltene: Where Are You? In *Proceedings Association of Asphalt Paving Technologists Technical Session*; Association of Asphalt Paving Technologists (AAPT), 1980; Vol. 49, pp 123–143.
- (29) Hildebrand, J. H. Solubility of Non-Electrolytes. In *American Chemical Society Monograph Series, No. 17*; Reinhold Publishing Corporation, New York, 1936; p 203.
- (30) Hansen, C. M. The Three Dimensional Solubility Parameter and Solvent Diffusion Coefficient. Their Importance in Surface Coating Formulation. *J. Paint Technol.* **1967**, 104.
- (31) Boduszynski, M. M.; Hurtubise, R. J.; Silver, H. F. Separation of Solvent-Refined Coal Into Compound-Class Fractions. *Anal. Chem.* **1982**, *54* (3), 375–381.
- (32) Boduszynski, M. M. Composition of Heavy Petroleum. 2. Molecular Characterization. *Energy Fuels* **1988**, *2* (5), 597.
- (33) Altgelt, K. H.; Boduszynski, M. M. Composition of Heavy Petroleum. 3. An Improved Boiling-Point Molecular-Weight Relation. *Energy Fuels* **1992**, *6* (1), 68–72.
- (34) Boduszynski, M. M.; Altgelt, K. H. Composition of Heavy Petroleum. 4. Significance of the Extended Atmospheric Equivalent Boiling-Point (AEBP) Scale. *Energy Fuels* **1992**, *6* (1), 72–76.
- (35) Mullins, O. C. Rebuttal to Strausz et Al. Regarding Time-Resolved Fluorescence Depolarization of Asphaltene. *Energy Fuels* **2009**, *23* (5), 2845–2854.
- (36) Purcell, J. M.; Merdrignac, I.; Rodgers, R. P.; Marshall, A. G.; Gauthier, T.; Guibard, I. Stepwise Structural Characterization of Asphaltene during Deep Hydroconversion Processes Determined by Atmospheric Pressure Photoionization (APPI) Fourier Transform Ion Cyclotron Resonance (FT-ICR) Mass Spectrometry. *Energy Fuels* **2010**, *24* (4), 2257–2265.
- (37) Gaspar, A.; Zellermann, E.; Lababidi, S.; Reece, J.; Schrader, W. Impact of Different Ionization Methods on the Molecular Assignments of Asphaltene by FT-ICR Mass Spectrometry. *Anal. Chem.* **2012**, *84*, 5257–5267.
- (38) Wang, W.; Taylor, C.; Hu, H.; Humphries, K. L.; Jaini, A.; Kitimet, M.; Scott, T.; Stewart, Z.; Ulep, K. J.; Houck, S.; Luxon, A.; Zhang, B.; Miller, B.; Parish, C. A.; Pomerantz, A. E.; Mullins, O. C.; Zare, R. N. Nanoaggregates of Diverse Asphaltene by Mass Spectrometry and Molecular Dynamics. *Energy Fuels* **2017**, *31* (9), 9140–9151.
- (39) Agrawala, M.; Yarranton, H. W. An Asphaltene Association Model Analogous to Linear Polymerization. *Ind. Eng. Chem. Res.* **2001**, *40* (21), 4664–4672.
- (40) Schuler, B.; Meyer, G.; Peña, D.; Mullins, O. C.; Gross, L. Unraveling the Molecular Structures of Asphaltene by Atomic Force Microscopy. *J. Am. Chem. Soc.* **2015**, *137* (31), 9870–9876.
- (41) Schuler, B.; Fatayer, S.; Meyer, G.; Rogel, E.; Moir, M.; Zhang, Y.; Harper, M. R.; Pomerantz, A. E.; Bake, K. D.; Witt, M.; Pena, D.; Kushnerick, J. D.; Mullins, O. C.; Ovalles, C.; Van Den Berg, F. G. A.; Gross, L. Heavy Oil Based Mixtures of Different Origins and Treatments Studied by Atomic Force Microscopy. *Energy Fuels* **2017**, *31*, 6856–6861.
- (42) Chen, P.; Joshi, Y. V.; Metz, J. N.; Yao, N.; Zhang, Y. Conformational Analysis of Nonplanar Archipelago Structures on a Cu (111) Surface by Molecular Imaging. *Energy Fuels* **2020**, *34* (10), 12135–12141.
- (43) Chacón-Patiño, M. L.; Rowland, S. M.; Rodgers, R. P. The Compositional and Structural Continuum of Petroleum from Light Distillates to Asphaltene: The Boduszynski Continuum Theory as Revealed by FT-ICR Mass Spectrometry. In *The Boduszynski Continuum: Contributions to the Understanding of the Molecular Composition of Petroleum*; Ovalles, C., Moir, M. E., Eds.; ACS Symposium Series, Vol. 1282; Washington, DC, 2018; pp 113–171.
- (44) Chen, P.; Metz, J. N.; Mennito, A. S.; Merchant, S.; Smith, S. E.; Siskin, M.; Rucker, S. P.; Dankworth, D. C.; Kushnerick, J. D.; Yao, N.; Zhang, Y. Petroleum Pitch: Exploring a 50-Year Structure Puzzle with Real-Space Molecular Imaging. *Carbon* **2020**, *161*, 456–465.
- (45) Schuler, B.; Zhang, Y.; Collazos, S.; Fatayer, S.; Meyer, G.; Pérez, D.; Guitián, E.; Harper, M. R.; Kushnerick, J. D.; Peña, D.; Gross, L. Characterizing Aliphatic Moieties in Hydrocarbons with Atomic Force Microscopy. *Chem. Sci.* **2017**, *8* (3), 2315–2320.
- (46) Scott, D. E.; Schulze, M.; Stryker, J. M.; Tykwinski, R. R. Deciphering Structure and Aggregation in Asphaltene: Hypothesis-Driven Design and Development of Synthetic Model Compounds. *Chem. Soc. Rev.* **2021**, *50*, 9202–9239.

- (47) Zhang, Y.; Schulz, F.; Rytting, B. M. K.; Walters, C. C.; Kaiser, K.; Metz, J. N.; Harper, M. R.; Merchant, S. S.; Mennito, A. S.; Qian, K.; Kushnerick, J. D.; Kilpatrick, P. K.; Gross, L. Elucidating the Geometric Substitution of Porphyrins by Spectroscopic Analysis and Atomic Force Microscopy Molecular Imaging. *Energy Fuels* **2019**, *33* (7), 6088–6097.
- (48) Mullins, O. C. The Modified Yen Model. *Energy Fuels* **2010**, *24* (4), 2179–2207.
- (49) Groenzin, H.; Mullins, O. C. Molecular Size and Structure of Asphaltenes from Various Sources. *Energy Fuels* **2000**, *14* (12), 677–684.
- (50) Groenzin, H.; Mullins, O. C. Asphaltene Molecular Size and Structure. *J. Phys. Chem. A* **1999**, *103* (50), 11237–11245.
- (51) Gray, M. R. Consistency of Asphaltene Chemical Structures with Pyrolysis and Coking Behavior. *Energy Fuels* **2003**, *17* (6), 1566–1569.
- (52) Karimi, A.; Qian, K.; Olmstead, W. N.; Freund, H.; Yung, C.; Gray, M. R. Quantitative Evidence for Bridged Structures in Asphaltenes by Thin Film Pyrolysis. *Energy Fuels* **2011**, *25*, 3581–3589.
- (53) Savage, P. E.; Klein, M. T.; Kukes, S. G. Petroleum Asphaltene Thermal Reaction Pathways. *ACS Div. Fuel Chem. Prepr.* **1985**, *30* (3), 408–419.
- (54) Chacón-Patiño, M. L.; Blanco-Tirado, C.; Orrego-Ruiz, J. A.; Gómez-Escudero, A.; Combariza, M. Y. Tracing the Compositional Changes of Asphaltenes after Hydroconversion and Thermal Cracking Processes by High-Resolution Mass Spectrometry. *Energy Fuels* **2015**, *29* (10), 6330–6341.
- (55) Speight, J. G. Thermal Cracking of Athabasca Bitumen, Athabasca Asphaltenes, and Athabasca Deasphalted Heavy Oil. *Fuel* **1970**, *49* (2), 134–145.
- (56) Wang, J.; Anthony, E. J. A Study of Thermal-Cracking Behavior of Asphaltenes. *Chem. Eng. Sci.* **2003**, *58* (1), 157–162.
- (57) Trejo, F.; Ancheyta, J.; Noyola, A.; Sámano, V. Cracking of Maya Crude Asphaltenes. *Pet. Sci. Technol.* **2014**, *32* (21), 2592–2598.
- (58) Rueda-Velásquez, R. I.; Freund, H.; Qian, K.; Olmstead, W. N.; Gray, M. R. Characterization of Asphaltene Building Blocks by Cracking under Favorable Hydrogenation Conditions. *Energy Fuels* **2013**, *27*, 1817–1829.
- (59) Trejo, F.; Ancheyta, J. Characterization of Asphaltene Fractions from Hydrotreated Maya Crude Oil. *Ind. Eng. Chem. Res.* **2007**, *46*, 7571–7579.
- (60) Ancheyta, J.; Centeno, G.; Trejo, F.; Marroquin, G. Changes in Asphaltene Properties during Hydrotreating of Heavy Crudes. *Energy Fuels* **2003**, *17* (6), 1233–1238.
- (61) Ancheyta, J.; Trejo, F.; Rana, M. S. Definition and Structure of Asphaltenes. In *Asphaltene Chemical Transformation during Hydroprocessing of Heavy Oils*; CRC Press, Taylor & Francis Group: Boca Raton, FL, USA, 2010; pp 1–86.
- (62) Strausz, O. P.; Mojelsky, T. W.; Lown, E. M.; Kowalewski, I.; Behar, F. Structural Features of Boscan and Duri Asphaltenes. *Energy Fuels* **1999**, *13* (2), 228–247.
- (63) Strausz, O. P.; Mojelsky, T. W.; Lown, E. M. The Molecular Structure of Asphaltene: An Unfolding Story. *Fuel* **1992**, *71* (12), 1355–1363.
- (64) Podgorski, D. C.; Corilo, Y. E.; Nyadong, L.; Lobodin, V. V.; Bythell, B. J.; Robbins, W. K.; McKenna, A. M.; Marshall, A. G.; Rodgers, R. P. Heavy Petroleum Composition. 5. Compositional and Structural Continuum of Petroleum Revealed. *Energy Fuels* **2013**, *27* (3), 1268–1276.
- (65) Sabbah, H.; Morrow, A. L.; Pomerantz, A. E.; Zare, R. N. Evidence for Island Structures as the Dominant Architecture of Asphaltenes. *Energy Fuels* **2011**, *25*, 1597–1604.
- (66) Chacón-Patiño, M. L.; Rowland, S. M.; Rodgers, R. P. Advances in Asphaltene Petroleomics. Part I: Asphaltenes Are Composed of Abundant Island and Archipelago Structural Motifs. *Energy Fuels* **2017**, *31* (12), 13509–13518.
- (67) Payzant, J. D.; Lown, E. M.; Strausz, O. P. Structural Units of Athabasca Asphaltene: The Aromatics with a Linear Carbon Framework. *Energy Fuels* **1991**, *5* (3), 445–453.
- (68) Peng, P.; Morales-Izquierdo, A.; Hogg, A.; Strausz, O. P. Molecular Structure of Athabasca Asphaltene: Sulfide, Ether, and Ester Linkages. *Energy Fuels* **1997**, *11* (6), 1171–1187.
- (69) Murgich, J.; Abanero, J. A.; Strausz, O. P. Molecular Recognition in Aggregates Formed by Asphaltene and Resin Molecules from the Athabasca Oil Sand. *Energy Fuels* **1999**, *13* (2), 278–286.
- (70) Strausz, O. P.; Mojelsky, T. W.; Faraji, F.; Lown, E. M.; Peng, P. Additional Structural Details on Athabasca Asphaltene and Their Ramifications. *Energy Fuels* **1999**, *13* (2), 207–227.
- (71) Artok, L.; Su, Y.; Hirose, Y.; Hosokawa, M.; Murata, S.; Nomura, M. Structure and Reactivity of Petroleum-Derived Asphaltene. *Energy Fuels* **1999**, *13* (2), 287–296.
- (72) Sinninghe Damsté, J. S.; Eglinton, T. I.; De Leeuw, J. W.; Schenck, P. A. Organic Sulphur in Macromolecular Sedimentary Organic Matter: I. Structure and Origin of Sulphur-Containing Moieties in Kerogen, Asphaltenes and Coal as Revealed by Flash Pyrolysis. *Geochim. Cosmochim. Acta* **1989**, *53* (4), 873–889.
- (73) Savage, P. E.; Klein, M. T.; Kukes, S. G. Asphaltene Reaction Pathways. 1. Thermolysis. *Ind. Eng. Chem. Process Des. Dev.* **1985**, *24* (4), 1169–1174.
- (74) Yasar, M.; Trauth, D. M.; Klein, M. T. Asphaltene and Resid Pyrolysis. 2. The Effect of Reaction Environment on Pathways and Selectivities. *Energy Fuels* **2001**, *15* (3), 504–509.
- (75) Savage, P. E.; Klein, M. T.; Kukes, S. G. Asphaltene Reaction Pathways. 3. Effect of Reaction Environment. *Energy Fuels* **1988**, *2* (12), 619–628.
- (76) Savage, P. E.; Klein, M. T. Asphaltene Reaction Pathways. 4. Pyrolysis of Tridecylcyclohexane and 2-Ethyltetralin. *Ind. Eng. Chem. Res.* **1988**, *27* (8), 1348–1356.
- (77) Mullins, O. C.; Sabbah, H.; Eyssautier, J.; Pomerantz, A. E.; Barré, L.; Andrews, A. B.; Ruiz-Morales, Y.; Mostowfi, F.; McFarlane, R.; Goual, L.; Lepkowitz, R.; Cooper, T.; Orbulescu, J.; Leblanc, R. M.; Edwards, J.; Zare, R. N. Advances in Asphaltene Science and the Yen–Mullins Model. *Energy Fuels* **2012**, *26*, 3986–4003.
- (78) Mullins, O. C.; Sheu, E. Y. *Structure and Dynamics of Asphaltenes*, First Edition; Springer Science+Business Media, LLC: New York, 1998; DOI: 10.1007/978-1-4899-1615-0.
- (79) Betancourt, S. S.; Johansen, Y. B.; Forsythe, J. C.; Rinna, J.; Christoffersen, K.; Skillingstad, P.; Achourov, V.; Canas, J.; Chen, L.; Pomerantz, A. E.; Zuo, J. Y.; Mullins, O. C. Gravitational Gradient of Asphaltene Molecules in an Oilfield Reservoir with Light Oil. *Energy Fuels* **2018**, *32* (4), 4911–4924.
- (80) Alshareef, A. H.; Scherer, A.; Tan, X.; Azyat, K.; Stryker, J. M.; Tykwinski, R. R.; Gray, M. R. Formation of Archipelago Structures during Thermal Cracking Implicates a Chemical Mechanism for the Formation of Petroleum Asphaltenes. *Energy Fuels* **2011**, *25* (5), 2130–2136.
- (81) McKenna, A. M.; Purcell, J. M.; Rodgers, R. P.; Marshall, A. G. Atmospheric Pressure Photoionization Fourier Transform Ion Cyclotron Resonance Mass Spectrometry for Detailed Compositional Analysis of Petroleum. In *Proceedings of the 9th International Conference on Petroleum Phase Behavior and Fouling*, Victoria, British Columbia, Canada, June 15–19, 2008; Abstract 17.
- (82) McKenna, A. M.; Purcell, J. M.; Rodgers, R. P.; Marshall, A. G. Nonpolar speciation of Athabasca bitumen by atmospheric pressure photoionization FT-ICR mass spectrometry. In *Petrophase 2009, 10th International Conference on Petroleum Phase Behavior and Fouling*, Rio de Janeiro, Brazil, 2009.
- (83) Rodgers, R. P.; Mapolelo, M. M.; Robbins, W. K.; Chacon-Patino, M. L.; Putman, J. C.; Niles, S. F.; Rowland, S. M.; Marshall, A. G. Combating Selective Ionization in the High Resolution Mass Spectral Characterization of Complex Mixtures. *Faraday Discuss.* **2019**, *218*, 29–51.
- (84) Klein, G. C.; Kim, S.; Rodgers, R. P.; Marshall, A. G.; Yen, A. Mass Spectral Analysis of Asphaltenes. II. Detailed Compositional

Comparison of Asphaltenes Deposit to Its Crude Oil Counterpart for Two Geographically Different Crude Oils by ESI FT-ICR MS. *Energy Fuels* **2006**, *20*, 1973–1979.

(85) Klein, G. C.; Kim, S.; Rodgers, R. P.; Marshall, A. G.; Yen, A.; Asoaming, S. Mass Spectral Analysis of Asphaltenes. I. Compositional Differences between Pressure-Drop and Solvent-Drop Asphaltenes Determined by Electrospray Ionization Fourier Transform Ion Cyclotron Resonance Mass Spectrometry. *Energy Fuels* **2006**, *20* (9), 1965–1972.

(86) Mckenna, A. M.; Purcell, J. M.; Rodgers, R. P.; Marshall, A. G. Identification of Vanadyl Porphyrins in a Heavy Crude Oil and Raw Asphaltene by Atmospheric Pressure Photoionization Fourier Transform Ion Cyclotron Resonance (FT-ICR) Mass Spectrometry. *Energy Fuels* **2009**, *23* (4), 2122–2128.

(87) Nyadong, L.; Lai, J.; Thompsen, C.; LaFrancois, C. J.; Cai, X.; Song, C.; Wang, J.; Wang, W. High-Field Orbitrap Mass Spectrometry and Tandem Mass Spectrometry for Molecular Characterization of Asphaltenes. *Energy Fuels* **2018**, *32* (1), 294–305.

(88) Rodgers, R. P.; Marshall, A. G.; Niles, S. F.; Chacón-Patiño, M. L.; Smith, D. F. Comprehensive Compositional and Structural Comparison of Coal and Petroleum Asphaltenes Based on Extrography Fractionation Coupled with Fourier Transform Ion Cyclotron Resonance MS and MS/MS Analysis. *Energy Fuels* **2020**, *34* (2), 1492–1505.

(89) Chacón-Patiño, M. L.; Rowland, S. M.; Rodgers, R. P. Advances in Asphaltene Petroleomics. Part 3. Dominance of Island or Archipelago Structural Motif Is Sample Dependent. *Energy Fuels* **2018**, *32* (9), 9106–9120.

(90) Dong, X.; Zhang, Y.; Milton, J.; Yerabolu, R.; Easterling, L.; Kenttämaa, H. I. Investigation of the Relative Abundances of Single-Core and Multicore Compounds in Asphaltenes by Using High-Resolution in-Source Collision-Activated Dissociation and Medium-Energy Collision-Activated Dissociation Mass Spectrometry with Statistical Consideration. *Fuel* **2019**, *246*, 126–132.

(91) Thomas, M. J.; Jones, H. E.; Palacio Lozano, D. C.; Gavard, R.; Carney, S.; Barrow, M. P. Comprehensive Analysis of Multiple Asphaltene Fractions Combining Statistical Analyses and Novel Visualization Tools. *Fuel* **2021**, *291*, 120132.

(92) Rüger, C. P.; Miersch, T.; Schwemer, T.; Sklorz, M.; Zimmermann, R. Hyphenation of Thermal Analysis to Ultrahigh-Resolution Mass Spectrometry (Fourier Transform Ion Cyclotron Resonance Mass Spectrometry) Using Atmospheric Pressure Chemical Ionization For Studying Composition and Thermal Degradation of Complex Materials. *Anal. Chem.* **2015**, *87* (13), 6493–6499.

(93) Niles, S. F.; Chacón-Patiño, M. L.; Chen, H.; Mckenna, A. M.; Blakney, G. T.; Rodgers, R. P.; Marshall, A. G. Molecular-Level Characterization of Oil-Soluble Ketone/Aldehyde Photo-Oxidation Products by Fourier Transform Ion Cyclotron Resonance Mass Spectrometry Reveals Similarity Between Microcosm and Field Samples. *Environ. Sci. Technol.* **2019**, *53*, 6887–6894.

(94) Radović, J. R.; Jaggi, A.; Silva, R. C.; Snowdon, R.; Waggoner, D. C.; Hatcher, P. G.; Larter, S. R.; Oldenburg, T. B. P. Applications of FTICR-MS in Oil Spill Studies. *Deep Oil Spills* **2020**, 355–373.

(95) Leyva, D.; Jaffe, R.; Fernandez-Lima, F. Structural Characterization of Dissolved Organic Matter at the Chemical Formula Level Using TIMS-FT-ICR MS/MS. *Anal. Chem.* **2020**, *92* (17), 11960–11966.

(96) Zark, M.; Christoffers, J.; Dittmar, T. Molecular Properties of Deep-Sea Dissolved Organic Matter Are Predictable by the Central Limit Theorem: Evidence from Tandem FT-ICR-MS. *Mar. Chem.* **2017**, *191*, 9–15.

(97) Ware, R. L.; Rowland, S. M.; Rodgers, R. P.; Marshall, A. G. Advanced Chemical Characterization of Pyrolysis Oils from Landfill Waste, Recycled Plastics, and Forestry Residue. *Energy Fuels* **2017**, *31* (8), 8210–8216.

(98) Cheng, F.; Dehghanizadeh, M.; Audu, M. A.; Jarvis, J. M.; Holguin, F. O.; Brewer, C. E. Characterization and Evaluation of

Guayule Processing Residues as Potential Feedstock for Biofuel and Chemical Production. *Ind. Crops Prod.* **2020**, *150* (March), 112311.

(99) Mazzoleni, L. R.; Saranjampour, P.; Dalbec, M. M.; Samburova, V.; Hallar, A. G.; Zielinska, B.; Lowenthal, D. H.; Kohl, S. Identification of Water-Soluble Organic Carbon in Non-Urban Aerosols Using Ultrahigh-Resolution FT-ICR Mass Spectrometry: Organic Anions. *Environ. Chem.* **2012**, *9* (3), 285–297.

(100) Choi, J. H.; Ryu, J.; Jeon, S.; Seo, J.; Yang, Y. H.; Pack, S. P.; Choung, S.; Jang, K. S. In-Depth Compositional Analysis of Water-Soluble and -Insoluble Organic Substances in Fine (PM_{2.5}) Airborne Particles Using Ultra-High-Resolution 15T FT-ICR MS and GC × GC-TOFMS. *Environ. Pollut.* **2017**, *225*, 329–337.

(101) Rodgers, R. P.; Marshall, A. G. Petroleomics: Advanced Characterization of Petroleum-Derived Materials by Fourier Transform Ion Cyclotron Resonance Mass Spectrometry (FT-ICR MS). In *Asphaltenes, Heavy Oils and Petroleomics*; Springer: New York, 2007; pp 63–93, DOI: 10.1007/0-387-68903-6_3.

(102) Gallegos, E. J.; Green, J. W.; Lindeman, L. P.; LeTourneau, R. L.; Teeter, R. M. Petroleum Group-Type Analysis by High Resolution Mass Spectrometry. *Anal. Chem.* **1967**, *39* (14), 1833–1838.

(103) Comisarow, M. B.; Marshall, A. G. Fourier Transform Ion Cyclotron Resonance. *Chem. Phys. Lett.* **1974**, *25* (2), 282–283.

(104) Comisarow, M. B.; Marshall, A. G. Theory of Fourier Transform Ion Cyclotron Resonance Mass Spectroscopy. I. Fundamental Equations and Low-Pressure Line Shape. *J. Chem. Phys.* **1976**, *64* (1), 110.

(105) Marshall, A. G.; Hendrickson, C. L.; Jackson, G. S. Fourier Transform Ion Cyclotron Resonance Mass Spectrometry: A Primer. *Mass Spectrom. Rev.* **1998**, *17*, 1–35.

(106) Marshall, A. G.; Rodgers, R. P. Petroleomics: The Next Grand Challenge for Chemical Analysis. *Acc. Chem. Res.* **2004**, *37* (1), 53–59.

(107) Petkewich, R. Cracking” the Structure of Petroleum. *Environ. Sci. Technol.* **2003**, *37* (11), 206A–207A.

(108) Rodgers, R. P.; Schaub, T.; Marshall, A. G. Petroleomics: MS Returns to Its Roots. *Anal. Chem.* **2005**, *77* (1), 20A–27A.

(109) Gaspar, A.; Zellermann, E.; Lababidi, S.; Reece, J.; Schrader, W. Characterization of Saturates, Aromatics, Resins, and Asphaltenes Heavy Crude Oil Fractions by Atmospheric Pressure Laser Ionization Fourier Transform Ion Cyclotron Resonance Mass Spectrometry. *Energy Fuels* **2012**, *26*, 3481–3487.

(110) Qi, Y.; Barrow, M. P.; Li, H.; Meier, J. E.; Van Orden, S. L.; Thompson, C. J.; O’Connor, P. B. Absorption-Mode: The next Generation of Fourier Transform Mass Spectra. *Anal. Chem.* **2012**, *84* (6), 2923–2929.

(111) Rogel, E.; Witt, M. Asphaltene Characterization During Hydroprocessing by Ultrahigh-Resolution Fourier Transform Ion Cyclotron Resonance Mass Spectrometry. *Energy Fuels* **2017**, *31* (4), 3409–3416.

(112) Nascimento, P. T. H.; Santos, A. F.; Yamamoto, C. I.; Tose, L. V.; Barros, E. V.; Gonçalves, G. R.; Freitas, J. C. C.; Vaz, B. G.; Romão, W.; Scheer, A. P. Fractionation of Asphaltene by Adsorption onto Silica and Chemical Characterization by Atmospheric Pressure Photoionization Fourier Transform Ion Cyclotron Resonance Mass Spectrometry. *Energy Fuels* **2016**, *30*, 5439–5448.

(113) Lu, H.; Shi, Q.; Ma, Q.; Shi, Y.; Liu, J.; Sheng, G.; Peng, P. Molecular Characterization of Sulfur Compounds in Some Special Sulfur-Rich Chinese Crude Oils by FT-ICR MS. *Sci. China: Earth Sci.* **2014**, *57* (6), 1158–1167.

(114) Rüger, C. P.; Neumann, A.; Sklorz, M.; Schwemer, T.; Zimmermann, R. Thermal Analysis Coupled to Ultrahigh Resolution Mass Spectrometry with Collision Induced Dissociation for Complex Petroleum Samples: Heavy Oil Composition and Asphaltene Precipitation Effects. *Energy Fuels* **2017**, *31*, 13144–13158.

(115) Islam, A.; Cho, Y.; Ahmed, A.; Kim, S. Data Interpretation Methods for Petroleomics. *Mass Spectrom. Lett.* **2012**, *3* (3), 63–67.

(116) Qian, K.; Edwards, K. E.; Mennito, A. S.; Freund, H.; Saeger, R. B.; Hickey, K. J.; Francisco, M. A.; Yung, C.; Chawla, B.; Wu, C.; Kushnerick, J. D.; Olmstead, W. N. Determination of Structural

Building Blocks in Heavy Petroleum Systems by Collision-Induced Dissociation Fourier Transform Ion Cyclotron Resonance Mass Spectrometry. *Anal. Chem.* **2012**, *84* (10), 4544–4551.

(117) Corilo, Y. E.; Vaz, B. G.; Simas, R. C.; Lopes Nascimento, H. D.; Klitzke, C. F.; Pereira, R. C. L.; Bastos, W. L.; Santos Neto, E. V.; Rodgers, R. P.; Eberlin, M. N. Petroleomics by EASI(\pm) FT-ICR MS. *Anal. Chem.* **2010**, *82* (10), 3990–3996.

(118) Vaz, B. G.; Silva, R. C.; Klitzke, C. F.; Simas, R. C.; Lopes Nascimento, H. D.; Pereira, R. C. L.; Garcia, D. F.; Eberlin, M. N.; Azevedo, D. A. Assessing Biodegradation in the Llanos Orientales Crude Oils by Electrospray Ionization Ultrahigh Resolution and Accuracy Fourier Transform Mass Spectrometry and Chemometric Analysis. *Energy Fuels* **2013**, *27*, 1277–1284.

(119) Jiang, B.; Zhan, Z. W.; Shi, Q.; Liao, Y.; Zou, Y. R.; Tian, Y.; Peng, P. Chemometric Unmixing of Petroleum Mixtures by Negative Ion ESI FT-ICR MS Analysis. *Anal. Chem.* **2019**, *91* (3), 2209–2215.

(120) Valencia-dávila, J. A.; Witt, M.; Blanco-tirado, C.; Combariza, M. Y. Molecular Characterization of Naphthenic Acids from Heavy Crude Oils Using MALDI FT-ICR Mass Spectrometry. *Fuel* **2018**, *231*, 126–133.

(121) Ramírez-Pradilla, J. S.; Blanco-Tirado, C.; Hubert-Roux, M.; Giusti, P.; Afonso, C.; Combariza, M. Y. Comprehensive Petroporphyrin Identification in Crude Oils Using Highly Selective Electron Transfer Reactions in MALDI-FTICR-MS. *Energy Fuels* **2019**, *33* (5), 3899–3907.

(122) Rojas-Ruiz, F. A.; Orrego-Ruiz, J. A. Distribution of Oxygen-Containing Compounds and Its Significance on Total Organic Acid Content in Crude Oils by ESI Negative Ion FT-ICR MS. *Energy Fuels* **2016**, *30*, 8185–8191.

(123) McKenna, A. M.; Marshall, A. G.; Rodgers, R. P. Heavy Petroleum Composition. 4. Asphaltene Compositional Space. *Energy Fuels* **2013**, *27*, 1257–1267.

(124) Ancheyta, J.; Centeno, G.; Trejo, F.; Marroquín, G.; García, J. A.; Tenorio, E.; Torres, A. Extraction and Characterization of Asphaltenes from Different Crude Oils and Solvents. *Energy Fuels* **2002**, *16* (5), 1121–1127.

(125) Ancheyta, J.; Trejo, F.; Rana, M. S. Fractionation of Heavy Crude Oils and Asphaltenes. In *Asphaltenes: Chemical Transformation during Hydroprocessing of Heavy Oils*; CRC Press, Taylor & Francis Group: Boca Raton, FL, USA, 2010; pp 371–416.

(126) Rogel, E.; Moir, M.; Witt, M. Atmospheric Pressure Photoionization and Laser Desorption Ionization Coupled to Fourier Transform Ion Cyclotron Resonance Mass Spectrometry To Characterize Asphaltene Solubility Fractions: Studying the Link between Molecular Composition and Physical Behav. *Energy Fuels* **2015**, *29* (7), 4201–4209.

(127) Rogel, E.; Moir, M.; Witt, M. Atmospheric Pressure Photoionization and Laser Desorption Ionization Coupled to Fourier Transform Ion Cyclotron Resonance Mass Spectrometry To Characterize Asphaltene Solubility Fractions: Studying the Link between Molecular Composition and Physical Behav. *Energy Fuels* **2015**, *29* (7), 4201–4209.

(128) Giraldo-Dávila, D.; Chacón-Patiño, M. L.; McKenna, A. M.; Blanco-Tirado, C.; Combariza, M. Y. Correlations Between Molecular Composition and the Adsorption, Aggregation and Emulsifying Behavior of Petrophase 2017 Asphaltenes and Their TLC Fractions. *Energy Fuels* **2018**, *32*, 2769.

(129) Cho, Y.; Na, J.; Nho, N.; Kim, S.; Kim, S. Application of Saturates, Aromatics, Resins, Asphaltenes Crude Oil Fractionation for Detailed Chemical Characterization of Heavy Crude Oils by Fourier Transform Ion Cyclotron Resonance Mass Spectrometry Equipped with Atmospheric Pressure Photoionization. *Energy Fuels* **2012**, *26*, 2558–2565.

(130) Rieger, C. P.; Grimmer, C.; Sklorz, M.; Neumann, A.; Streibel, T.; Zimmermann, R. Combination of Different Thermal Analysis Methods Coupled to Mass Spectrometry for the Analysis of Asphaltenes and Their Parent Crude Oils: Comprehensive Characterization of the Molecular Pyrolysis Pattern. *Energy Fuels* **2018**, *32* (3), 2699–2711.

(131) Chacón-Patiño, M. L.; Vesga-Martínez, S. J.; Blanco-Tirado, C.; Orrego-Ruiz, J. A.; Gómez-Escudero, A.; Combariza, M. Y. Exploring Occluded Compounds and Their Interactions with Asphaltene Networks Using High-Resolution Mass Spectrometry. *Energy Fuels* **2016**, *30* (6), 4550–4561.

(132) Rowland, S. M.; Chacon-Patino, M. L.; Rodgers, R. P. Single Nominal Mass Zoom-Inset for the Broadband MS. In *Petrophase 18th International Conference on Petroleum Phase Behavior and Fouling*; 2017.

(133) Krajewski, L. C.; Rodgers, R. P.; Marshall, A. G. 126264 Assigned Chemical Formulas from an Atmospheric Pressure Photoionization 9.4 T Fourier Transform Positive Ion Cyclotron Resonance Mass Spectrum. *Anal. Chem.* **2017**, *89*, 11318–11324.

(134) Palacio Lozano, D. C.; Gavard, R.; Arenas-Diaz, J. P.; Thomas, M. J.; Stranz, D. D.; Mejía-Ospino, E.; Guzman, A.; Spencer, S. E. F.; Rossell, D.; Barrow, M. P. Pushing the Analytical Limits: New Insights into Complex Mixtures Using Mass Spectra Segments of Constant Ultrahigh Resolving Power. *Chem. Sci.* **2019**, *10* (29), 6966–6978.

(135) Jarrell, T. M.; Jin, C.; Riedeman, J. S.; Owen, B. C.; Tan, X.; Scherer, A.; Tykwinski, R. R.; Gray, M. R.; Slater, P.; Kenttämä, H. I. Elucidation of Structural Information Achievable for Asphaltenes via Collision-Activated Dissociation of Their Molecular Ions in MSn Experiments: A Model Compound Study. *Fuel* **2014**, *133* (May), 106–114.

(136) Hurt, M. R.; Borton, D. J.; Choi, H. J.; Kenttämä, H. I. Comparison of the Structures of Molecules in Coal and Petroleum Asphaltenes by Using Mass Spectrometry. *Energy Fuels* **2013**, *27* (7), 3653–3658.

(137) Wu, Q.; Pomerantz, A. E.; Mullins, O. C.; Zare, R. N. Minimization of Fragmentation and Aggregation by Laser Desorption Laser Ionization Mass Spectrometry. *J. Am. Soc. Mass Spectrom.* **2013**, *24* (7), 1116–1122.

(138) Pomerantz, A. E.; Mullins, O. C.; Paul, G.; Ruzicka, J.; Sanders, M. Orbitrap Mass Spectrometry: A Proposal for Routine Analysis of Nonvolatile Components of Petroleum. *Energy Fuels* **2011**, *25* (7), 3077–3082.

(139) Tang, W.; Hurt, M. R.; Sheng, H.; Riedeman, J. S.; Borton, D. J.; Slater, P.; Kenttämä, H. I. Structural Comparison of Asphaltenes of Different Origins Using Multi-Stage Tandem Mass Spectrometry. *Energy Fuels* **2015**, *29* (3), 1309–1314.

(140) Qian, K.; Robbins, W. K.; Hughey, C. A.; Cooper, H. J.; Rodgers, R. P.; Marshall, A. G. Resolution and Identification of Elemental Compositions for More than 3000 Crude Acids in Heavy Petroleum by Negative-Ion Microelectrospray High-Field Fourier Transform Ion Cyclotron Resonance Mass Spectrometry. *Energy Fuels* **2001**, *15* (6), 1505–1511.

(141) Hughey, C. A.; Rodgers, R. P.; Marshall, A. G. Resolution of 11 000 Compositionally Distinct Components in a Single Electrospray Ionization Fourier Transform Ion Cyclotron Resonance Mass Spectrum of Crude Oil. *Anal. Chem.* **2002**, *74* (16), 4145–4149.

(142) Smith, L. M.; Kelleher, N. L. Proteomics, T. C. for T. D. Proteoform: A Single Term Describing Protein Complexity. *Nat. Methods* **2013**, *10*, 186–187.

(143) York, W. S.; Agravat, S.; Aoki-Kinoshita, K. F.; McBride, R.; Campbell, M. P.; Costello, E. C.; Dell, A.; Feizi, T.; Haslam, S. M.; Karlsson, N.; et al. MIRAGE: The Minimum Information Required for a Glycomics Experiment. *Glycobiology* **2014**, *24*, 402–406.

(144) Murphy, R. C. Challenges in Mass Spectrometry-Based Lipidomics of Neutral Lipids. *TrAC, Trends Anal. Chem.* **2018**, *107*, 91–98.

(145) Henriksen, T.; Juhler, R. K.; Svensmark, B.; Cech, N. B. The Relative Influences of Acidity and Polarity on Responsiveness of Small Organic Molecules to Analysis with Negative Ion Electrospray Ionization Mass Spectrometry (ESI-MS). *J. Am. Soc. Mass Spectrom.* **2005**, *16* (4), 446–455.

(146) Purcell, J. M.; Hendrickson, C. L.; Rodgers, R. P.; Marshall, A. G. Atmospheric Pressure Photoionization Proton Transfer for Complex Organic Mixtures Investigated by Fourier Transform Ion

Cyclotron Resonance Mass Spectrometry. *J. Am. Soc. Mass Spectrom.* **2007**, *18*, 1682–1689.

(147) Farenc, M.; Corilo, Y. E.; Lalli, P. M.; Riches, E.; Rodgers, R. P.; Afonso, C.; Giusti, P. Comparison of Atmospheric Pressure Ionization for the Analysis of Heavy Petroleum Fractions with Ion Mobility-Mass Spectrometry. *Energy Fuels* **2016**, *30* (11), 8896–8903.

(148) Purcell, J. M.; Hendrickson, C. L.; Rodgers, R. P.; Marshall, A. G. Atmospheric Pressure Photoionization Proton Transfer for Complex Organic Mixtures Investigated by Fourier Transform Ion Cyclotron Resonance Mass Spectrometry. *J. Am. Soc. Mass Spectrom.* **2007**, *18* (9), 1682–1689.

(149) Kauppila, T. J.; Kkuuranne, T.; Meurer, E. C.; Eberlin, M. N.; Kotiaho, T.; Kostianen, R. Atmospheric Pressure Photoionization Mass Spectrometry. Ionization Mechanism and the Effect of Solvent on the Ionization of Naphthalenes. *Anal. Chem.* **2002**, *74* (21), 5470–5479.

(150) Hughey, C. A.; Hendrickson, C. L.; Rodgers, R. P.; Marshall, A. G. Elemental Composition Analysis of Processed and Unprocessed Diesel Fuel by Electrospray Ionization Fourier Transform Ion Cyclotron Resonance Mass Spectrometry. *Energy Fuels* **2001**, *15* (5), 1186–1193.

(151) Kiontke, A.; Oliveira-Birkmeier, A.; Opitz, A.; Birkemeyer, C. Electrospray Ionization Efficiency Is Dependent on Different Molecular Descriptors with Respect to Solvent PH and Instrumental Configuration. *PLoS One* **2016**, *11*, e0167502.

(152) Krueve, A.; Kaupmees, K.; Liigand, J.; Leito, I. Negative Electrospray Ionization via Deprotonation: Predicting the Ionization Efficiency. *Anal. Chem.* **2014**, *86*, 4822–4830.

(153) Rebane, R.; Krueve, A.; Liigand, P.; Liigand, J.; Herodes, K.; Leito, I. Establishing Atmospheric Pressure Chemical Ionization Efficiency Scale. *Anal. Chem.* **2016**, *88*, 3435–3439.

(154) Pomerantz, A. E.; Hammond, M. R.; Morrow, A. L.; Mullins, O. C.; Zare, R. N. Two-Step Laser Mass Spectrometry of Asphaltenes. *J. Am. Chem. Soc.* **2008**, *130* (23), 7216–7217.

(155) Sabbah, H.; Morrow, A. L.; Pomerantz, A. E.; Mullins, O. C.; Tan, X.; Gray, M. R.; Azyat, K.; Tykwinski, R. R.; Zare, R. N. Comparing Laser Desorption/Laser Ionization Mass Spectra of Asphaltenes and Model Compounds. *Energy Fuels* **2010**, *24* (6), 3589–3594.

(156) Sabbah, H.; Morrow, A. L.; Pomerantz, A. E.; Mullins, O. C.; Tan, X.; Gray, M. R.; Azyat, K.; Tykwinski, R. R.; Zare, R. N. Comparing Laser Desorption/Laser Ionization Mass Spectra of Asphaltenes and Model Compounds. *Energy Fuels* **2010**, *24* (6), 3589–3594.

(157) Pomerantz, A. E.; Wu, Q.; Mullins, O. C.; Zare, R. N. Laser-Based Mass Spectrometric Assessment of Asphaltene Molecular Weight, Molecular Architecture and Nanoaggregate Number. *Energy Fuels* **2015**, *29* (5), 2833–2842.

(158) Sabbah, H.; Morrow, A. L.; Pomerantz, A. E.; Zare, R. N. Evidence for Island Structures as the Dominant Architecture of Asphaltenes. *Energy Fuels* **2011**, *25* (4), 1597–1604.

(159) Sabbah, H.; Pomerantz, A. E.; Wagner, M.; Müllen, K.; Zare, R. N. Laser Desorption Single-Photon Ionization of Asphaltenes: Mass Range, Compound Sensitivity, and Matrix Effects. *Energy Fuels* **2012**, *26* (6), 3521–3526.

(160) Mamyryn, B. A. Time-of-Flight Mass Spectrometry (Concepts, Achievements, and Prospects). *Int. J. Mass Spectrom.* **2001**, *206* (3), 251–266.

(161) Schuler, B.; Zhang, Y.; Liu, F.; Pomerantz, A. E.; Andrews, A. B.; Gross, L.; Pauchard, V.; Banerjee, S.; Mullins, O. C. Overview of Asphaltene Nanostructures and Thermodynamic Applications. *Energy Fuels* **2020**, *34*, 15082.

(162) Chacón-Patiño, M. L.; Rowland, S. M.; Rodgers, R. P. Advances in Asphaltene Petroleomics. Part 2: Selective Separation Method That Reveals Fractions Enriched in Island and Archipelago Structural Motifs by Mass Spectrometry. *Energy Fuels* **2018**, *32* (1), 314–328.

(163) Wang, W.; Taylor, C.; Hu, H.; Humphries, K. L.; Jaini, A.; Kitimet, M.; Scott, T.; Stewart, Z.; Ulep, K. J.; Houck, S.; Luxon, A.;

Zhang, B.; Miller, B.; Parish, C. A.; Pomerantz, A. E.; Mullins, O. C.; Zare, R. N. Nanoaggregates of Diverse Asphaltenes by Mass Spectrometry and Molecular Dynamics. *Energy Fuels* **2017**, *31* (9), 9140–9151.

(164) Kondyli, A.; Schrader, W. Evaluation of the Combination of Different Atmospheric Pressure Ionization Sources for the Analysis of Extremely Complex Mixtures. *Rapid Commun. Mass Spectrom.* **2020**, *34* (8), 1–9.

(165) Huba, A. K.; Huba, K.; Gardinali, P. R. Understanding the Atmospheric Pressure Ionization of Petroleum Components: The Effects of Size, Structure, and Presence of Heteroatoms. *Sci. Total Environ.* **2016**, *568*, 1018–1025.

(166) Kaiser, N. K.; Quinn, J. P.; Blakney, G. T.; Hendrickson, C. L.; Marshall, A. G. A Novel 9.4 T FTICR Mass Spectrometer with Improved Sensitivity, Mass Resolution, and Mass Range. *J. Am. Soc. J. Am. Soc. Mass Spectrom.* **2011**, *22* (8), 1343–1351.

(167) Nikolaev, E. N.; Vladimirov, G. N.; Jertz, R.; Baykut, G. From Supercomputer Modeling to Highest Mass Resolution in FT-ICR. *Mass Spectrom.* **2013**, *2*, S0010–S0010.

(168) Lobodin, V. V.; Marshall, A. G.; Hsu, C. S. Compositional Space Boundaries for Organic Compounds. *Anal. Chem.* **2012**, *84*, 3410–3416.

(169) Hsu, C. S.; Lobodin, V. V.; Rodgers, R. P.; McKenna, A. M.; Marshall, A. G. Compositional Boundaries for Fossil Hydrocarbons. *Energy Fuels* **2011**, *25*, 2174–2178.

(170) Cho, Y.; Kim, Y. H.; Kim, S. Planar Limit-Assisted Structural Interpretation of Saturates/Aromatics/Resins/Asphaltenes Fractionated Crude Oil Compounds Observed by Fourier Transform Ion Cyclotron Resonance Mass Spectrometry. *Anal. Chem.* **2011**, *83* (15), 6068–6073.

(171) Pereira, T. M. C.; Vanini, G.; Tose, L. V.; Cardoso, F. M. R.; Fleming, F. P.; Rosa, P. T. V.; Thompson, C. J.; Castro, E. V. R.; Vaz, B. G.; Romão, W. FT-ICR MS Analysis of Asphaltenes: Asphaltenes Go In. *Fuel* **2014**, *131* (April), 49–58.

(172) Farmani, Z.; Vetere, A.; Poidevin, C.; Auer, A. A.; Schrader, W. Studying Natural Buckyballs and Buckybowls in Fossil Materials. *Angew. Chem., Int. Ed.* **2020**, *59* (35), 15008–15013.

(173) Rowland, S. M.; Robbins, W. K.; Corilo, Y. E.; Marshall, A. G.; Rodgers, R. P. Solid-Phase Extraction Fractionation To Extend the Characterization of Naphthenic Acids in Crude Oil by Electrospray Ionization Fourier Transform Ion Cyclotron Resonance Mass Spectrometry. *Energy Fuels* **2014**, *28*, 5043–5048.

(174) Vasconcelos, G. A.; Pereira, R. C. L.; Santos, C. D. F.; Carvalho, V. V.; Tose, L. V.; Romão, W.; Vaz, B. G. Extraction and Fractionation of Basic Nitrogen Compounds in Vacuum Residue by Solid-Phase Extraction and Characterization by Ultra-High Resolution Mass Spectrometry. *Int. J. Mass Spectrom.* **2017**, *418*, 67–72.

(175) Clingenpeel, A. C.; Rowland, S. M.; Corilo, Y. E.; Zito, P.; Rodgers, R. P. Fractionation of Interfacial Material Reveals a Continuum of Acidic Species That Contribute to Stable Emulsion Formation. *Energy Fuels* **2017**, *31* (6), 5933–5939.

(176) Ramírez, F. A.; Morales, Y. R. Island versus Archipelago Architecture for Asphaltenes: Polycyclic Aromatic Hydrocarbon Dimer Theoretical Studies. *Energy Fuels* **2013**, *27*, 1791–1808.

(177) Ruiz-Morales, Y. HOMO-LUMO Gap as an Index of Molecular Size and Structure for Polycyclic Aromatic Hydrocarbons (PAHs) and Asphaltenes: A Theoretical Study. *J. Phys. Chem. A* **2002**, *106* (46), 11283–11308.

(178) Klein, G. C.; Angstrom, A.; Rodgers, R. P.; Marshall, A. G. Use of Saturates/Aromatics/Resins/Asphaltenes (SARA) Fractionation To Determine Matrix Effects in Crude Oil Analysis by Electrospray Ionization Fourier Transform Ion Cyclotron Resonance Mass Spectrometry. *Energy Fuels* **2006**, *20* (10), 668–672.

(179) Buenrostro-Gonzalez, E.; Andersen, S. I.; Garcia-Martinez, J. A.; Lira-Galeana, C. Solubility/Molecular Structure Relationships of Asphaltenes in Polar and Nonpolar Media. *Energy Fuels* **2002**, *16* (3), 732–741.

(180) Adams, J. J. Asphaltene Adsorption, a Literature Review. *Energy Fuels* **2014**, *28* (5), 2831–2856.

- (181) Pernyeszi, T.; Dékány, I. Sorption and Elution of Asphaltenes from Porous Silica Surfaces. *Colloids Surf., A* **2001**, *194*, 25–39.
- (182) Sullivan, A. P.; Kilpatrick, P. K. The Effects of Inorganic Solid Particles on Water and Crude Oil Emulsion Stability. *Ind. Eng. Chem. Res.* **2002**, *41*, 3389–3404.
- (183) McLean, J. D.; Kilpatrick, P. K. Comparison of Precipitation and Extrography in the Fractionation of Crude Oil Residua. *Energy Fuels* **1997**, *11* (3), 570–585.
- (184) Wang, S.; Liu, Q.; Xu, C.; Gray, M. Irreversible Surface Adsorption of Asphaltenes and Analogies to Proteins. In *Petrophase 17th International Conference on Petroleum Phase Behavior and Fouling*. 2016; p 134.
- (185) Juyal, P.; McKenna, A. M.; Fan, T.; Cao, T.; Rueda-Velásquez, R. I.; Fitzsimmons, J. E.; Yen, A.; Rodgers, R. P.; Wang, J.; Buckley, J. S.; Gray, M. R.; Allenson, S. J.; Creek, J. Joint Industrial Case Study for Asphaltene Deposition. *Energy Fuels* **2013**, *27* (4), 1899–1908.
- (186) Ballard, D. A.; Chacón-Patiño, M. L.; Qiao, P.; Roberts, K. J.; Rae, R.; Dowding, P. J.; Xu, Z.; Harbottle, D. Molecular Characterization of Strongly and Weakly Interfacially Active Asphaltenes by High-Resolution Mass Spectrometry. *Energy Fuels* **2020**, *34* (11), 13966–13976.
- (187) Qiao, P.; Harbottle, D.; Tchoukov, P.; Masliyah, J.; Sjöblom, J.; Liu, Q.; Xu, Z. Fractionation of Asphaltenes in Understanding Their Role in Petroleum Emulsion Stability and Fouling. *Energy Fuels* **2017**, *31* (4), 3330–3337.
- (188) Qiao, P.; Harbottle, D.; Li, Z.; Tang, Y.; Xu, Z. Interactions of Asphaltene Subfractions in Organic Media of Varying Aromaticity. *Energy Fuels* **2018**, *32*, 10478–10485.
- (189) Karimi, A.; Qian, K.; Olmstead, W. N.; Freund, H.; Yung, C.; Gray, M. R. Quantitative Evidence for Bridged Structures in Asphaltenes by Thin Film Pyrolysis. *Energy Fuels* **2011**, *25* (8), 3581–3589.
- (190) Chacón-Patiño, M. L.; Smith, D. F.; Hendrickson, C. L.; Marshall, A. G.; Rodgers, R. P. Advances in Asphaltene Petroleomics. Part 4. Compositional Trends of Solubility Subfractions Reveal That Polyfunctional Oxygen-Containing Compounds Drive Asphaltene Chemistry. *Energy Fuels* **2020**, *34*, 3013–3030.
- (191) Chacón-Patiño, M. L.; Moulian, R.; Barrère-Mangote, C.; Putman, J. C.; Weisbrod, C. R.; Blakney, G. T.; Bouyssièrè, B.; Rodgers, R. P.; Giusti, P. Compositional Trends for Total Vanadium Content and Vanadyl Porphyrins in Gel Permeation Chromatography Fractions Reveal Correlations between Asphaltene Aggregation and Ion Production Efficiency in Atmospheric Pressure Photoionization. *Energy Fuels* **2020**, *34* (12), 16158–16172.
- (192) Caumette, G.; Lienemann, C. P.; Merdrignac, I.; Bouyssièrè, B.; Lobinski, R. Fractionation and Speciation of Nickel and Vanadium in Crude Oils by Size Exclusion Chromatography-ICP MS and Normal Phase HPLC-ICP MS. *J. Anal. At. Spectrom.* **2010**, *25* (7), 1123–1129.
- (193) Desprez, A.; Bouyssièrè, B.; Arnaudguilhem, C.; Krier, G.; Vernex-Loset, L.; Giusti, P. Study of the Size Distribution of Sulfur, Vanadium, and Nickel Compounds in Four Crude Oils and Their Distillation Cuts by Gel Permeation Chromatography Inductively Coupled Plasma High-Resolution Mass Spectrometry. *Energy Fuels* **2014**, *28* (6), 3730–3737.
- (194) Putman, J. C.; Moulian, R.; Smith, D. F.; Weisbrod, C. R.; Chacón-Patiño, M. L.; Corilo, Y. E.; Blakney, G. T.; Rumancik, L. E.; Barrère-Mangote, C.; Rodgers, R. P.; Giusti, P.; Marshall, A. G.; Bouyssièrè, B. Probing Aggregation Tendencies in Asphaltenes by Gel Permeation Chromatography. Part 2: Online Detection by Fourier Transform Ion Cyclotron Resonance Mass Spectrometry and Inductively Coupled Plasma Mass Spectrometry. *Energy Fuels* **2020**, *34* (9), 10915–10925.
- (195) Panda, S. K.; Alawani, N. A.; Lajami, A. R.; Al-Qunaysi, T. A.; Muller, H. Characterization of Aromatic Hydrocarbons and Sulfur Heterocycles in Saudi Arabian Heavy Crude Oil by Gel Permeation Chromatography and Ultrahigh Resolution Mass Spectrometry. *Fuel* **2019**, *235* (9), 1420–1426.
- (196) Alawani, N. A.; Panda, S. K.; Lajami, A. R.; Al-Qunaysi, T. A.; Muller, H. Characterization of Crude Oils through Alkyl Chain-Based Separation by Gel Permeation Chromatography and Mass Spectrometry. *Energy Fuels* **2020**, *34* (5), 5414–5425.
- (197) Putman, J. C.; Gutiérrez Sama, S.; Barrère-Mangote, C.; Rodgers, R. P.; Lobinski, R.; Marshall, A. G.; Bouyssièrè, B.; Giusti, P. Analysis of Petroleum Products by Gel Permeation Chromatography Coupled Online with Inductively Coupled Plasma Mass Spectrometry and Offline with Fourier Transform Ion Cyclotron Resonance Mass Spectrometry. *Energy Fuels* **2018**, *32* (12), 12198–12204.
- (198) Gutierrez Sama, S.; Desprez, A.; Krier, G.; Lienemann, C. P.; Barbier, J.; Lobinski, R.; Barrère-Mangote, C.; Giusti, P.; Bouyssièrè, B. Study of the Aggregation of Metal Complexes with Asphaltenes Using Gel Permeation Chromatography Inductively Coupled Plasma High-Resolution Mass Spectrometry. *Energy Fuels* **2016**, *30* (9), 6907–6912.
- (199) Gascon, G.; Vargas, V.; Feo, L.; Castellano, O.; Castillo, J.; Giusti, P.; Acavedo, S.; Lienemann, C. P.; Bouyssièrè, B. Size Distributions of Sulfur, Vanadium, and Nickel Compounds in Crude Oils, Residues, and Their Saturate, Aromatic, Resin, and Asphaltene Fractions Determined by Gel Permeation Chromatography Inductively Coupled Plasma High-Resolution Mass Spectrometry. *Energy Fuels* **2017**, *31* (8), 7783–7788.
- (200) Barbier, J.; Marques, J.; Caumette, G.; Merdrignac, I.; Bouyssièrè, B.; Lobinski, R.; Lienemann, C. P. Monitoring the Behaviour and Fate of Nickel and Vanadium Complexes during Vacuum Residue Hydrotreatment and Fraction Separation. *Fuel Process. Technol.* **2014**, *119*, 185–189.
- (201) Ballard, D. A.; Chacón-Patiño, M. L.; Qiao, P.; Roberts, K. J.; Rae, R.; Dowding, P. J.; Xu, Z.; Harbottle, D. Molecular Characterization of Strongly and Weakly Interfacially Active Asphaltenes by High-Resolution Mass Spectrometry. *Energy Fuels* **2020**, *34* (11), 13966–13976.
- (202) McKenna, A. M.; Chacón-Patiño, M. L.; Weisbrod, C. R.; Blakney, G. T.; Rodgers, R. P. Molecular-Level Characterization of Asphaltenes Isolated from Distillation Cuts. *Energy Fuels* **2019**, *33* (3), 2018–2029.
- (203) Giraldo-Dávila, D.; Chacón-Patiño, M. L.; Orrego-Ruiz, J. A.; Blanco-Tirado, C.; Combariza, M. Y. Improving Compositional Space Accessibility in (+) APPI FT-ICR Mass Spectrometric Analysis of Crude Oils by Extrography and Column Chromatography Fractionation. *Fuel* **2016**, *185*, 45–58.
- (204) Salinas, S. L. D6560-12, Standard Test Method for Determination of Asphaltenes (Heptane Insolubles) in Crude and Petroleum Products. *Pet. Prod. Lubr. Foss. Fuels* **2013**, 1–6.
- (205) Jarvis, J. M.; Robbins, W. K.; Corilo, Y. E.; Rodgers, R. P. Novel Method to Isolate Interfacial Material. *Energy Fuels* **2015**, *29* (11), 7058–7064.
- (206) Clingenpeel, A. C.; Robbins, W. K.; Corilo, Y. E.; Rodgers, R. P. Effect of the Water Content on Silica Gel for the Isolation of Interfacial Material from Athabasca Bitumen. *Energy Fuels* **2015**, *29*, 7150–7155.
- (207) Chacon-Patino, M. L.; Rowland, S. M.; Rodgers, R. P. Molecular Composition and Structure of Asphaltene Compounds That Disproportionally Contribute to Emulsion Ageing and Stability. In *Proceedings of the Petrophase 19th International Conference on Petroleum Phase Behavior and Fouling*, 2018.
- (208) Zeegers-Huyskens, T. Importance of the Proton Affinities in Hydrogen Bond Studies. A New Exponential Expression. *J. Mol. Struct.* **1988**, *177* (C), 125–141.
- (209) Dega-Szafran, Z.; Hrynio, A.; Szafran, M. A Quantitative Comparison of Spectroscopic and Energy Data, in Solution, of NHO and OHO Hydrogen Bonds and Gas-Phase Proton Affinities: Complexes of Pyridines and Pyridine N-Oxides with Acetic Acids. *J. Mol. Struct.* **1990**, *240* (C), 159–174.
- (210) Mautner, M. The Ionic Hydrogen Bond and Ion Solvation. I. NH⁺···O, NH⁺···N, and OH⁺···O Bonds. Correlations with Proton Affinity. Deviations Due to Structural Effects. *J. Am. Chem. Soc.* **1984**, *106* (5), 1257–1264.

- (211) Ren, L.; Wu, J.; Qian, Q.; Liu, X.; Meng, X.; Zhang, Y.; Shi, Q. Separation and Characterization of Sulfoxides in Crude Oils. *Energy Fuels* **2019**, *33*, 796–804.
- (212) Laskin, J.; Futrell, J. H. Activation of Large Ions in FT-ICR Mass Spectrometry. *Mass Spectrom. Rev.* **2005**, *24* (2), 135–167.
- (213) Vala, M.; Szczepanski, J.; Oomens, J.; Steill, J. D. H₂ Ejection from Polycyclic Aromatic Hydrocarbons: Infrared Multiphoton Dissociation Study of Protonated 1,2-Dihydronaphthalene. *J. Am. Chem. Soc.* **2009**, *131* (18), 5784–5791.
- (214) Schuler, B.; Zhang, Y.; Liu, F.; Pomerantz, A. E.; Andrews, A. B.; Gross, L.; Pauchard, V.; Banerjee, S.; Mullins, O. C. Overview of Asphaltene Nanostructures and Thermodynamic Applications. *Energy Fuels* **2020**, *34* (12), 15082–15105.
- (215) McKenna, A. M.; Donald, L. J.; Fitzsimmons, J. E.; Juyal, P.; Spicer, V.; Standing, K. G.; Marshall, A. G.; Rodgers, R. P. Heavy Petroleum Composition. 3. Asphaltene Aggregation. *Energy Fuels* **2013**, *27* (3), 1246–1256.
- (216) Smith, D. F.; Schaub, T. M.; Rahimi, P.; Teclemariam, A.; Rodgers, R. P.; Marshall, A. G. Self-Association of Organic Acids in Petroleum and Canadian Bitumen Characterized by Low- and High-Resolution Mass Spectrometry. *Energy Fuels* **2007**, *21* (3), 1309–1316.
- (217) Biggs, W. R.; Fetzer, J. C.; Brown, R. J.; Reynolds, J. G. Characterization of Vanadium Compounds in Selected Crudes I. Porphyrin and Non-Porphyrin Separation. *Liq. Liq. Fuels Technol.* **1985**, *3* (4), 397–421.
- (218) Baker, E. W.; William Louda, J.; Orr, W. L. Application of Metalloporphyrin Biomarkers as Petroleum Maturity Indicators: The Importance of Quantitation. *Org. Geochem.* **1987**, *11* (4), 303–309.
- (219) Mironov, N. A.; Milordov, D. V.; Abilova, G. R.; Yakubova, S. G.; Yakubov, M. R. Methods for Studying Petroleum Porphyrins (Review). *Pet. Chem.* **2019**, *59* (10), 1077–1091.
- (220) Chacón-Patiño, M. L.; Nelson, J.; Rogel, E.; Hench, K.; Poirier, L.; Lopez-Linares, F.; Ovalles, C. Vanadium and Nickel Distributions in Pentane, In-between C5-C7 Asphaltenes, and Heptane Asphaltenes of Heavy Crude Oils. *Fuel* **2021**, *292*, 120259.
- (221) Zhao, X.; Shi, Q.; Gray, M. R.; Xu, C. New Vanadium Compounds in Venezuela Heavy Crude Oil Detected by Positive-Ion Electrospray Ionization Fourier Transform Ion Cyclotron Resonance Mass Spectrometry. *Sci. Rep.* **2015**, *4*, 1–6.
- (222) Qian, K.; Fredriksen, T. R.; Mennito, A. S.; Zhang, Y.; Harper, M. R.; Merchant, S.; Kushnerick, J. D.; Rytting, B. M. K.; Kilpatrick, P. K. Evidence of Naturally-Occurring Vanadyl Porphyrins Containing Multiple S and O Atoms. *Fuel* **2019**, *239*, 1258–1264.
- (223) Borton, D.; Pinkston, D. S.; Hurt, M. R.; Tan, X.; Azyat, K.; Scherer, A.; Tykwinski, R.; Gray, M.; Qian, K.; Kenttämaa, H. I. Molecular Structures of Asphaltenes Based on the Dissociation Reactions of Their Ions in Mass Spectrometry. *Energy Fuels* **2010**, *24* (10), 5548–5559.
- (224) Riedeman, J. S.; Kadasala, N. R.; Wei, A.; Kenttämaa, H. I. Characterization of Asphaltene Deposits by Using Mass Spectrometry and Raman Spectroscopy. *Energy Fuels* **2016**, *30* (2), 805–809.
- (225) Pomerantz, A. E.; Hammond, M. R.; Morrow, A. L.; Mullins, O. C.; Zare, R. N. Asphaltene Molecular-Mass Distribution Determined by Two-Step Laser Mass Spectrometry. *Energy Fuels* **2009**, *23* (3), 1162–1168.
- (226) Dong, X.; Lu, X.; Romanczyk, M.; Zhang, Y.; Kenttämaa, H. High-Resolution Broad Mass Range Collision-Energy Scanning Tandem Mass Spectrometry for Structural Characterization of Asphaltene Molecular Ions. In *66th ASMS Conference on Mass Spectrometry and Allied Topics*, San Antonio, TX, USA, June 5–9, 2016.
- (227) Vandenbroucke, M. Kerogen: From Types to Models of Chemical Structure. *Oil Gas Sci. Technol.* **2003**, *58* (2), 243–269.
- (228) Kelemen, S. R.; Walters, C. C.; Ertas, D.; Freund, H.; Curry, D. J. Petroleum Expulsion Part 3. A Model of Chemically Driven Fractionation during Expulsion of Petroleum from Kerogen. *Energy Fuels* **2006**, *20* (1), 309–319.
- (229) Rodgers, R. P.; Mapolelo, M. M.; Robbins, W. K.; Chacón-Patiño, M. L.; Putman, J. C.; Niles, S. F.; Rowland, S. M.; Marshall, A. G. Combating Selective Ionization in the High Resolution Mass Spectral Characterization of Complex Mixtures. *Faraday Discuss.* **2019**, *218*, 29.
- (230) Acevedo, N.; Moulian, R.; Chacon-Patino, M. L.; Mejia, A.; Radji, S.; Daridon, J.-L.; Barrere-Mangote, C.; Giusti, P.; Rodgers, R. P.; Piscitelli, V.; Castillo, J.; Carrier, H.; Bouyssiere, B. Understanding Asphaltene Fraction Behavior through Combined Quartz Crystal Resonator Sensor, FT-ICR MS, GPC ICP HR-MS and AFM Characterization. Part I: Extrography Fractionation. *Energy Fuels* **2020**, *34* (11), 13903–13915.
- (231) Wittrig, A. M.; Fredriksen, T. R.; Qian, K.; Clingenpeel, A. C.; Harper, M. R. Single Dalton Collision-Induced Dissociation for Petroleum Structure Characterization. *Energy Fuels* **2017**, *31* (12), 13338–13344.
- (232) Chawla, B.; Green, L. A. Multi-dimensional high performance liquid chromatographic separation technique (STAR7) for quantitative determinations of 7 fractions in heavy petroleum streams boiling above 550 degrees F, U.S. Patent No. US 8,114,678 B2, Feb. 12, 2012.
- (233) McLafferty, F. W.; Tureček, F. *Interpretation of Mass Spectra*, Fourth Edition; University Science Books, 1993; pp 27–28.
- (234) Hsu, C. S. Definition of Hydrogen Deficiency for Hydrocarbons with Functional Groups. *Energy Fuels* **2010**, *24* (7), 4097–4098.
- (235) Marshall, A. G.; Wang, T. C. L.; Ricca, T. L. Tailored Excitation for Fourier Transform Ion Cyclotron Mass Spectrometry. *J. Am. Chem. Soc.* **1985**, *107* (26), 7893–7897.
- (236) Guan, S.; Marshall, A. G. Stored Waveform Inverse Fourier Transform (SWIFT) Ion Excitation in Trapped-Ion Mass Spectrometry: Theory and Applications. *Int. J. Mass Spectrom. Ion Processes* **1996**, *157-158*, 5–37.
- (237) Shinn, J. H. From Coal to Single-Stage and Two-Stage Products: A Reactive Model of Coal Structure. *Fuel* **1984**, *63* (9), 1187–1196.
- (238) Lababidi, S.; Panda, S. K.; Andersson, J. T.; Schrader, W. Direct Coupling of Normal-Phase High-Performance Liquid Chromatography to Atmospheric Pressure Laser Ionization Fourier Transform Ion Cyclotron Resonance Mass Spectrometry for the Characterization of Crude Oil. *Anal. Chem.* **2013**, *85* (20), 9478–9485.
- (239) Lababidi, S.; Schrader, W. Online Normal-Phase High-Performance Liquid Chromatography/Fourier Transform Ion Cyclotron Resonance Mass Spectrometry: Effects of Different Ionization Methods on the Characterization of Highly Complex Crude Oil Mixtures. *Rapid Commun. Mass Spectrom.* **2014**, *28* (12), 1345–1352.
- (240) Ghislain, T.; Molnár G. L.; Schrader, W. Characterization of Crude Oil Asphaltenes by Coupling Size-Exclusion Chromatography Directly to an Ultrahigh-Resolution Mass Spectrometer. *Rapid Commun. Mass Spectrom.* **2017**, *31* (6), 495–502.
- (241) Molnár G. L.; Schrader, W. Argonation Chromatography Coupled to Ultrahigh-resolution Mass Spectrometry for the Separation of a Heavy Crude Oil. *J. Chromatogr. A* **2017**, *1484*, 41–48.
- (242) Gavard, R.; Jones, H. E.; Palacio Lozano, D. C.; Thomas, M. J.; Rossell, D.; Spencer, S. E. F.; Barrow, M. P. KairosMS: A New Solution for the Processing of Hyphenated Ultrahigh-Resolution Mass Spectrometry Data. *Anal. Chem.* **2020**, *92* (5), 3775–3786.
- (243) Marshall, A. G.; Hendrickson, C. L.; Jackson, G. S. Fourier Transform Ion Cyclotron Resonance Mass Spectrometry: A Primer. *Mass Spectrom. Rev.* **1998**, *17*, 1–35.
- (244) Smith, D. F.; Podgorski, D. C.; Rowland, S. M.; Hendrickson, C. L. 21 T FT-ICR Mass Spectrometer for Complex Mixture Analysis. In *Proceedings of the ASMS Asilomar Conference 2016*, Pacific Grove, CA, USA, Oct. 14–18, 2016.
- (245) Smith, D. F.; Podgorski, D. C.; Rodgers, R. P.; Blakney, G. T.; Hendrickson, C. L. 21 T FT-ICR Mass Spectrometer for Ultrahigh-Resolution Analysis of Complex Organic Mixtures. *Anal. Chem.* **2018**, *90* (3), 2041–2047.

- (246) Rowland, S.; Smith, D.; Blakney, G.; Hendrickson, C.; Rodgers, R. Online Coupling of Liquid Chromatography with Fourier Transform Ion Cyclotron Resonance Mass Spectrometry at 21 T Provides Fast and Unique Insight into Crude Oil Composition. *Anal. Chem.*, in press, DOI: 10.1021/acs.analchem.1c01169.
- (247) Putman, J. C.; Rowland, S. M.; Podgorski, D. C.; Robbins, W. K.; Rodgers, R. P. Dual-Column Aromatic Ring Class Separation with Improved Universal Detection across Mobile-Phase Gradients via Eluate Dilution. *Energy Fuels* 2017, 31, 12064–12071.
- (248) Kalli, A.; Smith, G. T.; Sweredoski, M. J.; Hess, S. Evaluation and Optimization of Mass Spectrometric Settings during Data-Dependent Acquisition Mode: Focus on LTQ-Orbitrap Mass Analyzers. *J. Proteome Res.* 2013, 12 (7), 3071–3086.
- (249) Page, J. S.; Bogdanov, B.; Vilkov, A. N.; Prior, D. C.; Buschbach, M. A.; Tang, K.; Smith, R. D. Automatic Gain Control in Mass Spectrometry Using a Jet Disrupter Electrode in an Electrodynamic Ion Funnel. *J. Am. Soc. Mass Spectrom.* 2005, 16 (2), 244–253.
- (250) Putman, J. C.; Moulian, R.; Smith, D. F.; Weisbrod, C. R.; Chacon-Patino, M. L.; Corilo, Y. E.; Blakney, G. T.; Rumancik, L. E.; Barrere-Mangote, C.; Bouysiere, B. Probing Aggregation Tendencies in Asphaltenes by Gel Permeation Chromatography. Part 2: Online Inductively Coupled Plasma Mass Spectrometry and Offline Fourier Transform Ion Cyclotron Resonance Mass Spectrometry. *Energy Fuels* 2020, 34, 10915.
- (251) Carboognani, L.; Rogel, E. Solvent Swelling of Petroleum Asphaltenes. *Energy Fuels* 2002, 16 (6), 1348–1358.
- (252) Carboognani, L.; Rogel, E. Solid Petroleum Asphaltenes Seem Surrounded by Alkyl Layers. *Pet. Sci. Technol.* 2003, 21 (3–4), 537–556.
- (253) Stachowiak, C.; Vigiú, J. R.; Grolier, J. P. E.; Rogalski, M. Effect of N-Alkanes on Asphaltene Structuring in Petroleum Oils. *Langmuir* 2005, 21 (11), 4824–4829.
- (254) Takanohashi, T.; Sato, S.; Saito, I.; Tanaka, R. Molecular Dynamics Simulation of the Heat-Induced Relaxation of Asphaltene Aggregates. *Energy Fuels* 2003, 17 (1), 135–139.
- (255) Flego, C.; Zannoni, C. Direct Insertion Probe-Mass Spectrometry: A Useful Tool for Characterization of Asphaltenes. *Energy Fuels* 2010, 24 (11), 6041–6053.
- (256) Neumann, A.; Chacón-Patiño, M. L.; Rodgers, R. P.; Rüger, C. P.; Zimmermann, R. Investigation of Island/Single-Core- And Archipelago/Multicore-Enriched Asphaltenes and Their Solubility Fractions by Thermal Analysis Coupled with High-Resolution Fourier Transform Ion Cyclotron Resonance Mass Spectrometry. *Energy Fuels* 2021, 35 (5), 3808.
- (257) Zhao, Y.; Gray, M. R.; Chung, K. H. Molar Kinetics and Selectivity in Cracking of Athabasca Asphaltenes. *Energy Fuels* 2001, 15, 751–755.
- (258) Hauser, A.; AlHumaidan, F.; Al-Rabiah, H.; Halabi, M. A. Study on Thermal Cracking of Kuwaiti Heavy Oil (Vacuum Residue) and Its SARA Fractions by NMR Spectroscopy. *Energy Fuels* 2014, 28 (7), 4321–4332.
- (259) Douda, J.; Alvarez, R.; Navarrete Bolanos, J. Characterization of Maya Asphaltene and Maltene by Means of Pyrolysis Application. *Energy Fuels* 2008, 22 (4), 2619–2628.
- (260) Chiaberge, S.; Guglielmetti, G.; Montanari, L.; Salvalaggio, M.; Santolini, L.; Spera, S.; Cesti, P. Investigation of Asphaltene Chemical Structural Modification Induced by Thermal Treatments. *Energy Fuels* 2009, 23, 4486–4495.
- (261) Materazzi, S.; Vecchio, S. Evolved Gas Analysis by Mass Spectrometry. *Appl. Spectrosc. Rev.* 2011, 46 (4), 261–340.
- (262) Geißler, R.; Saraji-Bozorgzad, M.; Streibel, T.; Kaisersberger, E.; Denner, T.; Zimmermann, R. Investigation of Different Crude Oils Applying Thermal Analysis/Mass Spectrometry with Soft Photoionisation. *J. Therm. Anal. Calorim.* 2009, 96 (3), 813–820.
- (263) Geißler, R.; Saraji-Bozorgzad, M. R.; Gröger, T.; Fendt, A.; Streibel, T.; Sklorz, M.; Krooss, B. M.; Fuhrer, K.; Gonin, M.; Kaisersberger, E.; Denner, T.; Zimmermann, R. Single Photon Ionization Orthogonal Acceleration Time-of-Flight Mass Spectrometry and Resonance Enhanced Multiphoton Ionization Time-of-Flight Mass Spectrometry for Evolved Gas Analysis in Thermogravimetry: Comparative Analysis of Crude Oils. *Anal. Chem.* 2009, 81 (15), 6038–6048.
- (264) Jayaraman, K.; Gokalp, I. Thermogravimetric and Evolved Gas Analyses of High Ash Indian and Turkish Coal Pyrolysis and Gasification. *J. Therm. Anal. Calorim.* 2015, 121 (2), 919–927.
- (265) Streibel, T.; Fendt, A.; Geißler, R.; Kaisersberger, E.; Denner, T.; Zimmermann, R. Thermal Analysis/Mass Spectrometry Using Soft Photo-Ionisation for the Investigation of Biomass and Mineral Oils. *J. Therm. Anal. Calorim.* 2009, 97 (2), 615–619.
- (266) Rüger, C. P.; Miersch, T.; Schwemer, T.; Sklorz, M.; Zimmermann, R. Hyphenation of Thermal Analysis to Ultrahigh-Resolution Mass Spectrometry (Fourier Transform Ion Cyclotron Resonance Mass Spectrometry) Using Atmospheric Pressure Chemical Ionization for Studying Composition and Thermal Degradation of Complex Materials. *Anal. Chem.* 2015, 87 (13), 6493–6499.
- (267) Lacroix-Andrivet, O.; Castilla, C.; Rüger, C.; Hubert-Roux, M.; Mendes Siqueira, A. L.; Giusti, P.; Afonso, C. Direct Insertion Analysis of Polymer-Modified Bitumen by Atmospheric Pressure Chemical Ionization Ultrahigh-Resolution Mass Spectrometry. *Energy Fuels* 2021, 35 (3), 2165–2173.
- (268) Zannoni, C.; Flego, C. Direct Insertion Probe - Mass Spectrometry in the Characterization of Opportunity Crudes. *Energy Fuels* 2013, 27, 46–55.
- (269) Käfer, U.; Gröger, T.; Rohbogner, C. J.; Struckmeier, D.; Saraji-Bozorgzad, M. R.; Wilharm, T.; Zimmermann, R. Detailed Chemical Characterization of Bunker Fuels by High-Resolution Time-of-Flight Mass Spectrometry Hyphenated to GC × GC and Thermal Analysis. *Energy Fuels* 2019, 33 (11), 10745–10755.
- (270) Kök, M. V.; Karacan, O. Pyrolysis Analysis and Kinetics of Crude Oils. *J. Therm. Anal. Calorim.* 1998, 52 (3), 781–788.
- (271) Käfer, U.; Gröger, T.; Rüger, C. P.; Czech, H.; Saraji-Bozorgzad, M.; Wilharm, T.; Zimmermann, R. Direct Inlet Probe – High-Resolution Time-of-Flight Mass Spectrometry as Fast Technique for the Chemical Description of Complex High-Boiling Samples. *Talanta* 2019, 202, 308–316.
- (272) Wohlfahrt, S.; Fischer, M.; Saraji-Bozorgzad, M.; Matuschek, G.; Streibel, T.; Post, E.; Denner, T.; Zimmermann, R. Rapid Comprehensive Characterization of Crude Oils by Thermogravimetry Coupled to Fast Modulated Gas Chromatography-Single Photon Ionization Time-of-Flight Mass Spectrometry. *Anal. Bioanal. Chem.* 2013, 405 (22), 7107–7116.
- (273) Streibel, T.; Geißler, R.; Saraji-Bozorgzad, M.; Sklorz, M.; Kaisersberger, E.; Denner, T.; Zimmermann, R. Evolved Gas Analysis (EGA) in TG and DSC with Single Photon Ionisation Mass Spectrometry (SPI-MS): Molecular Organic Signatures from Pyrolysis of Soft and Hard Wood, Coal, Crude Oil and ABS Polymer. *J. Therm. Anal. Calorim.* 2009, 96 (3), 795–804.
- (274) Grimmer, C.; Rüger, C. P.; Streibel, T.; Cuoq, F.; Kwakkenbos, G.; Cordova, M.; Peñalver, R.; Zimmermann, R. Description of Steam Cracker Fouling and Coking Residues by Thermal Analysis-Photoionization Mass Spectrometry. *Energy Fuels* 2019, 33 (11), 11592–11602.
- (275) Neumann, A.; Käfer, U.; Gröger, T.; Wilharm, T.; Zimmermann, R.; Rüger, C. P. Investigation of Aging Processes in Bitumen at the Molecular Level with High-Resolution Fourier-Transform Ion Cyclotron Mass Spectrometry and Two-Dimensional Gas Chromatography Mass Spectrometry. *Energy Fuels* 2020, 34 (9), 10641–10654.